A HOLOGRAPHIC STUDY

OF

TYMPANIC MEMBRANE VIBRATIONS IN CATS

by

SHYAM M. KHANNA

A dissertation submitted to the Graduate Faculty in Speech in partial fulfillment of the requirements for the degree of Doctor of Philosophy, The City University of New York.

1970

This manuscript has been read and accepted for the Graduate Faculty in Speech in satisfaction of the dissertation requirement for the degree of Doctor of Philosophy.

17 Feb. 1970
date

Chairman of Examining Committee

17 Feb 1970
date

Executive Officer

Supervisory Committee

The City University of New York

ACKNOWLEDGMENT

I would like to thank Professor E. N. Leith of the University of Michigan for his valuable advice on general holographic problems.

Mr. G. W. Johnson built most of the holographic components used in the experiments. Without his skilled work, the experiments could not have been conducted.

My special thanks go to Professor J. Tonndorf for his able guidance and advice. His deep knowledge of anatomy and his surgical skills contributed heavily towards the success of these experiments.

CONTENTS

Page No.

LIST OF TABLES

LIST OF ILLUSTRATIONS

Abstract

A HOLOGRAPHIC STUDY

OF

TYMPANIC MEMBRANE VIBRATIONS IN CATS

by

Shyam M. Khanna

Adviser: Professor Juergen Tonndorf

Time averaged holography developed by Powell and Stetson (1965) is a method for studying the vibration patterns of objects with amplitudes in excess of 10^{-5} cm. Both the shape and absolute magnitude of vibrations can be deduced from the contour lines visible in such holographic reconstructions. There are alternate bright and dark contour lines, each of them connecting points of equal vibration amplitude. They are comparable to the contour lines of a geodesic map. Numerical analysis is presented to show the dynamic range and accuracy of the method. In the application of this method for the study of the vibratory characteristics of the cat's tympanic membrane (T.M.), a number of technical difficulties were encountered:

(a) The T.M. is transparent. In order to make a good hologram, it must be uniformly coated with a reflecting material. This coat should not alter its mechanical properties. Finely ground bronze powder suspended in ether, was found to be a satisfactory coating material. A uniform thin coat was obtained by spraying the liquid with an artist's air brush.

(b) Photographic shutters are noisy and set the T.M. into undesirable vibrations. A silent shutter was devised; its principles and design are described.

(c) The low stiffness of the T.M. required high mechanical stability. Methods used to achieve such stability are described.

(d) Because of the small size of the T.M., high optical resolution is required. Factors affecting the quality of time averaged holography in this regard are evaluated.

Time averaged holograms of the T.M. in cat cadavers were obtained for various frequencies and sound pressure levels. Photographs of the reconstructions are shown.

These reconstructions are pictures of the T.M. with superimposed iso-amplitude contour lines.

Comparisons are made between the holographic data and data obtained from living animals by different methods to show that the experimental method (i.e., the use of cadavers and the coating of the T.M.) did not affect the results.

Results may be summarized as follows: (a) Vibratory patterns remain substantially unchanged in their first mode up to a frequency of 2000 Hz. In this mode, there are peak displacement regions in the posterior and anterior quadrants. At the posterior peak the amplitude is three times larger than that at the mallar tip, and at the anterior peak it is about the same as at the mallar tip.

(b) Above 3000 Hz, the vibration pattern undergoes a sharp change. First posteriorly and then, above 4000 Hz, also anteriorly, the vibrations break up into small sectional patterns. Consequently, in the frequency range above 3000 Hz, anterior and posterior amplitudes become relatively larger than those of the malleus. This difference increases with frequency.

Essentially the same results were obtained in a study using human cadaver specimens (Tonndorf and Khanna 1970). The peak displacement regions were located in the anterior and posterior quadrants of

the T.M. and there was no sign of a lower fold or hinged-plate motion of the T.M.

The present data do not support the notion of Bekesy that the mode of vibration of the T.M. is that of a hinged stiff plate. However, they are compatable with the proposal of Helmholtz, i.e., that the mode of vibration obeys the catenary principle. The tympanic membrane, owing to its shape, acts as a force transformer so that the force transmitted to the malleus is larger than merely that given by sound pressure times the area of the T.M. The average value of the catenary force transformation ratio is estimated to be between 1.3 and 3.0. The transformer ratio of the entire middle ear is discussed in the light of these findings.

A. INTRODUCTION

Due to its ready accessability and relatively large size, the tympanic membrane has been a subject of study for quite some time. Over one hundred years ago (1869), Helmholtz presented the concept of the mechanism of curved membranes in which he proposed that the tympanic membrane, owing to its shape, acts as a force transformer. The force transmitted to the malleus will be larger than merely that given by pressure times the area of the tympanic membrane. At the time of Helmholtz there were no tools available with which the vibratory pattern of the tympanic membrane could be studied directly. He had to rely on indirect static measurements to arrive at his conclusions.

In 1941, the vibratory pattern of the human tympanic membrane was studied by Bekesy by means of a capacitive probe. His observations indicated that the tympanic membrane vibrates at low and middle frequencies like a hinged stiff plate, and that the inferior part of the tympanic membrane was a loose fold (the "lower fold") to allow such a motion. According to this concept, the force acting on the malleus would be: pressure times two-thirds the area of the tympanic membrane, the loose fold not contributing

to the force transformation.

On the strength of Bekesy's experiment, the concept of Helmholtz was discarded and the concept of the hinged stiff plate was accepted. This concept appeared to be supported by middle ear impedance measurements of Zwislocki and Møller.

Invention of the laser in 1960 introduced a powerful optical tool. Using lasers, Leith, Upatnieks, and their group at the University of Michigan, advanced the wavefront reconstruction process proposed by Gabor in 1948. Their work made the present-day, high resolution, holograms possible (Leith and Upatnieks 1962, 1963, 1964). Powell and Stetson from the Michigan group, in 1965, introduced the technique of time averaged holography, an excellent technique for vibration analysis.

In 1966 at the Boston Acoustical Society meeting, Carl Stetson gave a paper on time average holography. It became clear that this method could be used to determine both absolute amplitudes and modes of vibrations of objects vibrating with amplitudes in excess of 10^{-5}cm.

We immediately recognized it as an important tool for the analysis of tympanic membrane vibrations,

and asked Stetson if we could have a setup made. In June, 1967, we started to use this setup to make holograms and time averaged holograms of vibrating earphone membranes that were relatively large. While the setup was quite satisfactory for the latter purpose, time averaged holography of the tympanic membrane turned out to be a difficult task, and two years elapsed before any results could be obtained from the tympanic membrane. During this period, every single part of the original setup was redesigned, and many additional parts were added. Some of the problems encountered and their solutions are presented in the following sections, along with some of the observations on the vibrations of the membrane and their analysis.

The theory of time averaged holography as proposed by Powell and Stetson is presented in Section B. Detailed analysis of their equations from a practical point of view is presented with numerical data.

The basic experimental arrangements, both optical and acoustical, are discussed in Section C.

Some of the mechano-acoustical vibration problems which spoiled the early attempts at vibration holography of the tympanic membrane are discussed in Section D.

The noise made by photographic shutters was causing undesirable motions of the tympanic membrane. Since silent shutters are not available commercially, we had to design our own. The principles used and the design and performance of such a shutter are shown in Section E.

The cat's tympanic membrane is transparent. In order to make a hologram, it had to be coated with a reflecting material. This material, however, should not affect the mechanical properties of the membrane. The search for a suitable material and an appropriate method of application is described in Section F.

The quality of holograms is dependent on a number of factors. Considerations, which led to the selection of laser power output, holographic plates, etc., are discussed in Section G.

Processing of holographic plates is described in Section H.

Experiments were carried out in fresh cadaver specimens of cats. Surgical procedures used for the exposure of the tympanic membrane are discussed in Section I.

A series of reconstructions of vibration holograms,

obtained at different intensities of a 600 Hz signal, and their interpretations are described in Section J.

Holographic reconstructions must be recorded for both analysis and publication purposes. Some of the problems associated with photography are discussed in Section K.

Calculations of malleus amplitudes and of the axis of rotation are given in Section L.

Detailed evidence is presented in Section M to show that the coat of powder applied to the tympanic membrane does not affect its vibratory properties, and that the results obtained from cadaver experiments compare well with those derived from other experiments performed on living animals.

Changes in the vibratory pattern of the tympanic membrane with frequency are presented in Section N along with an analysis of these data.

The discussion of Section O makes the point that the present data do not support the notion that the mode of vibration of the tympanic membrane is that of a hinged stiff plate. However, they are compatible with the proposal of Helmholtz, made more than one hundred years ago, that the mode of vibration obeys the

catenary principle. Further experiments will be performed at a later date to assess the magnitude of the force transformation by the mechanism of curved membranes.

B. PRINCIPLES OF TIME AVERAGED HOLOGRAPHY

1. Theory

The theory and technique of holographic vibration analysis was first described by Powell and Stetson (1965). According to Powell and Stetson, if the vibrations

$$\gamma = m(x_o,y_o) \cos [\omega t + \mu(x_o,y_o)] \qquad (1)$$

of an object are recorded in a hologram, the reconstructed image is described by

$$I(x_1,y_1) = J_o \left[\left(\frac{2\pi}{\lambda}\right) (\cos\theta_1 + \cos\theta_2)\, m(x_o,y_o) \right] \cdot I_{st}(x_1,y_1). \qquad (2)$$

In these equations,

γ = Instantaneous value of displacement;

$m(x_o,y_o)$ = Peak displacement of the object at point (x_o,y_o)

$\mu(x_o,y_o)$ = Phase angle of displacement at point (x_o,y_o);

ω = 2π Frequency;

t = Time;

$I(x_1,y_1)$ = Image point (x_1,y_1) corresponding to the object point (x_o,y_o);

$Ist(x_1,y_1)$ = Image point (x_1,y_1) corresponding to the object point (x_o,y_o) when the object is stationary;

λ = Wavelength of the laser light;

θ_1 = Angle between the axis of observation and the vector displacement;

θ_2 = Angle between the direction of propagation of the incident light and the vector displacement.

Furthermore in equation (2)

$$J_o\left[\left(\frac{2\pi}{\lambda}\right)(\cos\theta_1 + \cos\theta_2)\, m(x_o, y_o)\right] = J_o(P),$$

and represents a Bessel function.

The geometry of the situation is described in Figure 1.

When the object is not vibrating, ($\underline{m = o}$) and $\underline{J_o(P) = 1}$, and the classical Leith-Upatnieks hologram is obtained. The reconstructed image is three-dimensional and looks as if the real object were being directly observed. The properties of such holograms were first described by Leith and Upatnieks (Leith and Upatnieks, 1962, 1963, 1964).

When the object is vibrating, the stationary image $\underline{I_{st}(x_1, y_1)}$ is modulated by the function $\underline{J_o(P)}$, and a series of dark and bright fringes appear on the reconstructed image of the object. The number and spacings of these fringes is related to the function $\underline{J_o(P)}$ which in turn is related to the vibration amplitude of the object.

Both the shape and the absolute amplitude of vibrations could be deduced from the contour lines (dark and bright fringes) that connect points of equal-vibration amplitude.

An example of reconstruction from a time averaged hologram of a vibrating earphone membrane is shown in Figure 2.

In order to understand the nature of these fringes, it is important to study the properties of function $J_o(P)$. A plot of function $J_o(P)$ vs P is shown in Figure 3. When $P = 0, 3.8, 7.0$ --- etc., the function has maxima. When $P = 2.4, 5.5, 8.7$ --- etc., the function is zero. Thus, whenever the vibration amplitude $m(x_o,y_o)$ of a point (x_o,y_o) on the object is such that $P = 0, 3.8, 7.01$ --- etc., the corresponding image point (x_1,y_1) in the reconstruction will be bright. When the amplitude is such that $P = 2.4, 5.5, 8.7,$ --- etc., the image point will be dark. A dark fringe will therefore appear on the object passing through all points where $P = 2.4$. A similar fringe will appear connecting all points where $P = 5.5$. Dark and bright fringes, therefore, are contour lines of equal displacement of the object. They are directly

comparable to the contour lines of a geodesic map and permit assessment of the pattern of vibration of the object.

2. Absolute Amplitude of Vibration

The magnitude of vibration can be determined by

$$m(x_o, y_o) = \frac{P}{\left(\frac{2\pi}{\lambda}\right)(\cos\theta_1 + \cos\theta_2)}$$

if $\theta_1 = \theta_2 = 0$;

then $m(x_o, y_o) = \frac{\lambda P}{4\pi} = 5.03 \times 10^{-6} P$,

since $\lambda = 6.328 \times 10^{-5}$ cm for the helium-neon laser used in the present experiments.

The peak vibration amplitude corresponding to the 1st dark fringe ($P = 2.4$) is approximately 1.211×10^{-5}cm. This is the lowest amplitude of vibration that can be measured with this technique using a helium-neon laser. Vibration amplitudes corresponding to the first ten successive maxima and zeros are shown in Table I and Figure 4. The amplitude ratio between the first ten successive dark fringes (zeros) is given in Table II.

Between the first two dark dringes, the ratio is about seven dB, and it decreases with the fringe number. The ratio between the 9th and 10th zero is only 0.9dB.

If a linearly vibrating object is under study and the sound pressure has been adjusted so as to obtain one fringe on the surface, then an additional seven dB of pressure are required to obtain two fringes. To obtain three fringes, an additional pressure of four dB is required. It may be desirable to keep the total number of fringes below 10, as the clarity of the higher fringes is poorer.

The dynamic range of the technique is therefore from 1.2×10^{-5}cm to approximately 15×10^{-5}cm, a range of about twenty dB.

Any vibrations under study must have an amplitude in the above range in order that they may be analyzed clearly by time averaged holography.

When vibrations are induced by sound, the objects under study may be so stiff that the highest obtainable sound pressure is unable to produce vibrations as high as 10^{-5}cm. In such a case, time averaged holography is not a usable tool. If, on the other extreme, the object under study is too yielding, it may move about slowly, for example, under the effect of thermal air currents. Once again, in such a case, vibration holography is difficult. Only when the average position of the object, (i.e., its

resting position with no signal being applied) is stationary to within a fraction of a wavelength of the laser light during the time of exposure, can a good time averaged hologram be obtained.

3. Relative Light Intensity of the Fringes

The relative light intensity of the fringes, according to Brown, et al, 1969, is given by

$$I = [J_o(P)]^2 \qquad (4)$$

where I = Intensity of the fringe and $J_o(P)$ = zero order Bessel function as described above (Sect. B, 1). With the aid of a table of zero-order Bessel functions (Chemical Rubber Handbook, 1967), a plot of intensity as a function of P can be readily obtained; it is shown in Figure 5.

It is clear from Figure 5 that the intensity of successive bright fringes is not uniform. The first bright fringe is very intense (unity intensity), the intensity of the second bright fringe is only 16% of that of the first one, and the fifth about 5% of it. The fringe intensity, therefore, sharply decreases as the fringe number increases.

If $\theta_1 = \theta_2 = 0$ and $\lambda = 6.328 \times 10^{-5}$cm, then

$$P = \frac{4\pi}{\lambda} \, m(x_o, y_o) = \frac{m(x_o, y_o)}{5.03 \times 10^{-6}} ,$$

As already mentioned, the light intensity of the fringes can now be expressed in terms of vibration amplitude. The relationship between vibration amplitude and light intensity of the fringes is shown in Figure 6.

When the vibration amplitude is zero, i.e., the object is stationary, the intensity is maximum. The intensity drops sharply as the vibration amplitude approaches 10^{-5}cm. The intensity of all successive bright fringes is only a small fraction of the intensity of the object when it is stationary.

It has been suggested that the sharp drop in intensity following the first maximum (Figures 5 and 6) may be used to identify the stationary parts from the vibrating parts (Brown, et al, 1969).

The intensity of the bright fringes decreases rapidly as the vibration amplitude increases. This change reduces the contrast between the higher-order dark and bright fringes, i.e., the higher-order fringes become poorly defined.

This reduction in contrast of the higher-order fringes puts a practical limit to the maximum vibration amplitude that may be measured with the aid of this method.

4. Errors in Determination of Absolute Amplitudes

Calculated vibration amplitudes as a function of fringe numbers were shown in Table I. These calculations were based on the assumptions that $\theta_1 = \theta_2 = 0$, i.e., that the axis of vibrations, the direction of the incident beam, and the axis of observation coincided with one another. In practice, however, this is not the case. For example, different parts of the object may vibrate in different directions. Due to the finite size of the spatial filter and of the plate holder (cf. Figure 1; for details cf. Figure 11 later), angles θ_1 and θ_2 are usually larger than zero. Moreover, if the object is large, or if a large plate is used, θ_1 and θ_2 vary from point to point over the object and also over the plate.

When the shape of the object is irregular and the direction of vibration changes from point to point over the surface, determination of θ_1 and θ_2 for each point becomes impractical.

A rough estimate of the maximum values of θ_1 and θ_2 can usually be obtained. This estimate may be used to determine the magnitude of the error

introduced by not directly accounting for the angles θ_1 and θ_2.

The function $(\cos\theta_1 + \cos\theta_2)$ is shown in Figure 7. For fixed values of $(\theta_1 + \theta_2)$, i.e., 15^o, 30^o, and 60^o. The curves show that the error can be minimized when $\theta_1 = \theta_2$, i.e., when the direction of vibration lies exactly between the two beams. Angles as large as 30^o can be used with errors as low as 3% to 4%.

In our present setup $(\theta_1 + \theta_2)$, (i.e., the angle between the center of the object beam and the viewing axis through the center of the holographic plate; cf. Figure 1) was about 35^o. The error due to the angle between the incident beam and the reflected beam was about 4%.

5. Identification of Fringes

In order to determine absolute vibration amplitudes of any point on a given object, it is necessary to identify the particular fringe which passes through the point. The necessary procedure can best be illustrated with the aid of Figure 8. That figure shows the sequence of fringes that appear on the face of a hypothetical, clamped, circular, membrane vibrating in its fundamental mode. Consider

the amplitude of vibrations of a point at the center of the membrane. In Figure 8a, the amplitude is zero. When the center of the membrane is dark (first zero) the center is vibrating at an amplitude of 1.21×10^{-5}cm (Figure 8b).

In Figure 8c, the center is bright again (2nd maximum), and this corresponds to a vibration amplitude of 1.92×10^{-5}cm.

One method of identifying the fringe number is to count, in a sequence of holographic reconstructions taken at successively higher amplitudes, the number of times a given spot has become dark (zeros) and bright (maxima) again. Reference to Table I will then help to translate this information into absolute amplitudes.

The second method of identification is also demonstrated in Figure 8 (a-h). Since the edges of the membrane were assumed to be clamped, vibrations amplitude is always zero at the edges. The fringes in this case are formed at the center (at the point of maximum vibration) and move towards the edge with increasing amplitude. The highest fringe number is invariably located at the center (point of maximum vibration) and the lowest at the edge. To identify a particular fringe one simply has to count the

total number of fringes from the edge towards the center up to the fringe in question. The advantage of this second method is that a sequence of holograms is not required to identify a certain fringe number.

Examples of fringe identification with the aid of the latter method may also be seen in Figure 8 (a-h). A number of bright and dark fringes, with their numbers (M = maximum or bright; Z = zero or dark), and the absolute amplitudes at the center of the membrane are shown. Application of this method implies, however, that all vibrating parts of the membrane be visible. More often than not, this is not the case. When parts of the membrane are not visible, identification of fringes becomes a difficult problem. This situation is shown in Figure 9 (a-h). The membrane is identical to the one used in Figure 8 except that parts of it are not visible owing to the casing holding the membrane.

Vibration amplitudes of the membrane in Figures 8, a to h, are identical to those of corresponding numbers (a to h) of Figure 9.

Comparing the two sets of figures, it is clear that only a fraction of the total number of fringes is visible in most of the pictures of Figure 9. The

direct counting method, thus, gives a wrong identification of the fringes when only part of the vibrating surface is visible. In such cases, the direct counting method becomes unreliable, and one has to resort to a sequence of holograms taken at closely spaced amplitudes intervals.

The question may arise at this point as to the need for multiple fringes on the reconstructed surface of the vibrating object. The answer is that the vibratory pattern of an object is much easier determined when there are a number of fringes on the surface (5 to 10) as compared to only a few fringes (1-2). Also amplitude determination is more precise with higher fringe numbers. This will be dealt with in detail in the following section (Sect. b, 6).

At which intervals should signal amplitudes be spaced so that fringes may be followed from one reconstruction to the other without missing a count? Table II shows that, ideally, optimal spacing should vary with amplitude. The amplitude ratio between the second zero and the first one is 2.25:1 or 7.04 dB. The ratio between the third zero and the second one is only 1.56:1 or 3.86 dB.

This means that the signal may be increased by

7.04 dB from the level where the first zero is obtained to that where the second zero makes its appearance. An additional increase of 3.86 dB in signal will then produce the third zero. If the exact signal which yields the first zero is known, then the subsequent zeros can be easily traced by increasing signal amplitude according to Table II.

Normally, however, the signal levels required to obtain the first zero are not known or only approximately known. In such cases, holograms may be taken at uniform spacings of signal amplitude in decibels.

If the vibratory properties of the object under study are completely unknown, a series of holograms may first be taken at relatively large amplitude spacings of 10 or 20 dB. After the set was developed and viewed, a second set was made at narrower amplitude intervals (say 2 dB) over a limited range of amplitudes as determined from the first set. Generally, amplitude spacings of 2 dB were considered satisfactory for following individual fringes.

6. Accuracy of Amplitude Determination by Fringe Counting

It is clear from the plot of fringe intensity

vs vibration amplitude (Figure 6) that small increments in amplitude produce gradual changes in light intensity. The latter case is illustrated in Figure 10. As the vibration amplitude is gradually increased (Figure 10, a-d), the center of the vibrating membrane becomes gradually darker. Which one of these levels corresponds precisely to the first zero? If a series of holograms is taken at small amplitude intervals, this level is simple to determine. Inspection of the series of reconstructions of Fig. 10 indicates that the amplitude in Figure 10d is nearest to that of the first zero. In this case, the maximum error is approximately one-half the interval in dB between two successive pictures, *i.e.*, $\pm$ 1 dB in the present example.

If a series of reconstructions is not available, then it is only possible to conclude from inspection of any given reconstruction (say Figure 10c), that the amplitude is less than that corresponding to the first zero. Similarly, from inspection of Figure 10e, it is clear that the amplitude must be somewhere between those corresponding to the first zero and to the second maximum. The best estimate would be that the amplitude is the average of these two limits.

If amplitude is determined in this manner, the maximum error involved is shown in Table III. It shows the maximum percentage error as a function of the fringe number.

The error is fairly large (30%) when the first zero is used for amplitude determdination. It decreases rapidly with higher fringe numbers, being down to about 6% when the fifth zero is chosen for amplitude determination.

The precision of this determination improves as the fringe numbers increase. It is thus desirable to use higher-order fringes for greater precision in amplitude determination.

7. Effects of Noise and Harmonic Distortion

We must recall that a given fringe is the resultant of optical interference. Whether this interference is constructive (bright fringe) or destructive (dark fringe) depends upon the displacement amplitudes at that point of the surface as they relate to the wavelength of the laser light. Displacement amplitudes due to noise and/or harmonic distortion at any point must add vectorially to the amplitude due to the signal present at the same point. Such

additions may change the interference through any number of constructive or destructive cycles, i.e., fringe numbers. For example, a small amount of noise may convert a given bright fringe into the next higher or lower dark fringe.

When noise and/or distortion are present, the pattern over the entire surface is the resultant of these additions at all points. This means the clarity of the image due to the signal is being affected. The actual amount of noise and/or harmonic distortion that can be tolerated depends upon a number of complex factors and, thus, is usually determined emperically. However, one can arrive at a conservative estimate by setting a somewhat arbitrary limit, i.e., that the minimum amount of noise that will change the number of any fringe at more than a few points on the object will also disrupt the pattern.

The amplitude intervals between consecutive fringes change with their number. They become more closely spaced as the fringe number increases (cf. Table I). Therefore, a relatively small amount of noise and/or distortion must have a more deleterious effect upon higher-numbered fringes than upon lower-numbered ones.

To a first approximation, the estimate of the maximum percentage error in Table III also indicates the maximum tolerable distortion levels still permitting a clear resolution of the various fringes.

It is apparent from Table III that very low distortion of the sound signal is of prime importance. Low signal distortion at high sound intensities is always difficult to obtain.

8. Concluding Remarks

Time averaged holography, at the present time, is the only method permitting simultaneous assessment of vibration amplitudes at all points of a vibrating object. The vibrations, however, can only be measured when their amplitude exceeds a value of 1.2×10^{-5} cm. [Newer modifications of the technique (Metherall *et al*, 1969) permit an extension of the sensitivity by approximately one order of magnitude.] The interference process records the peak values of sinusoidial vibrating events; therefore, all results are read in terms of peak amplitude. The dynamic range of the method is limited by the resolution of higher order fringes. From a practical standpoint, a twenty

dB dynamic range appears to be realistic with respect to the vibrations of small objects.

The course of the iso-amplitude contour lines (fringes) and their spacings in various parts of the object indicate the prevailing vibration pattern.

The method is self-calibrating due to the extreme consistency of the wavelength of the laser light. The accuracy of measurement depends upon a number of factors. An accuracy of $\pm$ 1 dB can easily be realized. Successful application of the method requires a high purity of signals (freedom of distortion) and extreme mechanical stability of the object.

A final note: the method is not phase sensitive. Newer modifications, however, permit some assessment of phase (Metherell *et al.*, 1969).

C. EXPERIMENTAL ARRANGEMENT FOR TIME AVERAGED HOLOGRAPHY

Figure 11 shows the experimental arrangement used for time averaged holography in this laboratory.

A Spectra Physics, model 124, Helium-Neon cw laser with an output power of fifteen milliwatts was used as the source of light. The laser beam was reflected into an enclosed box by a front-surfaced mirror, through a small opening in the box. The laser itself was thermally isolated from the box.

The reflected beam passed through an opening in a specially designed silent shutter. This shutter could be operated electrically from outside the soundproof room and was used to turn the laser beam on and off. The construction and operation of this shutter are described in detail in Section E.

The beam was reflected once more by front-surfaced mirror 2 to change its direction and then split in two parts by a partially silvered mirror. The transmission of the beam splitter was about 90% and its reflection 10%.

The weaker beam was passed through a continuously variable optical attenuator (Jodon VBA 200), and a lens/pinhole arrangement, LP1 (20 x objective, 12μ pinhole), to form the reference beam.

The reference beam could be deflected in any direction by means of a front surfaced mirror which could be rotated in two planes. This reference mirror was set so that the central axis of the reference beam coincided with the center of the holographic plate.

Intensity of the reference beam could be adjusted by means of the variable optical attenuator.

The stronger of the two beams was deflected towards the object with the aid of front-surfaced mirror 3. The beam passed through a lens/pinhole arrangement, LP-2 (5 x objective, 25μpinhole), to form the object beam which illuminated the object.

Reflections from both the object and reference beams fell onto the holographic plate when the shutter was open.

A specially designed plate holder was used for the holographic plates. This holder has been described earlier (Tonndorf and Khanna, 1970). The key feature of this holder lies in the precision of relocating the plates to their original position on repeated trials. Replacement accuracy of a fraction of the wavelength of light is readily obtainable.

The relative position of the optical elements

was quite critical. The reference be . the object beam, the object, and the holographic plate were positioned with respect to each other so that (1) the angle between the object and the viewing axis was minimized, and so that (2) the angle between the object beam and the direction of vibrations was approximately equal to the angle between the direction of vibration and the viewing axis ($\theta_1 = \theta_2$; cf. Figure 1).

Sound was produced by a Jensen 100 watt driver located outside the box (see Figure 12) and brought in the box via a short length of garden hose terminated by the flared horn of a trumpet.

Sound pressure levels were monitored by means of a probe microphone located just at the edge of the tympanic membrane.

The orientation of the specimen was very critical. It had to be placed so that the anterior, posterior, and inferior portions of the tympanic membrane reflected equally well (i.e., appeared equally bright); at the same time the malleus had to be clearly visible. Failure to achieve such an orientation resulted in holographic reconstructions in which only parts of the tympanic membrane were visible.

This orientation was carried out by the use of multiple joints in the head-holder assembly which allowed rotation of the head in any of the three planes. The head holder-assembly was tightly locked, once the desired orientation had been obtained.

The intensity of the object beam was measured at the plane of the holographic plate. Then the intensity of the reference beam was measured and set one stop higher than that of the object beam by means of the optical attenuator.

The exposure time was set according to the reference beam intensity and the plate sensitivity (see later: Sect. G, 2).

The laser beam was cut off by means of the silent shutter. A photographic plate was loaded into the plate holder in the dark and the box enclosing the holographic setup closed. A two minute waiting period was allowed for equalization of temperature and settling of the air motions created by loading the plate. The sound signal was switched on at the desired level and an exposure taken with the aid of the shutter.

The plate was removed for processing. It was developed, fixed, washed, and dried. It was then returned to the plate holder and viewed through a long-focus, binocular, surgical microscope (Zeiss). The object beam was turned off during viewing.

D. MECHANICAL AND ACOUSTICAL ISOLATION OF THE HOLOGRAPHIC SETUP

1. General

While attempting to reconstruct high resolution, time averaged, holograms of vibrating circular plates (Tonndorf and Khanna, 1970), it became clear that a loss in resolution ensues if (a) any of the mirrors, pinholes, or the holographic plate are allowed to vibrate; (b) the reference-beam geometry is changed between exposure and reconstruction; and/or (c) the holographic plate is not returned for reconstruction to exactly the same location in which the original picture had been taken.

To minimize mechanical rocking of any optical component and accidental shifts in their position, all components were mounted on heavy bases (6 to 10 lbs. each). The bases were machined flat and bolted to an aluminum surface plate, two inches in thickness, which formed the top of the experimental table. Three bolts were used to tie down each base. The aluminum surface plate weighed approximately two hundred pounds and thus represents the main thermal inertia of the system.

Mechanical vibrations were minimized by the

fact that the aluminum surface plate had been bolted to a 500 pound granite block which in turn was suspended on a combination of rubber and spring isolation mounts (Figure 12). This combined system markedly attenuated the mechanical vibrations reaching the holographic setup for all frequencies above a few Hertz.

As already mentioned (Sect. C), a special holographic plate holder was designed to assure precise repeatability in the placement of holographic plates. Replacement accuracy was first checked mechanically by means of mechanical indicators up to their limits of 1/20,000 of an inch (5×10^{-4}cm). It was later verified with the aid of real-time holography, i.e., an interference was produced between a stationary object and its own reconstructed hologram. It was found that zero fringe patterns could be obtained every time the holographic plate was developed and returned to the holder. The replacement accuracy was thus better than a fraction of a wavelength of the laser light. In fact, the total system was so stable that the zero fringe pattern was maintained over periods of more than 24 hours (Tonndorf and Khanna, 1970).

In these earlier experiments, excellent vibration holograms had been obtained using the diaphragm of a magnetic earphone as the object. The resolution obtained was very good: up to 40 fringes could be counted with the aid of a microscope, on a diaphragm, 5 cm in diameter.

2. Special Problems Related to the Tympanic Membrane

The tympanic membrane (T.M.) has a very low stiffness compared to the metal plates on which vibration studies by means of holography had been made previously (Powell and Stetson, 1965; Tonndorf and Khanna, 1970).

This low stiffness of the T.M. led to several problems listed below along with their solutions.

(a) The T.M. is very sensitive to any acoustic signal. All spurious acoustic noises had thus to be eliminated in order to record responses to the desired signals. This problem was minimized by having located the entire holographic setup in an I.A.C. double walled, sound attenuating, room.

(b) Because of its low stiffness, minute air currents due to thermal gradients also cause the T.M.

to move. A successful high-resolution vibration hologram requires that the average position of the vibrating object be stationary within fractions of a wavelength of light during the time of exposure (cf Sect. G, 3). Movements of the T.M. due to air currents were therefore very undesirable. The air currents were somewhat reduced by the double walled, sound attenuating, room, except for the air circulating in its air ducts.

To minimize air currents around the holographic setup further, an air-tight box was constructed. This box, made of 1" thick pressboard, was provided with several airtight lids which gave access to the various holographic components inside (Figure 12). However, this box created two major acoustical problems: (i) Because of the reflection from the walls of the box, strong standing-wave patterns were set up, resulting in large variations of the SPL from point to point over small distances. These standing waves made measurements of SPL at the T.M. a difficult task. (ii) The box started to vibrate when the acoustical signal was turned on inside the box. These vibrations were transmitted to the holographic components mechanically, thereby spoiling

the holograms. Satisfactory holograms could only be made when a closed system was used delivering sound to the bulla tympanica. Whenever an open sound system was employed the time averaged holograms were found to be of very poor quality especially at frequencies above 2000 Hz.

These problems were minimized by (i) lining the box with lead to dampen the mechanical vibrations; (ii) lining the inside of the box with acoustic tiles to reduce reflections; and (iii) floating the box on a layer of soft putty so that the transmission of mechanical vibrations to the aluminum surface plate was minimized. Good time-averaged holograms using an open sound system were obtained after these steps had been taken.

(c) Temperature changes will cause the air volume in the middle ear to change, displacing the tympanic membrane. To avoid this occurrence, a thin capillary tube was cemented into the bulla wall for pressure equalization. The use of this tube has been discussed in detail in an earlier paper (Tonndorf and Khanna, 1968). The capillary was so chosen that it did not affect the acoustical properties of the ear in the region of interest.

E. SILENT SHUTTER

Shutters used in photography open and close with considerable noise. The response to this noise is recorded on the hologram in addition to that due to the applied signal, thus spoiling the vibration pattern due to the latter. (This was discussed in some detail in Section B, 7.) In order to eliminate this problem, a silent shutter was devised. The principle of operation of this shutter is described in Figure 13. A pendulum is held in one of its two extreme positions by electromagnets M_1 or M_2 respectively. By switching the current from one magnet to the other, the pendulum can be made to change position from one side to the other. A slit is attached to the pendulum in such a way that it allows light to pass through during part of the swing. The exposure time is dependent on the natural frequency of the pendulum as well as on the width of the slit. By changing both of these quantities simultaneously, a large range of exposure times can be obtained.

No sound is involved in releasing the pendulum. By the time it reaches the other side and is captured by the second electromagnet, the shutter is already

closed. No sound is therefore generated by the shutter before and during the exposure.

A compound pendulum shaped like a circular disc was used in the design of the shutter (Figure 14). The frequency of oscillation of such a pendulum is given by (Lindsay, 1933):

$$f_o = \frac{1}{2\pi} \quad \frac{2\,mg\ell}{r^2}$$

where,

f_o = frequency of oscillation in Hz;

m.g = weight of the disc;

r = radius of the disc;

ℓ = distance between center of mass and center of rotation.

The frequency of oscillations of the pendulum can be controlled by changing ℓ, the distance between the center of mass and the center of rotation. When $\ell = 0$, i.e., the pendulum is perfectly balanced, $f_o = 0$. As the pendulum is unbalanced the frequency increases.

The lowest useful frequency is determined by the friction of the bearings. As the pendulum is adjusted towards its balanced condition, the force available to drive the pendulum gradually decreases until it is so small that it cannot overcome the

friction in the bearings. The lesser the friction, the lower may be the frequency at which the pendulum will still oscillate reliably.

To reduce friction to a minimum, jewel pivot bearings were used for suspending the pendulum.

Figure 15 shows some of the components of the shutter. Two discs, A & B, constitute the pendulum as well as the slit. The slit is adjusted by rotating the two discs symmetrically with the aid of thumb screw K. The discs are attached to a small pendulum I, acting as the pole piece for the magnets. The pendulum is fastened to shaft P. The two discs, A and B, and the pendulum rotate together. When the pole piece I is held by either electromagnet M_1 or M_2, the slit is off the vertical and the beam is cut off. To actuate the shutter the current is switched to the other electromagnet, the pendulum swings to the other side, and is caught by the newly energized electromagnet. This sequence of events is shown in Figure 16.

The exposure time is adjusted by rotating plates A and B. This changes (1) the width of the slit and (2) the location of the center of mass. The plates are shaped in such a way that when the slit is wide open

the pendulum is almost perfectly balanced. The wide slit together with the low velocity of the pendulum gives a long exposure time (approximately 1 second). When the slit is closed, the center of mass moves down increasing the velocity by a factor of five. A narrow slit together with a high velocity of the pendulum, gives shorter exposure times (approximately 1/100th second). Figure 17 shows the relationship between slit width and exposure time.

F. COATING THE TYMPANIC MEMBRANE

The cat's T.M. is almost transparent. In order to obtain a hologram, the T.M. must be made to reflect laser light. The T.M. must be coated with a material that has to satisfy several requirements.

(1) Effects of Coating upon the T.M.

The material should not alter the vibration characteristics of the T.M.

(a) It should not be toxic: Toxic material may cause severe damage to the T.M. such as drying (and subsequent tearing) edema, or chemical alterations of the fibers of T.M. Each of these changes will affect the vibratory characteristics of the T.M.

(b) It should not stiffen the T.M.: If the coating layer is too thick or too stiff compared to the properties of the T.M., one would be observing the properties of the coat rather than those of the T.M.

(c) It should not mechanically load the T.M., i.e., the total mass of the coating should be small.

(2) Reflectivity

The material should have good reflectivity:

(a) The T.M. is a very small object. If reflectivity is poor the total amount of light reflected from it will be very small, and long exposure times will be needed to make a hologram. Long exposure times put severe stability requirements on the T.M.

(b) Poor reflectivity also means greater absorption of laser light over longer periods of exposure, thus heating up the T.M. and the air within the middle-ear cavity. This in turn means expansion of air and movement of the T.M.

(3) Uniformity of Coat

The material should form a thin uniform coat.

(a) It was found in preliminary experiments that the maximum resolution available from a hologram is closely related to the surface texture of the object. When the coat contained particles of 50-100μ in size, the resolution was very poor. As the size of the particles was reduced in steps down to 1μ , the resolution continued to improve. For technical reasons, it was not possible to reduce particle size to less than 1μ .

(b) A uniform coat is essential for avoiding intensity variations over the surface. The pattern of such variations will invariably be superimposed upon the recorded fringe pattern. Such occurrence must be avoided.

(4) Coating Materials

The problem of finding a suitable coating material and a suitable coating method took considerable time and effort. A large variety of materials and solvents were tested. Some of the materials tested are listed in the following:

(a) Powders: Several white powders including talc were used. The powder was deposited on the T.M. by using a powder blower, rendering the T.M. semi-transparent. Deposits were coarse and lumpy due to the stickiness of the particles. The reflection was totally insufficient for holographic purposes.

(b) Water colors: Water colors and poster colors were tried. White color was used because of its good reflectivity. Thick coats of poster color gave satisfactory opaque coatings. However, the thick layer required rendered the T.M. too stiff. Another

problem with such coats was posed by the natural wax coat of the T.M. which caused the coating material to collect in patches, unless the wax was first dissolved. The solvents, more often than not, proved to be toxic for the T.M.

(c) Oil colors: Quick drying paints produced uniform coatings with good reflection. However the coats were too stiff and the paint solvents were generally too toxic for the T.M.

(d) Inks: India inks and other printing inks were experimented with. Unsatisfactory semi-transparent coatings were obtained with white India inks.

A red printing ink ("red lexographic ink"), especially made for us by the Borden Chemical Co., was tried. The maximum reflectance of this ink was near the red laser wavelength. This ink produced very uniform opaque coatings on the T.M., and excellent light reflection was obtained. With its aid, the first good time averaged holograms of the T.M. were obtained which were in fairly good agreement with later observations. Unfortunately, the solvents of the ink and its drying agents were found to be toxic to the T.M.

(e) Stains: Several tissue dyes were tried. Dyes are absorbed by the tissues and produce uniform staining without affecting the surface. Eosin, Congo red, and Ponceau red were used among others. However, as the membrane remained semi-transparent, the stain was only helpful with regard to visual observations, but totally unsatisfactory for holography.

Relatively speaking, the best staining results were obtained with Ponceau red dissolved in a mixture of glycerol and water. The stain was quite intense, but still insufficient for holographic purposes.

(f) Metallic powders: Metallic powders held promise from the very beginning because of their excellent reflectivity. The main problem was to find a suitable way of dispensing these materials so that a thin uniform coat could be obtained. When bronze powder was used suspended in a liquid (alcohol, benzene, chloroform), the particles tended to lump together during the drying process, and nonuniform coats were obtained.

A thin solution of rubber cement in benzene was used to suspend the bronze particles - this worked very well for a time. The benzene evaporated quickly leaving behind a very thin layer of rubber cement with the bronze particles embedded. The particle size being used at this time was 44 microns.

A number of time averaged holograms were obtained at this stage. Two problems were associated with such paints. (i) The rubber-cement layer would not always stick to the T.M., and on several occasions we found ourselves measuring the vibration characteristics of the detached rubber membrane. (ii) Vibrations of only one portion of the tympanic membrane (i.e., anterior, posterior, or inferior) could be studied at any one time depending on which part of the surface was adjusted so as to give maximum reflection. The remaining parts of the membrane appeared dark. We learned later that this problem was being caused by the large particles suspended in this paint. They caused the spatial frequency content of the scene to exceed the resolution limits of the holographic plates.

Next, bronze powder with a particle size of four microns was used, still suspended in

benzene/rubber-cement solutions. This improved the resolution to a considerable degree - at the same time, vibrations of the anterior, posterior, as well as the inferior parts of the eardrum could be discerned simultaneously in a single reconstruction.

With a view to help us improve the resolution further, the Atlantic Powdered Metals, Inc. specially ground for us, in their laboratories, bronze powder with 1 micron particle size. After receipt of this material, we realized that the benzene/rubber solutions could be dispensed with all together. The particle size had become so small that the cement was no longer needed. However, attempts to produce a uniform coat by dispensing dry powder were not successful.

Liquids with very low surface tension were required to suspend the particles because of their small size. Ether was found most suitable for several reasons. It evaporated rapidly leaving behind a very uniform coat adhering directly to the T.M. and consisting of nothing but a thin layer of bronze powder. There was no binding material anymore that might become stiff, detach itself from the T.M. to form a separate layer, or be toxic to the T.M. Furthermore,

the rapid evaporation of ether in the container automatically kept the bronze particles stirred up well, and suspensions remained uniform while being sprayed. All studies of the vibrations of the T.M. reported here were carried out by using the 1μ particles of bronze powder suspended in ether for coating the T.M.

(5) Air Brush

In earlier phases of the study, paints were applied to the T.M. with the aid of a fine brush. It soon became apparent that, even with the smallest brush, too much paint was being dispensed; moreover, a very uneven coat was being obtained. This resulted in holograms of rather poor resolution. In order to improve the quality of coating, an air brush was employed. This device, used by artists, is shown in Figure 18. It is essentially a miniature spray gun. The material to be sprayed is filled in the paint cup. The air inlet is connected to a source of high pressure air (8-10 lbs/sq in). The air gun is about the same size as a writing pen and is used in a similar manner. The amount of material sprayed is controlled by the control knob, giving a uniform and thin coat.

(6) Evaluation of Coats

To evaluate the quality of coats employed throughout this series, the T.M. was illuminated with laser light and examined through a Zeiss operating microscope. It was seen that, whenever the T.M. was well defined and its surface features clearly visible, a good hologram could be obtained.

After a promising coat was found, it was necessary to investigate its effects upon the vibration characteristics of the T.M. Two sets of time averaged holograms were made: (a) with only the malleus coated and, (b) with both malleus and tympanic membrane coated. Both sets of holograms were made at identical frequencies and sound pressure levels. Fringes on the malleus were compared between the two sets to check if the coating of the T.M. had altered the amplitude of malleus vibrations. Up to 4000 Hz, the differences found were within the experimental error. This point will be discussed once more in greater detail in Sect. M.

G. FACTORS AFFECTING THE QUALITY OF TIME AVERAGED HOLOGRAMS

In normal photography, the brightness of the scene, film speed, shutter speed, and the lens opening are all interrelated. Increases in brightness or film speed permit the use of shorter exposure times. A faster film, however, has generally a lower resolving power. In normal photography, the resolution is rarely limited by the film, and movements of the object being photographed seldom present a serious problem.

In holography, similar considerations apply. Brightness of the scene, film speed, and shutter speed are interrelated factors. The film resolution and the movements of the object, however, limit the quality of the hologram. Unlike photography, the spatial frequency components being recorded on a hologram often exceed the film resolution. As already mentioned (Sect. D), the stability requirements for the object are also critical in holography. Object movements must be limited to a small fraction of a wavelength during the time of exposure in order to make a successful hologram.

Some of the factors which influence the quality of a hologram are listed below.

1. Intensity of illumination;
2. Stability of the object;
3. Resolution of the holographic plates;
4. Relative intensities of object and reference beams;
5. Exposure time.

In the following, these factors will be discussed in order and in some detail.

1. Intensity of Illumination

Increases in light intensity decrease the exposure time and relax the stability requirements. However, higher intensities also increase the temperature of the object under study, thus introducing thermal instability. A coat that minimizes heat absorption helps to reduce this effect. In an earlier series of the present experiments, a Perkin Elmer, one milliwatt, cw laser was used. This was found to be too low a power, requiring exposure times that were much too long (40 seconds). Furthermore, when viewing the finished hologram under magnification the light

intensity was insufficient for clear observation.

A 15 milliwatt, Spectra Physics, model 124, cw gas laser was employed in all experiments upon which this report is based. The use of this laser resulted in a reduction of the exposure time by a factor of fifteen.

The object beam was utilized more efficiently by employing separate lens-pinhole arrangement (cf. Figure 11). This spatial filter was so located that the object beam just filled the area of the T.M., concentrating the total amount of light on the object.

2. Stability of the Object

For general holography, movements of the object should be less than $\lambda/5$, or approximately 10^{-5} cm, during the time of exposure. For perfect imaging, the tolerance may be even smaller, $\lambda/15$, according to Brown et al. (1969).

For time averaged holography, the tolerances are still smaller. For example, movements on the order of 0.8×10^{-5}cm will completely wipe out the 10th fringe recorded on the hologram (see Table I and Sect. B, 7). Stability of at least

$\lambda/80$, or 0.88×10^{-6} cm, during the time of exposure is essential for a good quality, time averaged, hologram. Details of the steps taken to achieve this order of stability were given above in Section D.

3. Resolution of the Holographic Plates

According to Leith, Upatnieks, Hildebrand, and Haines (1965), the plate resolution requirements for holography are set by both the field and the object. Diffusely scattering objects often contain spatial frequencies on the order of 1000 lines/mm.

In the present case, the object is rather small compared to the size of the holographic plate. The field requirement, therefore, is less important than the object requirement. The bandwidth requirements were minimized by the following steps: (a) reducing the angle of separation in the spatial carrier method of Leith and Upatnieks (cf. Leith & Upatnieks, 1962); (b) locating the point of origin of the reference bean near the object plane; (c) coating the object to reduce the resolution requirement. (The coating technique was discussed at some length above in Section F.)

Kokak 649F high resolution plates were used in the earlier phases of the present experiments. The resolution of these plates is excellent, about 4000 lines/mm. These plates, however, turned out to be too slow for the present purpose. Agfa-Gevaert 10E70 plates were used in all the experiments upon which this report is based. These plates, although having a resolution of only 2000 lines/mm, are about twenty times faster than the Kodak 649F plates. The combination of the 15 milliwatt laser and the Agfa plates reduced the exposure time to about 1/15th sec. This made time averaged holography of the tympanic membrane a reality.

4. Relative Intensities of Object and Reference Beams

According to Leith and Upatnieks (1967), ratios from 10:1 to 2:1 between the intensities of the reference beam and of the object beam are satisfactory in general holography.

A series of time averaged holograms was made from the same vibrating object (i.e., the T.M.). The object beam intensity was measured with a Luna-Pro exposure meter. The reference beam intensity was then adjusted with the aid of the continuously variable

optical attenuator (cf. Figure 11). A ratio of 2:1 gave best time averaged holograms. This ratio was maintained in all subsequent holographic experiments.

5. Exposure Time

The optimum exposure time was determined experimentally in a series in which the exposure was varied and the quality of the resultant holograms judged. A time of 1/15th second was found best and maintained in all subsequent experiments.

H. PROCESSING OF PLATES

All chemical solutions, as well as the water used for washing the plates, were maintained at room temperature. The holographic plates were developed in complete darkness for four min in Kodak H.R.P. developer, briefly rinsed in tap water, and fixed in Kodak Rapid Fix for five min. Thereafter, the plates were washed in running tap water for fifteen min, drained, and then bathed in 95% alcohol for three min. About ten to fifteen minutes drying time was needed before the plates could be used for reconstruction.

A time of about forty to forty-five minutes elapsed between exposing a holographic plate and viewing it. Because of this long delay, it is impractical to process each hologram and view it for the determination of signal parameters for the following hologram. It is much more economical in time to expose a batch of plates at different frequencies and intensities and then look at them together to select the desired range.

In our original setup, only two plates could be processed at the same time. This was found to be too cumbersome and too time consuming - it took

eighteen hours to process a set of fifty plates. The arrangement was then changed so that sixteen plates could be processed simultaneously, drastically reducing the processing time. Eighty holograms could now be easily processed during the course of one morning (three hours).

The only problem in processing that many plates at the same time is to maintain exact identification of individual plates. This problem was solved by numbering the plate developing hangers (Kodak) individually and loading the exposed plates in a predetermined sequential order.

I. SURGICAL EXPOSURE OF THE TYMPANIC MEMBRANE

Healthy young cats weighing 2.0 to 2.5 kg, were used in the present experiments.

A combination of chlorpromazine and nembutal was used for anesthesia. (14mg/kg wt and 22mg/kg wt respectively.) To achieve high mechanical stability, a head holder described earlier was employed (Tonndorf and Khanna, 1968). The skull was screwed tightly to a thick brass plate at three points. The brass plate somewhat conformed to the shape of the skull. The head was fastened in the holographic setup by means of a steel rod welded to the brass plate. Compound joints in the head-holder assembly allowed rotation and movement of the head along three axes.

After surgical removal of the pinna, the posterior third of the zygomatic arch and the entire ascending part of the lower jaw were resected. This was done in order to give wide exposure of the T.M. area from anteriorly.

While the soft tissues of the ear canal were kept intact, the bony ear canal was removed as far as possible with the aid of a dental drill until the skin and periostial lining became very thin. This was done to avoid bone dust falling on the T.M.,

which is easily lacerated when being cleaned. Moreover, some of the finer dust particles cannot be cleaned away, which causes loss of resolution in the holograms due to the rough texture of the surface. Usually, only a few overhanging areas had to be thinned down after removal of the soft tissues. These overhangs cast shadows and thus obscure the vibration patterns in some areas. Normally, due to the shape of the residual bony overhang around the rim of the T.M., small parts of the inferior and posterior areas of the membrane remained obscured.

To keep the pressure in the middle ear equalized, a capillary tube was cemented into the bulla. Earlier experiments had shown that this tube did not affect the response of the middle ear in the frequency region of interest (Tonndorf and Khanna, 1968).

At this point, the animal was sacrificed using an intercardiac injection of 5.00 cc of a 10% nembutal solution.

The T.M. was coated as described in Section F.

The animal's head was removed and fastened in the holographic setup with the aid of the head-holder

assembly. First holograms were taken within thirty minutes of sacrificing an animal and continued to be taken for as long as six hours thereafter.

J. VIBRATION PATTERN OF THE TYMPANIC MEMBRANE OF A CAT AT 600 Hz

A series of time averaged holograms of a cat's left T.M. is given in Figures 19 (A to N). Each hologram was taken at a SPL 2 dB higher than that of the preceeding one. The first hologram (A) was taken at 89 dB SPL, while the last one (L) was taken at 115 dB SPL.

Evidently, below 89 dB SPL the vibrations of the T.M. are smaller than 10^{-5} cm and as such do not show up on the holographic reconstructions, i.e., the entire surface looks brightly illuminated. As the sound pressure is increased, those parts of the membrane which vibrate most show up first.

In Figure 19 A, the first dark fringe appears in the posterior part of the T.M. indicating that the vibration amplitude of this part is approaching 1.2×10^{-5} cm, but also that this part of the membrane vibrates more than any other part.

A two dB increase in SPL (Figure 19 B) further darkens the posterior fringe. Since additional increases in SPL (Figure 19 C) introduce a bright fringe in the center of the first dark fringe, it is clear that in Figure 19 B the posterior part of

the tympanic membrane had reached an amplitude of 1.2×10^{-5} cm.

The appearance of a bright fringe in Figures 19 C and D shows that the posterior part of the T.M. has reached the 2nd maximum (1.85×10^{-5}cm). The outline of the 1st zero fringe gives a good idea of the shape of the vibration pattern in the posterior part of the tympanic membrane. Figure 19 E shows that at 97 dB SPL the posterior part has reached a vibration amplitude corresponding to the 2nd zero, or 2.8×10^{-5}cm; the anterior part is just reaching an amplitude corresponding to the first zero, or 1.21×10^{-5}cm.

At 99 dB SPL, (Figure 19 F) the posterior part has reached an amplitude corresponding to the 3rd bright fringe, while in the anterior part the 2nd bright fringe has appeared. The first dark fringe has just crossed the tip of the malleus indicating that its vibration amplitude has a value of 1.21×10^{-5}cm.

In Figure 19 G, both posterior and anterior parts have acquired one additional fringe, and the first dark fringe has moved half-way up the malleus

indicating that now the center of the malleus is vibrating with an amplitude of 1.21×10^{-5}cm.

Figures 19 (H, I, J, K,) show the effect of further increases in SPL over a total range of 8 dB. In Figure 19 I, the second dark fringe is reaching the tip of the malleus. If a series of holograms were not taken, it would be hard, if not impossible, to tell if this was the first fringe as in Figure 19 F, or, indeed, the 2nd fringe. In the posterior quadrant, the first dark fringe is now hidden under the rim, and it is only possible to correctly identify all fringes by following them through successive pictures.

At still higher sound pressure levels, (Figures 19 L, M, N,) the number of fringes simultaneously present on the malleus increases to two and eventually to three. In Figure 19 L, the second and third fringes are seen in various positions along the malleus, and in Figure 19 M, the second, third, and fourth fringes appear simultaneously along the malleus representing the vibration amplitudes of different parts of this structure. The simultaneous presence of two or more fringes along the malleus at higher sound pressure levels can be used to advantage in calculating the dynamic point of rotation of the malleus. This

calculation is described in a later section, (sect. L.).

As was mentioned in sect. B-7, noise and distortion produce a low contrast between higher order fringes, such effects begin to show up in Figure 19 N, where the fringes in the posterior quadrant appear very fuzzy.

A simplified line drawing of Figure 19 L is shown in Figure 20. The numbers identify the dark fringes on the surface of the T.M. and on the malleus. From Figure 20, the vibratory pattern of the T.M. can be readily deduced. The posterior quadrant vibrates approximately in the shape of a slice of an orange with the maximum located in the posterior superior part of the T.M. The anterior quadrant vibrates approximately in the shape of a spoon with the handle located inferiorly. However, both patterns are connected together inferiorly.

Because of the difference in their respective amplitudes of vibration, those of the posterior and anterior quadrant and of the malleus are best determined from different holograms. For example, while Figures 19 I and J are well suited for determination of posterior amplitudes, they are not well suited for

determination of anterior amplitudes which are better shown in Figures 19 K or L.

Malleus amplitude is easiest to determine at a SPL, at which a fringe is just touching the tip of the malleus, (e.g., Figures 19 E, I, K).

Malleus amplitude can also be determined from any hologram with the fringes being located anywhere along the malleus. This method of calculation is shown in a later section, (sect. L). This method, however, is complicated by the fact that is requires knowledge of the length and the axis of rotation of the malleus.

Table IV shows amplitude ratios in dB between any two of the first five bright or dark fringes. For example, the ratio between the 4th bright fringe (top row) and the 5th dark fringe (left column) is 3.29 dB. Such information is useful in either of two situations; (1) when one is looking at a hologram shot for trial purposes and wants to determine what the correct amplitude range should be in which further holograms are to be taken; (2) when one is comparing two holograms taken at a known intensity interval and wishes to identify fringe numbers.

It is seen from Figure 19 that fringes, whenever

present on the malleus, are not perpendicular to the mallar axis. Invariably, they form at an angle of approximately 30^{o} to that axis.

In Appendix 1, it will be shown by simple analysis that isodisplacement contours on a flat rectangular plate, vibrating along two mutually perpendicular axes, are formed parallel to their resultant axis. The axis of rotation and the fringes formed on the malleus of a cat are shown in Figure 21. This figure shows the anatomical basis for the fringe tilt observed in the holographic experiments. (Further evidence for the location and course of the axis of rotation will be presented in sect. L.)

It is clear from the above series of photographs (Fig. 19) that, because amplitudes of vibration in the anterior and posterior parts of the tympanic membrane and along the malleus are not equal, sound pressure levels best suited for observing fringes on each part are not the same. It is therefore necessary to take a series of holograms at different amplitudes of each of the frequencies under investigation.

Table V lists the frequencies and the range of SPL's used at each frequency for four animals. In each

case, holograms were recorded in two dB steps between the minimum and the maximum sound pressure levels indicated. Only some selected holograms from this set will be shown in the following sections.

K. PHOTOGRAPHY OF HOLOGRAPHIC RECONSTRUCTIONS

Reconstructions of time averaged holograms obtained in the present T.M. experiments are of excellent quality. Fifteen or more fringes may be counted on the posterior surface of the T.M. when the particular reconstruction is viewed directly through a good quality microscope. However, most of the details that can be observed in the original are lost in the photographic copying process.

In fact, photography of these reconstructions turned out to be a major problem which required redesigning a camera and part of the holographic assembly. Without going into all the details, some of the important points will be discussed in the following:

(1) A holographic reconstruction represents a three-dimensional image and is optically identical to the original object. On the other hand, a photograph is a two-dimensional image. Only one view may be recorded; moreover depth information is completely lost. This is the first cause of the loss in pictorial detail.

(2) Due to the limited depth of focus of the camera, not all parts of the object can be perfectly

focused at the same time. Definition of some parts is therefore reduced.

(3) Since the object size is very small, magnification of the image is mandatory to facilitate studying and analyzing the photographs. It is not practical to enlarge the photographic prints because of the characteristic speckled background of holographic images. (This speckled pattern is caused by the monochromatic laser light.) Direct enlargement (in which the first photographic image is made as large as possible) is preferred because the size of the speckles is then independent of the magnification. This need for magnification puts severe requirements on camera optics and depth of focus.

(4) The need for an enlarged image, together with the fact that the original illumination of the object had a fairly low intensity, results in a weak image on the camera screen. Often, the image was so dim that focusing became virtually impossible. Every effort was made to increase the intensity of this image. (a) The optical attenuator in the reference beam path (cf. Fig. 11) was turned up so that the reference beam intensity was at its maximum.

(b) A special assembly was designed for the beam splitter (cf. Fig. 11) so that, during reconstructions, the partially silvered mirror (10% reflection) could be replaced by a front surface mirror, increasing the reference beam intensity by a factor of 10. The requirements in this interchange of mirrors were such that the geometry of the reference beam had to be maintained exactly in the two cases, i.e., the two mirror surfaces had to be parallel to each other and in the same plane, to an accuracy of one millionth of an inch. (This was done to maintain the exact geometry of the reference beam.)

(5) Additional problems arose from the fact that the intensity of the reconstructions depends strongly on the number of fringes recorded on the T.M. Since an exposure meter could not be employed, a tiral and error method had to be used to obtain correct exposures. Furthermore, the exposures were very critical. One-half stop adjustments were needed in many cases.

These changes in technique resulted in a substantial improvement in picture quality. Yet most photographs are rather poor in quality as compared to the direct

viewing of holographic reconstructions. In fact, many of them cannot be reproduced by means of conventional photographic techniques. Contrast enhancement is currently being tried with some success to improve the contrast in pictures for use in publications.

L. CALCULATION OF MALLAR AMPLITUDE AND AXIS OF ROTATION

As shown in Section J, the mallar amplitude is easily determined when a fringe just touches the tip of the malleus. It is more difficult to determine the amplitude at the tip when fringes are located somewhere else along the manubrium.

Vibration amplitudes of points along the malleus are proportional to their perpendicular distances from the axis of rotation. If the amplitude at any point R along the malleus is known, the amplitude at the tip is given by: amplitude at point R x perpendicular distance of the tip from the axis of rotation/perpendicular distance of point R from the axis of rotation (Figure 22).

In the holographic reconstructions of the T.M. shown in Sections J and N, only part of the malleus is visible (up to the short process). The axis of rotation of the malleus is not exposed.

The geometry involved in mallar vibrations around its axis of rotation, xy, is shown in some detail in Figure 22.

Both the location of the axis xy and its angle with respect to the malleus must be known before the

lengths ℓ_x, ℓ_y, and ℓ_n can be determined.

When a fringe n appears at a distance ℓn from line OP through the short process and parallel to the axis of rotation (cf. Figure 22A), vibration amplitude at the tip of the malleus may be calculated with the aid of Figure 22B.

$$D = A_n \frac{(\ell_y + \ell_x)}{\ell_n + \ell_x} \qquad (6)$$

where

D = vibration amplitude of the tip of the malleus;

A_n = vibration amplitude corresponding to nth fringe number;

ℓ_x = perpendicular distance from the short process to the axis of rotation;

$\ell_x + \ell_y$ = perpendicular distance from the tip of the malleus to the axis of rotation;

ℓ_n = perpendicular distance from the axis of the nth fringe to the short process.

1. Determination of the Axis of Rotation

It was shown above that in order to calculate the mallar amplitude the location of the axis along, and its angle with, the malleus must be determined.

(a) Angle between the axis of rotation and the malleus: It is shown in Appendix (i) that the lines of equal displacement amplitude on the surface of a rectangular vibrating plate are in a direction parallel to the axis of rotation.

In Appendix (ii), it is shown that slightly curved surface (like that of the malleus) may be approximated by a flat plate. We may therefore conclude that the direction of fringes on the malleus is parallel to its axis of rotation.

(b) Position of the axis: If two or more fringes appear simultaneously on the malleus, it is relatively simple to calculate the perpendicular distance $\underline{\ell_x}$ from the short process to the axis of rotation.

The geometry describing this situation is shown in Figure 23. Sine equation (6) is valid for either of the fringes $\underline{m}$ or $\underline{n}$, we have:

$$D = A_m \quad \frac{(\ell_y + \ell_x)}{\ell_m + \ell_x} \quad , \tag{7}$$

and

$$D = A_n \quad \frac{(\ell_y + \ell_x)}{\ell_n + \ell_x} \quad , \tag{8}$$

where

A_m = vibration amplitude corresponding to the mth fringe;

A_n = vibration amplitude corresponding to the nth fringe;

ℓ_m = perpendicular distance between the line representing fringe m and the short process;

ℓ_n = perpendicular distance between the line representing fringe n and the short process.

Dividing equation (7) by equation (8) we have:

$$1 = \frac{A_n}{A_m} \frac{(\ell_m + \ell_x)}{\ell_n + \ell_x} , \qquad (9)$$

or

$$\ell_x = \frac{(A_n \ell_m - A_m \ell_n)}{A_m - A_n} . \qquad (10)$$

Since all parameters on the right-hand side of equation (10) can be easily determined from a holographic reconstruction such as Figure 19N in Section J, the value of ℓ_x can be calculated.

It must be emphasized here that, since the values ℓ_m and ℓ_n are obtained from a relative value

which applies only to that particular photograph. In order to obtain absolute values of length suitable scaling must be employed.

The following is an example of the application of equation (10): From an enlargement of Figure 19N, the following measurements were obtained:

ℓ_y = 1.25cm;

ℓ_5 = 1.10cm;

ℓ_4 = 0.75 cm;

ℓ_3 = 0.42cm;

A_5 = 7.52×10^{-5}cm;

A_4 = 5.94×10^{-5}cm;

A_3 = 4.36×10^{-5}cm.

Using the data for the 4th and the 5th fringe and substituting the pertinent values in equation (10) we have

$$\ell_x = \frac{5.94\times10^{-5}\times1.10 - 7.52.10^{-5}\times0.75}{7.52\times10^{-5} - 5.9\times10^{-5}} = 0.554\text{cm}.$$

Similarly using the data for the 3rd and 4th fringe we have

$$\ell_x = \frac{4.36\times10^{-5}\times0.75 - 5.94\times10^{-5}\times0.42}{5.94\times10^{-5} - 4.36\times10^{-5}} = 0.487\text{cm}.$$

The average value of ℓ_x = 0.52cm.

and $\ell_y / \ell_x = \frac{1.25}{0.52} = 2.4$.

(c) Anatomical measurements - The calculated results shown above can be cross-checked by anatomical measurements on the malleus. These measurements are based upon the description of the rotational axis of the major ossicles, by Barany, i.e., that the axis runs from the anterior mallar ligament to the posterior incudal ligament. For such measurements, the exposure made originally (cf. Section I) was simply extended by opening the lateral wall of the attic so that the head of the malleus and the body of the incus were completely exposed -- It might be mentioned in passing that the conclusions underlying Figure 21 were reached from inspection of such a preparation.

Measurements were made on such specimens with the aid of a calibrated binocular microscope. P the distance between the rotational axis and the short process and Q the distance between the short process and the tip of the malleus were measured (cf. Figure 24).

1st specimen Q = .575 cm

P = .24cm

2nd specimen Q = .52cm

P = .22cm

Avg. value of Q = 0.55cm

Avg. value of P = 0.23cm

It can be seen from Figure 24 that

$$\ell_y / \ell_x \approx \frac{Q}{P} = \frac{0.55}{0.23} = 2.5.$$

This figure compares very well with the ratio obtained from the dynamic measurements, and indicates that indeed the axis of rotation is a line running from the anterior mallar process to the posterior incudal ligament, as Barany had found in 1938.

2. Calculation of Mallar Amplitude

Using the data from Figure 19N, which were tabulated in Section L,1,b., and substituting them in equation (6), we obtain the amplitude D at the tip of the malleus.

From the 5th fringe

$$D = 7.52 \times 10^{-5} \cdot \frac{(1.25 + 0.52)}{(1.10 + 0.52)} = 8.2 \times 10^{-5} \text{cm};$$

From the 4th fringe

$$D = 5.94\times10^{-5} \cdot \frac{(1.25 + 0.52)}{(0.57 + 0.52)} = 8.3\times10^{-5}\text{cm};$$

From the 3rd fringe

$$D = 4.36\times10^{-5} \cdot \frac{(1.25 + 0.52)}{(0.42 + 0.52)} = 8.2\times10^{-5}\text{cm}.$$

There is close agreement between the values of mallar displacement calculated from three sets of fringes. Since the fringes are located on different parts of the malleus, this agreement indicates that the malleus vibrates as a stiff beam and there is no measurable bending along its length (within the accuracy of our measurements, approximately 1%).

M. VALIDITY OF EXPERIMENTAL RESULTS

1. Physical Effects of the Powder Coat

An objection may be raised that the coating of the T.M. may have altered its physical properties.

The effect of the powder coat on the properties of the T.M. was investigated in a series of experiments. Consecutively in the same preparation, (a) the malleus was coated alone (while the T.M. remained untouched); and (b) the T.M. was also coated. Under both conditions, time averaged holograms were made at four frequencies and over a wide range of amplitudes.

Mallar displacements for a given SPL were compared between the two sets of experiments. One such comparison for a frequency of 969 Hz and at a SPL of 108 dB is shown as an example in Figure 25.

The lack of clarity of fringes above 3000 Hz in this particular case prevented extending the comparison to higher frequencies.

The comparison for the four frequencies of Table VI shows that the difference, if any, was less than one dB up to a frequency of 3000 Hz. Such

differences are within the experimental error.

Between the two sets of this experiment, the head had to be taken out of the holographic setup for coating the T.M. When the head was placed back, it was oriented so as to obtain optimal reflections from the T.M. There were some unavoidable differences between the viewing angles in the two situations, and these differences could easily have caused a systematic error of one dB.

The loading of the T.M. due to the bronze powder coat was thus proved to be a negligible factor up to 3000 Hz.

2. Comparison of Cadaver Data with Data from Living Animals

It had originally been planned to perform the holographic experiments on living animals; enough space was allowed to accomodate an animal. During the intervening two years, until time averaged holography of the tympanic membrane became practical, a number of optical components were added to solve some of the optical and mechanical problems that had arisen. The remaining space was insufficient to accomodate a whole animal.

(i) Earlier experiments (Tonndorf and Khanna, 1968) using a laser interferometer had shown that for a given SPL the amplitude of mallar vibrations in cats remains unchanged for several hours after the sacrifice of the animal;

(ii) It was much easier experimentally to obtain high quality, time averaged, holograms on cadavers due to the lack of breathing motions;

(ii) Redesigning the entire setup to accommodate living animals might have cost at least a year's time.

For these three reasons, it was decided to proceed with cadaver experiments.

(a) Comparison of mallar displacements: A number of comparisons may be made to show that the cadaver data from the present experiments are consistent with those obtained with the aid of other techniques. For example, mallar displacement data on living animals are available from an earlier study in which a laser interferometer had been employed.

Both the present holographic experiments and the interferometer experiments of 1968 were performed with the bulla closed and almost the same exposure of the T.M. A comparison of the data from the two types of experiments is shown in Figure 26,

in which SPL required to produce an umbo displacement of 10^{-7}cm is plotted as a function of frequency. In the frequency range from 500 Hz to 3000 Hz, holographically measured data are within five to six dB of those measured by the interferometer. Above 2000 Hz, holographic data shows a relatively greater displacement of the malleus for a given SPL. The reasons for these small, but consistent, differences between the two sets of data are not understood at the present time.

(b) Comparison of holograms taken at different times

It was mentioned in section I that the first holograms were taken within thirty minutes of sacrificing the animal. At this time two holograms at each frequency under test were first taken, one at the lowest intensity level and the other at the highest intensity level. The remaining holograms (about 10 per frequency) continued to be taken for as long as six hours.

The reconstructions from these holograms were compared later. The comparison showed that T.M. vibration amplitudes recorded thirty minutes after sacrificing the animal were consistent with

those recorded six hours later.

Changes if any were equivalent to less than one decibel change in SPL.

(c) Comparison of volume displacements:

A comparison of volume displacements, calculated from holographic data, with those obtained from measurements of middle-ear impedance provides another check on the validity of cadaver experiments.

(i) Calculation of volume displacement from holographic reconstructions: The volume displacement is determined by the product of area and amplitude of displacement in each part of the T.M.

Since each of the bright and dark fringes (cf. Figure 19) represent different vibration amplitudes, it is relatively simple to cut out from a photographic enlargement areas associated with a given vibration amplitude. An example of such cut-outs is shown in Figure 27. There are five cut-outs corresponding to the first bright, the first dark; the 2nd bright, the 2nd dark; and the 3rd bright fringes. The areas of the different pieces was found by weighing them on a chemical balance. Since the total area of the cat tympanic membrane is 42 square

millimeter (Wever and Lawrence, 1954), these weights can be converted into absolute areas. An example of such a calculation is shown in Table VII.

A plot of volume displacement vs frequency, derived from one of the holographic experiments, is shown in Figure 28.

(ii) Calculation of volume displacement from middle ear impedance: Volume displacements for a given SPL, may also be obtained from acoustic impedance data measured in living cats.

Acoustic impedance = sound pressure/volume velocity;

volume velocity = pressure/impedance.

Since volume velocity = 2π x frequency x volume displacement, volume displacement = pressure/2π x frequency x impedance. If, for instance, the pressure = 100 dB SPL = 20 dynes/ sq cm,

volume displacement = 3.18/frequency x impedance.

Using Møller's data on the acoustic impedance of the cat's middle ear (Møller 1960; 1963), two curves for volume displacement as a function of frequency were calculated; these are shown in Figure 28.

The same figure includes volume displacements calculated from holographic reconstructions (Sect. M,2,b,i.) for ready comparison.

(iii) Comparison of data: Volume displacements at frequencies above 1500 Hz, determined from holographic data, are very slightly higher than those determined from Møller's data. These differences are however less than two dB.

Volume displacement data from holographic experiments were calculated under the assumption that all parts of the membrane vibrate in phase. The above agreement supports this assumption.

In view of the evidence presented, it is clear that the mechanical properties of the coated T.M. as used in the present cadaver experiments are very close to those deduced from experiments in living cats. Changes indeed, if any, are small and difficult to detect by the techniques used.

N. CHANGE IN VIBRATION PATTERN WITH FREQUENCY

The changes in the shape of the vibration pattern of the cat T.M. with frequency are shown in two sets of photographs of holographic reconstructions. Figure 29 A-D shows vibration amplitudes of the malleus and the T.M. at frequencies of 600, 969, 2007, and 3050 Hz. Figure 30 A-J gives similar data from a different animal at frequencies of 385, 600, 980, 1519, 1998, 2459, 2967, 4001, 5176, and 5937 Hz.

Observations were limited to the above frequency range by our inability to produce sufficient sound pressure levels in an open sound system, in excess of 100 dB SPL at frequencies below 400 Hz, and in excess of 120 dB SPL at frequencies above 6000 Hz, without severely distorting the waveform.

These levels can be obtained if the sound is applied to the bulla cavity in a closed system. Some of the earlier experiments were conducted with such a system. It, however, introduced in the observations an unnecessary complication, i.e., a change in the transfer function of the middle ear. The open sound system was therefore utilized in all the present experiments.

1. Vibration Patterns With Constant Mallar Amplitude

Both sets of photographs (Fig. 29 A-D, Fig. 30 A-J) were selected from a large series. They were selected so that the malleus amplitudes are equal at each of the frequencies (1st zero 1.21×10^{-5}cm). The sound pressure levels, however, had to be different at each frequency. The vibration pattern remains substantially the same from low frequencies (385 Hz) to mid frequencies (2500 Hz). Around 3000 Hz, the vibration pattern undergoes a sharp change. First posteriorly and then, above 4000 Hz also anteriorly the T.M. vibrations break up into sectional patterns. The location of the amplitude peak in the posterior portion moves postero-superiorly at higher frequencies.

2. Anterior, Posterior and Mallar Amplitudes

Amplitudes at the peak regions of the anterior and posterior quadrants of the T.M., and the amplitudes of the mallar tip, observed at 100 dB SPL are given for two animals in Figures 31 and 32. These graphs are based on the experimental data shown in Table VIII. Amplitudes in the peak region of the anterior quadrant are approximately

the same as those at the tip of the malleus, up to frequencies of 3000 Hz. Above this frequency, the anterior amplitudes become larger than those of the malleus. This difference increases with frequency. Amplitudes in the peak region of the posterior quadrant are about three times larger than those at the mallar tip and of the anterior quadrant, up to a frequency of 2000 Hz.

Throughout the frequency range the amplitude of the posterior quadrant is consistently larger than that of the anterior quadrant and that of the mallar tip (umbo).

3. Ratios between Anterior, Posterior, and Mallar Amplitudes

Consider Figure 33, in which ratios of anterior, posterior, and mallar amplitudes are shown. The ratios of anterior to malleus amplitudes are unity up to about 4000 Hz but increase at higher frequencies. The ratios of posterior to mallar amplitudes are about three up to about 1500 Hz. Thereafter, these ratios increase to values between 6 and 10 at 4000 Hz.

Since the sound pressure acts on the membrane which in turn drives the malleus, it is

clear that the larger posterior portion begins to loose its efficiency in driving the malleus around 1500 Hz, while the smaller anterior portion looses this efficiency around 4000 Hz.

4. Ratios between the Averaged Amplitudes of the Entire T.M. and the Mallar Amplitudes

Averaged amplitudes of the T.M. were obtained by dividing the total volume displacement (cf section M, 2, b, i.) by the area of the T.M. The ratios of averaged amplitudes with those of the malleus are also shown in Figure 33. The averaged T.M. amplitude is about 1.3 higher than the mallar amplitude, up to a frequency of 2000 Hz. Thereafter, it increases with frequency to reach a value of approximately three at 4000 Hz.

0. DISCUSSION

Several points are emerging from the present results -

1. a confirmation of the axis of ossicular rotation;
2. a new set of measurements of mallar amplitudes for given SPL's;
3. the first observations of vibration patterns of the T.M. for various frequencies;
4. data on the direct measurement of volume displacement of the T.M. for given SPL's;
5. data allowing the calculation of the magnitude of the curved membrane effect; and, finally,
6. a new look at the problems of the middle ear transformer ratio and impedance matching.

These points will now be taken up in order.

1. Axis of Rotation

The axis of rotation of the major ossicles was first correctly described by Barany in 1938, as running from the anterior mallar ligament to the

incudal ligament in a general antero-posterior direction. For audio frequencies, malleus and incus vibrate together as a unit. Tonndorf and Khanna (1967) described an exception from this rule: in the cat, there is some slippage in the incudo-mallar joint at low frequencies, first noticeable at around 60 Hz and increasing with inverse frequency.

From the anatomical standpoint, it may be stated that in man the manubrium mallei forms a right angle with the axis of rotation, except for its actual tip which points slightly forward. In the cat however the manubrium runs sharply forward from the neck of the malleus, thus forming an angle of approximately 30^{o} with the axis of rotation (cf. Figure 21). This, as is recalled, was the reason for the apparent tilt of the fringes as they cross over the malleus. In general our results, specially those of Section L-1, fully confirm Barany's original concept.

2. Mallar Amplitude

The amplitude of mallar displacements for given sound pressure levels has been measured earlier by a number of different investigators using various techniques: (a) Bekesy (1941) - capacitivie probe; (b) Gilad et al. (1967) - Mossbauer effect;

(c) Guinan and Peake (1967) - Stroboscope; (d) Tonndorf and Khanna (1968) - laser interferometer.

From the present results, a new set of data was derived (Section L-2 and N-1). Results of mallar amplitude vs frequency for an SPL of 100 dB are presented in Figure 34. The general shape of the curve, as well as the magnitude of the mallar displacement for a given SPL agrees fairly well with the respective results of earlier studies. An example of such a comparison was given in Figure 26. The curve showing mallar displacement in Figure 34 is almost flat between the frequencies of 400 Hz and 2000 Hz; above the latter value, it slopes down. In particular, the flatness of the curve around 1000 Hz is in contrast with the observations of Møller (1965) and of Guinan and Peake (1967) both of whom found a broad hump in this frequency region. The present results confirm our own earlier observations obtained with the aid of the laser interferometer (Tonndorf and Khanna, 1968).

3. Vibration Patterns of the Tympanic Membrane

The only previous measurement of the vibratory pattern of the T.M. is that of Bekesy (1941). His

results were given for a human T.M. (right ear), at frequencies below 2000 Hz. They are shown in Figure 35A.

According to Bekesy, it would appear that the T.M. vibrates as a stiff plate, hinged at its upper margin. Because of the right-angle relationship between the malleus and the axis of ossicular rotation found in man, lines of equal amplitude are seen to cross the malleus perpendicularly and to continue in the same direction fairly far onto the anterior and posterior portions of the T.M. This course would indicate that mallar amplitudes and those of the adjacent portions of the T.M. are really one and the same. (In other words, the T.M. and the manubrium really represent a stiff plate.) The amplitude was lowest superiorly, i.e., close to the axis of rotation, but increased progressively towards the inferior quadrant where it was largest. That is to say, in order to allow for the hinged motion, as shown in Figure 35A, the inferior quadrant had to be very loosely coupled to the malleus. This area was therefore called the "lower fold". In Bekesy's opinion then, the middle ear transformer was given by the area ratio between the T.M. and the stapes footplate (with

a small additional contribution due to the ossicular leverage). The lower fold would not contribute to the force transformation. The effective area of the T.M. was thus given as approximately two thirds of its total area. Bekesy, and also Wever and Lawrence (1954), independently, were able to verify this latter value in other experiments (provided the hinged plate concept was accepted).

Figure 35B, once more, shows an example of the present results for cats (left ear) at a frequency of 969 Hz. This pattern is very different from that found by Bekesy. (The fact that in cats the manubrium runs at an angle of 30°, open anteriorly, with respect to the axis of rotation was already mentioned in Sections J and 0-1.)

According to the present findings, the lines of equal amplitude run approximately parallel to the malleus over fairly long distances on both of its sides, indicating that the amplitude of the malleus is not equal to that of the adjacent parts of the T.M. at all. Invariably, the amplitude of the T.M. is higher both posteriorly and anteriorly than the mallar amplitude at corresponding places. The point of maximum vibration of the entire surface

is located in the postero-superior region of the T.M. Here, amplitude is approximately twice that of the anterior or inferior regions. There is no indication of a "lower fold" (in the sense of Bekesy) in the inferior quadrant.

Figure 36 shows the information of Figure 35B in a different manner. Given are the amplitudes of vibration along five selected cross sections, two approximately parallel to the malleus and three perpendicular to it. (In this particular presentation, the actual cross sectional shape of the T.M. at rest is disregarded.) Cross sections 2, 3, and 4 show that in most regions, especially anteriorly and posteriorly, the membrane vibrates with an amplitude greater than that of the malleus.

Essentially the same results were obtained in a study using human cadaver specimens (Tonndorf and Khanna 1970). The peak displacement regions were located in the anterior and posterior quadrants of the T.M. and there was no sign of a lower fold or hinged-plate motion of the T.M.

According to the present findings then, the T.M. does not vibrate like a stiff plate. However, the vibration pattern of the T.M., as presented

here, is wholly compatible with the catenary principle proposed by Helmholtz in 1868. As was already mentioned in the introduction, the force developed by the sound pressure acting upon the membrane is transmitted to the malleus by the tension of the membrane; therefore the force acting upon the malleus is larger than merely that given by the product of sound pressure and the area of the T.M. The cross sectional shape of the T.M. and the angle of attachment of the membrane to the malleus are two other important factors supporting Helmholtz' concept.

4. Volume Displacement

The volume displacement of the cat's T.M. was given in Section M-2, as 3.18/frequency x impedance.

Møller (1960, 1963) has given impedance measurements of the T.M. in cats at two different occasions. From two of Møller's individual measurements, two curves representing volume displacement as a function of frequency were calculated (cf. Figure 28). Included in the same graph was a third curve derived from the results of the present experiments. These curves appear to have three distinct sections: (i) in the low frequency region up to about 800 Hz, the

volume displacement is independent of frequency; (ii) between 800 and 3000 Hz, there is a transition region in which volume displacement decreases with frequency; (iii) above 3000 Hz, volume displacement is once more independent of frequency, its magnitude being approximately one fifth of that found at low frequencies below 800 Hz.

Whenever volume displacement is independent of frequency, volume velocity must increase with frequency at a rate of 6 dB/oct. This implies that at frequencies below 800 Hz and above 3000 Hz the impedance is capacitive in nature. This conclusion is generally borne out by Møller's findings.

5. Magnitude of the Catenary Effect

According to the catenary principle, the force acting upon the malleus is larger by a factor $\underline{k}$ than that acting upon the T.M.; the factor $\underline{k}$ is the force transformation ratio due to the curved membrane effect. An estimate of this ratio is obtained in Appendix (III) by an extension of Esser's calculations. (Esser 1947) These simplified calculations based on static considerations only, give a force transformation ratio of approximately two. ($\underline{k} = 2$). The precise magnitude of this ratio must be

determined from direct measurement of the forces involved. Such experiments are presently being planned.

6. The Middle-Ear Transformer Ratio

For the cat, a complete set of data is available for calculation of the ideal transformer ratio irrespective of the mechanism involved. It is a well known fact that in a system in which a transformer is used for the purpose of obtaining optimal power transfer between a given source and a given load, the required transformer ratio can be expressed as the square root of the ratio between the load impedance and the source impedance. (This rule is, of course, only correct under some restrictive assumptions.)

Inner ear impedance data for the cat in c.g.s. units are available from Tonndorf et al. (1966), and middle ear impedance data, also for cats and in c.g.s. units, from Møller (1963). (It should be noted that these data did not come from the same animals.)

The results of these calculations for a series of seven frequencies between 200 and 4000 Hz

is given in Table IX. The average value of the ideal transformer ratio is sixty-five. Based upon the then accepted concept of the middle ear transformer, Wever and Lawrence (1954) presented the following calculation, also for the cat: They assumed the T.M. to act as a stiff hinged plate; the effective area ratio between the T.M. and the stapes footplate was taken as 24.3 and the ossicular lever ratio as 2.5. They obtained a result of the overall transformer ratio of 60.7.

Even if we accept for the moment the hinged-plate concept as being correct, there are two points in the later calculation which are at least debatable.

(a) The area ratio of Wever and Lawrence included the effective area of the T.M. (approximately 2/3 of the total area) and the total area of the stapes footplate. Considering the relative stiffness of the annular ligament, however, it must be assumed that some portion of it displaces together with the footplate, making the area of the footplate larger from the functional standpoint. The required correction would reduce the numerical value of the transformer ratio.

(b) Another uncertainty involves the use of ossicular lever ratio. First of all, Guinan and Peake (1967) and also Tonndorf and Khanna (1967), obtained lower values namely 2.0 and 2.2 respectively.

Insertion of these values would also reduce the numerical results of the calculations of Wever and Lawrence.

There is one more serious point we wish to raise. The ossicular lever ratio as employed by Wever and Lawrence in their calculations was based on the assumption thatthe entire force due to the sound pressure acts at the very tip of the manubrium. Even if the T.M. would function as a stiff plate, the latter assumption is not correct. The force might better be said to act at the geometrical center of the effective area, a point that lies certainly higher than the tip of the manubrium.

If the following corrections are made:

(i) If the diameters of the stapes footplate are enlarged by approximately 5%, the functional area is increased by 10%;

(ii) the ossicular lever ratio is reduced from 2.5 to a value of 2.1; and

(iii) if the geometrical center is assumed to be the true center of the upper 2/3 of the T.M., the force might be said to act at a place that lies at the half way point of the manubrium; the transformer ratio based on the hinged plate concept reduces from 60.7 to an unrealistically low value of approximately 23.

Although, admittedly, an exact numerical calculation of the middle ear transformer ratio that considers the catenary principle cannot be given at this time, a number of comments may be made.

Going back to Helmholtz' original concept, one may state the transformer ratio in the following manner

$$r = \text{Ossicular lever ratio} \times \text{catenary lever ratio} \times \frac{\text{Area of the T.M.}}{\text{Area of the footplate}} . \qquad (12)$$

The catenary lever ratio is not constant over the entire T.M. It changes as the inverse curvature of the surface in a given region. In the region of the short process, the curvature of both anterior and posterior quadrants is small (consequently, the catenary lever ratio is large). As one progresses towards the tip

of manubrium, the curvature becomes gradually larger (consequently, the catenary lever ratio becomes smaller). In the same manner, the ossicular lever ratio increases from a value of less than one at the short process to about 2.1 at the tip of the malleus.

Considering this point together with the displacement pattern of the T.M., as shown for example in Figure 19, indicates that in first approximation the product of the force provided by the catenary effect in each section and the corresponding force along the malleus (the ossicular lever ratio) is constant.

Thus, it appears that the entire area of the T.M. participates in the transformation process to approximately equal degrees. Furthermore, this transformation process makes use of the entire force due to the pressure acting upon the T.M. In other words, the effective area is now the total area of the T.M.

At this point, it is not possible to give an exact numerical solution to equation (12), especially since the force transformation has not yet been measured. The only data of this kind are those of Bekesy (1941). However, they were taken from human cadaver specimens.

P. CONCLUSIONS

(1) Time averaged holography is used in vibration analysis of cat's T.M.

(2) Under the experimental conditions employed, the mode of T.M. vibrations remained unchanged for several hours after the sacrifice of the animal.

(3) The dynamic axis of rotation of the malleus makes an angle of 30^{o} with that of the manubrium. This finding confirms the course of this axis as originally described by Barany.

(4) T.M. vibrations remained substantially the same up to a frequency of about 2500 Hz, above which sharp changes occur.

(5) At all frequencies the magnitude of vibrations was largest in the posterior quadrant, less in the anterior quadrant, and least in the inferior quadrant of the T. M.

(6) The amplitude of any point along the malleus was less than that of the adjacent parts of the T. M. on either side.

(7) The cat's T. M. was not found to vibrate like a stiff hinged plate as proposed by Bekesy

for the case of the human T. M. Rather, the vibration patterns are consistent with the curved membrane principle of Helmholtz.

(8) The action of the middle ear transformer is determined by three mechanisms of force transformation:

(a) An increase in force due to the large area of the T. M. as compared to the small area of the footplate.

(b) An increase in the force acting upon the malleus due to the curvature of the T. M. (its average value is estimated to be about 2.0).

(c) An increase in force due to the ossicular lever ratio (its average value is estimated to be about 1.4).

(9) The concept of the effective area (2/3 of the total area of the T. M.) is no longer valid.

(10) The effective value of the ossicular lever ratio is lower than that accepted up to the present time.

Q. APPENDIX I

Calculation of isodisplacement contours on a plate, formed by its rotation around two axes.

Consider the coordinates of the point (x, y, 0) in Figure 37 due to rotation of the plane A, B, C, D, around the y axis, at the extreme excursion the new coordinates are given by

$$x_1 = x \cos\theta$$

$$y_1 = y$$

$$z_1 = \pm x \sin\theta$$

Similarly the coordinates of the point (x, y, 0) in Figure 38 due to rotation of the plane A, B, C, D, around the x axis are given by

$$x_2 = x$$

$$y_2 = y \cos\psi$$

$$+z_2 = \pm y \sin\psi$$

If both rotations occur simultaneously (Figure 39) then the coordinates of the points are given by

$$x_3 = x_1 + x_2 = x (1 + \cos\theta)$$

$$y_3 = y_1 + y_2 = y (1 + \cos\psi)$$

$$z_3 = z_1 + z_2 = x \sin\theta + y \sin\psi$$

The displacement is being viewed along the z axis, and the angles θ and ψ are very small. Under these conditions

$$\cos\theta \approx 1 \quad \text{and} \quad \sin\theta \approx \theta.$$

The total change in the z coordinates at the two ends of excursion are given by

$$\Delta z = 2\ (x\theta + y\psi\ )$$

Therefore when viewed along the z axis, the lines of equal displacement on the surface are given by

$$x\theta + y\psi = k$$

when $\psi = 0$, the lines of equal displacement are given by

$$x = k.$$

These are lines parallel to the x axis.

Similarly when $\theta = 0$, i.e., the plate is displaced around the x axis only, the lines of equal displacement are given by

$$y = k.$$

These are lines parallel to the y axis, i.e., the lines are parallel to the axis of rotation.

When both θ and ψ rotation are present

$$y = -\frac{\theta}{\psi}\ x + \frac{k}{\psi}$$

$$\text{Tan}\ \gamma = \frac{\theta}{\psi}$$

Along the axis of rotation there is no change in coordinates with rotation.

$$\Delta z = 0 = 2(x\theta + y\psi)$$

The axis of rotation is therefore given by

$$y = -\frac{\theta}{\psi} x = \gamma x$$

The lines of equal displacement run at an angle γ to the y axis. The lines are parallel to the axis of rotation as shown in Figure 40.

R. APPENDIX II

Displacement of Points on the segment of a Circle when the chord is rotated through an Angle.

In Figure 41, the arc OA is rotated through an angle θ to the position OB. The Y displacement of points along the arc, produced by the rotation, will be determined in the following analysis.

Coordinates of the center P (x_1, y_1) are

$$y_1 = -r \sin\alpha \quad ;$$

and

$$x_1 = r \cos\alpha \quad .$$

Equation for the circle with x_1 and y_1 as center

$$(x - x_1)^2 + (y - y_1)^2 = r^2 \qquad (1)$$

Since this circle passes through (0, 0),

$$x_1^2 + y_1^2 = r^2 \qquad (2)$$

Expanding equation (1) we have:

$$x^2 - 2 xx_1 + x_1^2 + y_1^2 - 2 yy_1 + y_1^2 = r^2$$

Combining with (2) simplifies it to:

$$x^2 - 2 xx_1 + y^2 - 2 yy_1 = 0 \qquad (3)$$

Rewriting (3) we have:

$$y^2 - 2y_1 y + (x^2 - 2xx_1) = 0$$

$$y = \frac{2\, y_1 \pm \sqrt{4\, y_1^{\,2} - 2\,(x^2 - 2\, xx_1)}}{2}$$

$$= y_1 \pm (y_1^{\,2} - x^2 + 2\, xx_1)^{\frac{1}{2}} \qquad (4)$$

consider a case in which the radius r is much longer than the chord OA.

$\therefore\ y_1 \gg x_1$, and x.

Rewriting equation (4) we obtain:

$$y = y_1 \left[1 \pm \left\{ 1 - \frac{x^2 + 2\, xx_1}{y_1^{\,2}} \right\} \right]^{\frac{1}{2}} \qquad (5)$$

Since $\dfrac{(x^2 + 2\, xx_1)}{y_1^{\,2}} \ll 1$, therefore

expanding equation (5) by Binomial Theorem and neglecting the higher order terms gives:

$$y = y_1 \left[1 \pm \left\{ 1 - \tfrac{1}{2} \frac{x^2 - 2\, xx_1}{y_1^{\,2}} \right\} \right] \qquad (6)$$

Since we are only interested in points with the positive values of y, equation (6) may be simplified to,

$$y = \tfrac{1}{2}\left[\frac{x^2 - 2xx_1}{y_1}\right] \qquad (7)$$

Coordinates of the center Q (x_2, y_2) are,

$$x_2 = r\cos(\alpha - \theta),$$
$$= r(\cos\alpha\cos\theta + \sin\alpha\sin\theta),$$
$$= x_1\cos\theta - y_1\sin\theta,$$

and

$$y_2 = -r\sin(\alpha - \theta),$$
$$= -r(\sin\alpha\cos\theta - \cos\alpha\sin\theta),$$
$$= y_1\cos\theta + x_1\sin\theta,$$

Equation for the circle with (x_2, y_2) as center

$$(x - x_2)^2 + (y - y_2)^2 = r^2$$

Substituting for x_2 and y_2 in the above equation results in,

$$(x - x_1\cos\theta + y_1\sin\theta)^2 + (y - y_1\cos\theta - x_1\sin\theta)^2 = r^2 \quad (8$$

Since this circle also passes through (0 , 0) therefore,

$$x_2^2 + y_2^2 = r^2$$

or

$$(x_1\cos\theta - y_1\sin\theta)^2 + (y_1\cos\theta + x_1\sin\theta)^2 = r^2 \qquad (9)$$

The expansion of equation (8) gives,

$$x^2 + (x_1\cos\theta - y_1\sin\theta)^2 - 2x\,(x_1\cos\theta - y_1\sin\theta) + y^2$$

$$+ (y_1\cos\theta + x_1\sin\theta)^2 - 2y(y_1\cos\theta + x_1\sin\theta) = r^2$$

Combining it with equation (9) simplifies the results to,

$$y^2 - 2y(y_1\cos\theta + x_1\sin\theta) + x^2 - 2x(x_1\cos\theta - y_1\sin\theta) = 0$$

$$y = \tfrac{1}{2}\left[2(y_1\cos\theta + x_1\sin\theta) \pm \left[4(y_1\cos\theta + x_1\sin\theta)^2 - 4\left\{x^2 - 2x(x_1\cos\theta - y_1\sin\theta)\right\}\right]\right]^{\frac{1}{2}}$$

or $$y = (y_1\cos\theta + x_1\sin\theta) \pm \left[(y_1\cos\theta + x_1\sin\theta)^2 - \left\{x^2 - 2x\,(x_1\cos\theta - y_1\sin\theta)\right\}\right]^{\frac{1}{2}} \qquad (10)$$

Since we are only interested in points above x axis, ie + ve values of y

$$y = (y_1\cos\theta + x_1\sin\theta) - \left[(y_1\cos\theta + x_1\sin\theta)^2 - \left\{x^2 - 2x\,(x_1\cos\theta - y_1\sin\theta)\right\}\right]^{\frac{1}{2}} \qquad (11)$$

In our case θ is a very small angle, therefore

$\cos\theta = 1$ and $\sin\theta = \theta$

Rewriting equation (11) we have:

$$y = (y_1 + x_1\theta) - \left[(y_1 + x_1\theta)^2 - \left\{x^2 - 2x(x_1 - y_1\theta)\right\}\right]^{\frac{1}{2}} \qquad (12)$$

considering the case in which the radius r is much longer than the chord.

i.e. $y_1 \gg x_1$ or x

According to equation (12)

$$y = (y_1 + x_1\theta)\left[1 - \left[1 - \left\{\frac{x^2 - 2x(x_1 - y_1\theta)}{(y_1 + x_1\theta)^2}\right\}\right]^{\frac{1}{2}}\right] \quad (13)$$

Applying Binomial theorem and neglecting higher terms results in:

$$y = (y_1 + x_1\theta)\left[1 - \left[1 - \tfrac{1}{2}\left\{\frac{x^2 - 2x(x_1 - y_1\theta)}{(y_1 + x_1\theta)^2}\right\}\right]\right] \quad (14)$$

$$= \tfrac{1}{2}\left[\frac{x^2 - 2x(x_1 - y_1\theta)}{y_1 + x_1\theta}\right] \quad (15)$$

The total change in y coordinates is given by the difference between the y coordinates calculated in equation (15) and those in equation (7)

$$y' = \tfrac{1}{2}\left[\frac{x^2 - 2x(x_1 - y_1\theta)}{y_1 + x_1\theta} - \frac{x^2 - 2xx_1}{y_1}\right] \quad (16)$$

since $y_1 \gg x_1$ and $\theta \ll 1$

Equation (16) simplifies to $y' = x\theta$ (17)

The displacement of the chord OA can be described by

$$y = x \text{ Tan } \theta$$

since θ is small

$$y = x\theta$$

Thus the displacements of points on the segment approximate the displacements of points on the chord when each is rotated through the same angle θ, provided the angleθ is small and the chord is small compared to the radius of the curvature of the segment.

S. APPENDIX III

Magnitude of the force transformation ratio due to the curved membrane effect.

According to the curved membrane principle, the force acting upon the malleus is larger by a factor k than that acting upon the T.M.; factor k might be called the force transformation ratio due to the curved membrane effect.

Esser (1947) calculated the forces acting upon an idealized T.M. (the T.M. was shaped like a circular flared cone, attached to the malleus only at its tip) and derived an estimate of k

It was shown earlier that the bending of the malleus is negligible (sect L.2.), taking this into account in one of his equations, one obtains the force transformation ratio k as:

$$k = \frac{\Delta v}{\Delta x} \cdot \frac{1}{\pi r^2} \qquad (1)$$

where k = Force on malleus/ Force on T.M.;

Δv = volume displacement of the T.M.;

Δx = displacement amplitude of the malleus;

πr^2 = area of the T.M.

Equation (1) may be restated as:

Force on the T.M. x Average displacement of T.M. = Force on malleus x Displacement at the tip of malleus;

or

Work done on the T.M. = Work done on the malleus.

It was assumed in the above calculation that all the forces acting on the T.M. are applied at one point on the malleus, its tip. In reality, these forces are distributed along the entire malleus. A precise knowledge of this distribution is essential in evaluating the effective force transformation ratio. If the assumption is made that there is no power mismatch between the T.M. and the malleus, then the product of force times the lever ratio for each point along the malleus must be approximately constant. Since the displacement at each point along the malleus is also proportional to the ossicular lever ratio (cf. Figure 42) (different for each point on the malleus), it follows that:

$$a_p \times f_p = \frac{W_m}{(d_m - d_s)}\, d\ell \,, \qquad (2)$$

where

a_p = amplitude at point p;

f_p = force at point p;

W_m = total work done in displacing the malleus;

d_m = perpendicular distance between the tip of malleus and its axis of rotation;

d_s = perpendicular distance between the short process and the axis of rotation of the malleus.

Since $a_p = \frac{d_p}{d_m} a_u$;

it then follows from equation (2) that:

$$f_p = \frac{W_m}{(d_m - d_s)} \cdot \frac{d_m}{a_w \cdot d_p} \cdot d\ell \qquad (3)$$

where

d_p = perpendicular distance of point p from the axis of rotation of the malleus;

a_w = displacement of the mallar tip.

The total force acting on the malleus is given by:

$$F_m = \int_{d_s}^{d_m} \frac{W_m}{(d_m - d_s)} \cdot \frac{d_m}{a_u \cdot d_p} \, d\ell \qquad (4)$$

$$= \frac{W_m}{(d_m - d_s)} \cdot \frac{d_m}{a_u} \log_e \frac{d_m}{d_s} \qquad (5)$$

The value of the force acting on the malleus can now be numerically evaluated.

Since $\frac{d_m}{d_s} = 2.5$;

and $\frac{d_m}{(d_m - d_s)} = 1.66$;

then $F_m = 1.51 \frac{W_m}{a_u}$. (6)

As work done on the malleus is assumed to be equal to the work done on the T.M., equation (6) may be rewritten as:

$$\frac{F_m}{F_{T.M.}} = 1.51 \frac{\text{Average displacement of T.M.}}{\text{Displacement at tip of malleus}} \quad (7)$$

The total force acting on the tip of incus is similarly given by

$$F_i = \int_{d_i}^{d_m} \frac{d_m}{d_i \cdot a_u} \cdot \frac{W_m}{(d_m - d_s)} \cdot d\ell \quad (8)$$

$$= \frac{d_m}{d_i \cdot a_u} \cdot W_m \quad (9)$$

where

F_i = total force acting at the tip of the incus;

d_i = perpendicular distance from the tip of the incus to the axis of rotation of the both major ossicles.

Since

$$\frac{d_m}{d_i} = 2.1$$

equation 9 may be written as:

$$\frac{F_i}{F_{T.M.}} = 2.1 \cdot \frac{\text{Avg. displacement of T.M.}}{\text{Displacement at tip of malleus}} \quad ; \quad (10)$$

the effective value of the ossicular lever ratio is therefore given by:

$$\frac{F_i}{F_m} = \frac{F_i}{F_{T.M.}} \cdot \frac{F_{T.M.}}{F_m} = 1.4 \cdot$$

It was shown in section N.4, that the average displacement of the T.M. is about 1.3 times that of the tip of the malleus (i.e., below 2000 Hz). Substituting this datum in equation (7), we obtain the magnitude of the force transformation ratio due to the curved membrane effect.

$$\frac{F_m}{F_{T.M.}} = 1.96.$$

It is important to note that Esser's calculations and the present extension of his results are both based on static considerations only and thus represent an oversimplification of the complex dynamic situation. The precise magnitude of the force transformation ratio due to the curved membrane effect must be determined from direct measurements of the forces involved. Such experiments are presently being planned.

T. BIBLIOGRAPHY

1. Barany, E. A. Contribution to the Physiology of Bone Conduction. Acta-Oto-Laryng. Suppl. 26, 1938.

2. Bekesy, G. Von. Experiments in Hearing. McGraw-Hill Book Co. New York, 1960.

3. Brown, G. M., Grant, R. M. and Stroke, G. W. Theory of Holographic Interferometry. J. Acoust. Soc. Am. 45: 1166-1179, 1969.

4. Esser, M. H. M. The Mechanism of the Middle Ear: Part II The Drum. Bull. Math. Biophysics 9:75-91, 1947.

5. Gabor, D. A. New Microscope Principle. Nature 161:777-778, 1948.

6. Gilad, P. et al. Application of the Mossbauer Method to Ear Vibrations. J. Acoust. Soc. Am. 41:1232-1236, 1967.

7. Guinan, J. J. and Peake, W. T. Middle Ear Characteristics of Anesthetized Cats. J. Acoust. Soc. Am. 41:1237-1261, 1967.

8. Helmholtz, H. The Mechanism of the Ear and Membrana Tympani. Pfluger's Archiv. fur Physiologie (1869).

9. Leith, E. N. and Upatnieks, J. Reconstructed Wavefronts and Communication Theory. J. Opt. Soc. Am. 52: 1123-1130, 1962.

10. Leith, E. N. and Upatnieks, J. Wavefront Reconstruction with Continuous - Tone Objects. J. Opt. Soc. Am. 53:1377-1381, 1963.

11. Leith, E. N. and Upatnieks, J. Wavefront Reconstruction with Diffused Illumination and Three Dimensional Objects. J. Opt. Soc. Am. 54:1295-1301, 1964.

12. Leith, E. N. and Upatnieks, J. Recent Advances in Holography in Progress in Optics. ed. E. Wolf. North Holland Publishing Co. Amsterdam, 1967.

13. Lindsay, R. B. Physical Mechanics. D. Van Nostrand Co. New York, 1933.

14. Metherell, A. F., Pinak, S. S. and Pisa, E. J. Subfringe Interferometric Holography for Linearly Recording Small Displacements. Opt. Soc. Am. Oct. 1969 Meeting.

15. Moller, A. R. Transfer Function of the Middle Ear. J. Acoust. Soc. Am. 35: 1526-1534, 1963.

16. Moller, A. R. An Experimental Study of the Acoustic Impedance of the Middle Ear and its Transmission Properties. Acta-Oto-Laryng. 6:129-149, 1960.

17. Monahan, M. A. and Bromley, K. Vibration Analysis by Holographic Interferometry. J. Acoust. Soc. Am. 44:1225-1231, 1968.

18. Powell, R. L. and Stetson, K. A. Interferometric Vibration Analysis by Wavefront Reconstruction. J. Opt. Soc. Am. 55:1593-1598, 1965.

19. Selby, S. M. (editor) Handbook of Tables for Mathematics. Chemical Rubber Co. 1967.

20. Stetson, K. and Elion, H. A. Holographic Visualization of Sound Fields using Lasers. J. Acoust. Soc. Am. 39:1215, 1966.

21. Tonndorf, J. et al. The Input Impedance of the Inner Ear in Cats. Ann. Otol. Rhino., & Laryng. 75:752-763, 1966.

22. Tonndorf, J. and Khanna S. M. Some Properties of Sound Transmission in the Middle and Outer Ears of Cats. J. Acoust. Soc. Am. 44: 513-521, 1967.

23. Tonndorf, J. and Khanna, S. M. Submicroscopic Displacement Amplitudes of the Tympanic Membrane (cat) measured by a Laser Interferometer. J. Acoust. Soc. Am. 44: 1546-1554, 1968.

24. Tonndorf, J., Khanna, S. M. and Janecka, I. Vibratory Patterns observed in real time by Interferometric Holography. Opt. Soc. Am. October 1969 meeting, (Abstract).

25. Tonndorf, J. and Khanna, S. M. Function of the Tympanic Membrane. J. Acoust. Soc. Am. 47:60, 1970, (Abstract).

26. Tonndorf, J., Khanna, S. M. and Janecka. I. Vibratory Patterns Observed in Real Time by Interferometric Holography (under preparation) 1970.

27. Wever, E. G. and Lawrence, M. Physiological Acoustics. Princeton University Press. Princeton, N. J. 1954.

Fringe No.	Vibration Amplitude in cm
1st max	0
1st zero	1.211×10^{-5}
2nd max	1.928×10^{-5}
2nd zero	2.779×10^{-5}
3rd max	3.532×10^{-5}
3rd zero	4.355×10^{-5}
4th max	5.132×10^{-5}
4th zero	5.936×10^{-5}
5th max	6.709×10^{-5}
5th zero	7.517×10^{-5}
6th max	8.293×10^{-5}
6th zero	9.098×10^{-5}
7th max	9.878×10^{-5}
7th zero	10.679×10^{-5}
8th max	11.459×10^{-5}
8th zero	12.260×10^{-5}
9th max	13.040×10^{-5}
9th zero	13.843×10^{-5}
10th max	14.627×10^{-5}
10th zero	15.424×10^{-5}

Table I. Vibration amplitudes corresponding to the first ten maxima (bright fringes) and zeros (dark fringes).

No of Zero	Ratio $(A_n+1)/A_n$	Ratio dB 20 Log $\frac{(A_n+1)}{A_n}$
1		
2	2.25	7.2
3	1.56	3.87
4	1.33	2.67
5	1.27	2.1
6	1.21	1.66
7	1.17	1.36
8	1.15	1.21
9	1.13	1.06
10	1.11	0.91

Table II. Amplitude ratio's between the first ten successive dark fringes.

Fringe No.	Best Estimated Amplitude x 10^{-5}cm	Max % Error
1st max		
1st zero		
2nd max	1.57	29.6%
2nd zero	2.35	22%
3rd max	3.16	13.5%
3rd zero	3.94	11.6%
4th max	4.74	8.8%
4th zero	5.53	7.9%
5th max	6.32	6.5%
5th zero	7.11	6.0%
6th max	7.91	5.1%
6th zero	8.70	4.8%
7th max	9.49	4.2%
7th zero	10.28	4.0%
8th max	11.07	3.6%
8th zero	11.86	3.4%
9th max	12.65	3.1%
9th zero	13.44	3.0%
10th max	14.24	2.8%
10th zero	15.03	2.7%

Table III. Best estimates of amplitude and % error if the fringe number is determined from a single hologram.

	1D	2B	2D	3B	3D	4B	4D	5B	5D
1D	0	4.03	7.2	9.31	11.1	12.51	13.8	14.87	15.9
2B	4.03	0	3.17	5.24	7.08	8.46	10.21	10.83	11.8
2D	7.2	3.17	0	2.08	3.87	5.3	6.57	7.64	8.77
3B	9.31	5.24	2.08	0	1.8	3.23	4.51	5.58	6.53
3D	11.1	7.08	3.87	1.8	0	1.44	2.67	3.75	4.77
4B	12.51	8.46	5.3	3.23	1.44	0	1.29	2.34	3.29
4D	13.8	10.21	6.57	4.51	2.67	1.29	0	1.06	2.1
5B	14.87	10.83	7.64	5.58	3.75	2.34	1.06	0	1.06
5D	15.9	11.8	8.77	6.53	4.77	3.29	2.1	1.06	0

Table IV. 20 Log [Ratio of vibration amplitude between any two of the first five bright and dark fringes]

Cat	Frequency Hz	Min. SPL dB	Max. SPL dB
J	600	89	125
L	600	109	113
	968	102	120
	2042	103	123
	2960	103	125
	4005	108	130
	5118	102	118
	6310	110	114
M	385	98	102
	600	93	113
	980	90	110
	1519	95	115
	1998	93	113
	2459	94	116
	2967	93	117
	4001	93	119
	5176	92	116
	5937	94	114
N	600	93	111
	969	90	112
	2007	93	113
	3050	93	113

Table V. Range of sound pressure level used at each frequency in four experiments.

Frequency Hz	SPL for Equal Malleus Displacement		Difference dB
	Malleus Coated	T.M. Coated	
600	107	107	0
969	106	107	+1
2007	106	107	+1
3050	109	110	+1

Table VI. Comparison of SPL for the same mallar displacement.

No	Fractional Weight (in gms)	Area (in sq cm)	Fringe Number	Vibration Amplitude (in cm)	Volume Displacement
1	229	.166	1B	0	0
2	182	.132	1D	1.211×10^{-5}	16.03×10^{-7}
3	90	.065	2B	1.928×10^{-5}	12.59×10^{-7}
4	69.5	.050	2D	2.78×10^{-5}	14.01×10^{-7}
5	8.0	.006	3B	3.53×10^{-5}	2.05×10^{-7}
Total 579		0.42			44.68×10^{-7}

Table VII. Calculation of volume displacement (3050 Hz, 109 dB SPL)

(1) Area = $\frac{\text{fractional weight}}{\text{total weight}} \times 0.42$;

(2) Volume displacement = area x vibration amplitude.

Table VIII. Anterior and Posterior Amplitude related to malleus amplitude

Holo. No.	Frequency Hz	SPL dB	Malleus Fringe No.	Ant. Fringe No.	Post Fringe No.	Ant. Amp. dB Ref. Malleus Amp.	Post. Amp. dB Ref. Malleus Amp.
L-2	600	109	3Z	3Z	10Z	0	11.0
L-11	968	104	2Z	2Z	6Z	0	10.3
L-22	2042	107	2Z	2Z	7Z	0	11.7
L-34	2960	107	1Z	1Z	4Z	0	13.8
L-43	4005	117	1Z	1Z	8Z*	0	20.1
L-57	5118	108	1Z	4B	9Z*	12.5	21.1
M-98	385	102	1Z	1Z	3B	0	9.3
M-19	600	101	1Z	1Z-2B	3Z	2	11.1

Holo. No.	Frequency Hz	SPL dB	Malleus Fringe No.	Ant. Fringe No.	Post. Fringe No.	Ant. Amp. dB	Post. Amp. dB
						Ref. Malleus Amp.	
M-22	600	107	2Z	2Z	6B	0	9.5
M-3	980	100	1Z	1Z	2Z	0	9.0
M-31	980	107	2Z	2Z	6B	0	9.5
M-36	1519	101	1Z	1Z	3B	0	9.3
M-39	1519	107	2Z	2Z-3B	5Z	1.0	8.77
M-47	1998	101	1Z	1Z	3B	0	9.3
M-52	1998	109	2Z	3B	6Z	2.08	10.3
M-59	2459	104	1Z	1Z	3B	0	9.3
M-63	2459	112	2Z	3B	7B	2.08	11.0
M-74	2967	111	1Z	2B	4B	4.03	12.5

Holo. No.	Frequency Hz	SPL dB	Malleus Fringe No.	Ant. Fringe No.	Post. Fringe No.	Ant. Amp. dB Ref. Malleus Amp.	Post. Amp. dB Ref. Malleus Amp.
M-86	4001	115	1Z	2B	5Z*	4.03	16.0
M-92	5176	109	1Z	2B	5Z*	4.03	16.0
M-15	5937	114	1Z	4Z	5B*	13.80	15.0
N-30	600	95	1Z	2B	3B	4.03	9.31
N-33	600	101	2Z	3B	6B	2.08	9.45
N-42	969	96	1Z	2B	3B	4.03	9.31
N-45	969	102	2Z	3B	5Z	2.08	8.77
N-54	2007	99	1Z	2B	3B	4.03	9.31
N- 7	2007	106	2Z	3B	6B	2.08	9.45
N-71	3050	111	1Z	2B	4B	4.03	12.51

Frequency in Hz	Inner Ear Impedance $x10^6$ C.G.S. Units	Middle Ear Impedance C.G.S. Units	Impedance Ratio	Ideal Transformer Ratio
200	6.0	1585	$3.8x10^3$	62
400	4.2	767	$5.4x10^3$	73.5
800	2.1	422	$5.0x10^3$	71.0
1000	1.7	422	$4.2x10^3$	65.0
2000	1.2	380	$3.2x10^3$	57.0
3000	1.9	485	$3.9x10^3$	63.0
4000	1.3	317	$4.1x10^3$	64.0

Table IX. Inner ear impedance of cat, its middle ear impedance and ideal transformer ratio for matching.

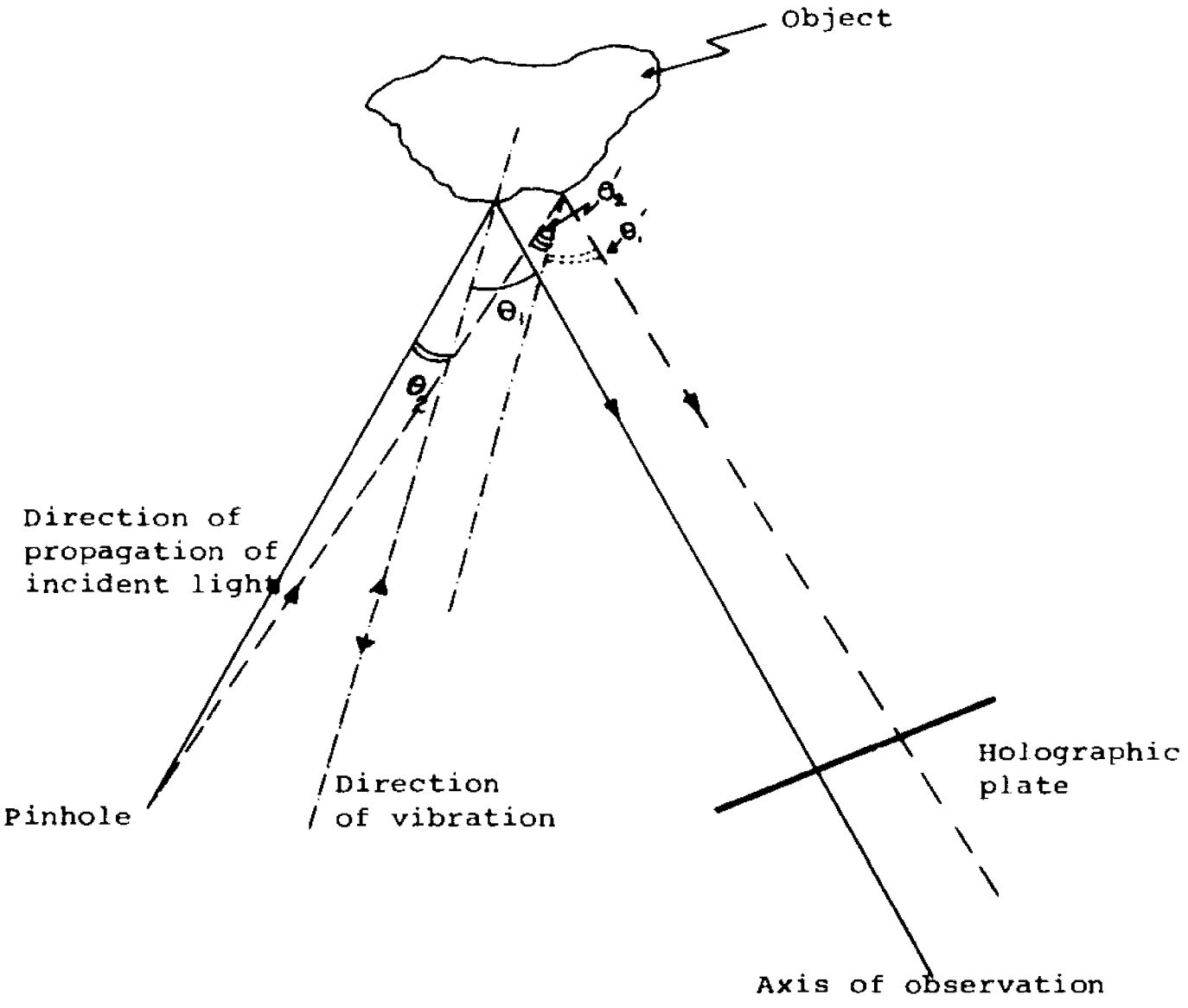

Figure 1.

Angles θ_2 and θ_1 between direction of incident beam, direction of vibration, and axis of observation. Both angles θ_2 and θ_1 are different for each point on the hologram.

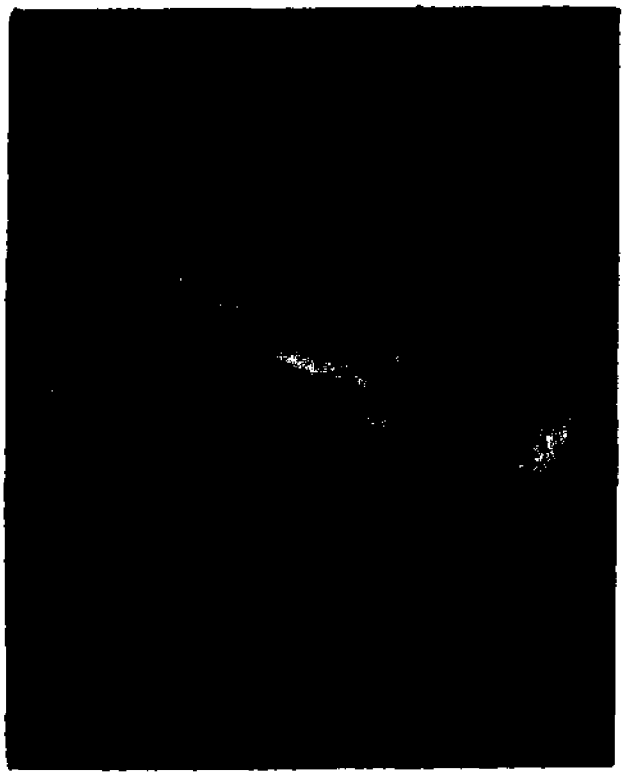

Figure 2

Holographic reconstruction of a vibrating earphone membrane. Dark and bright fringes connect points of equal vibration amplitude.

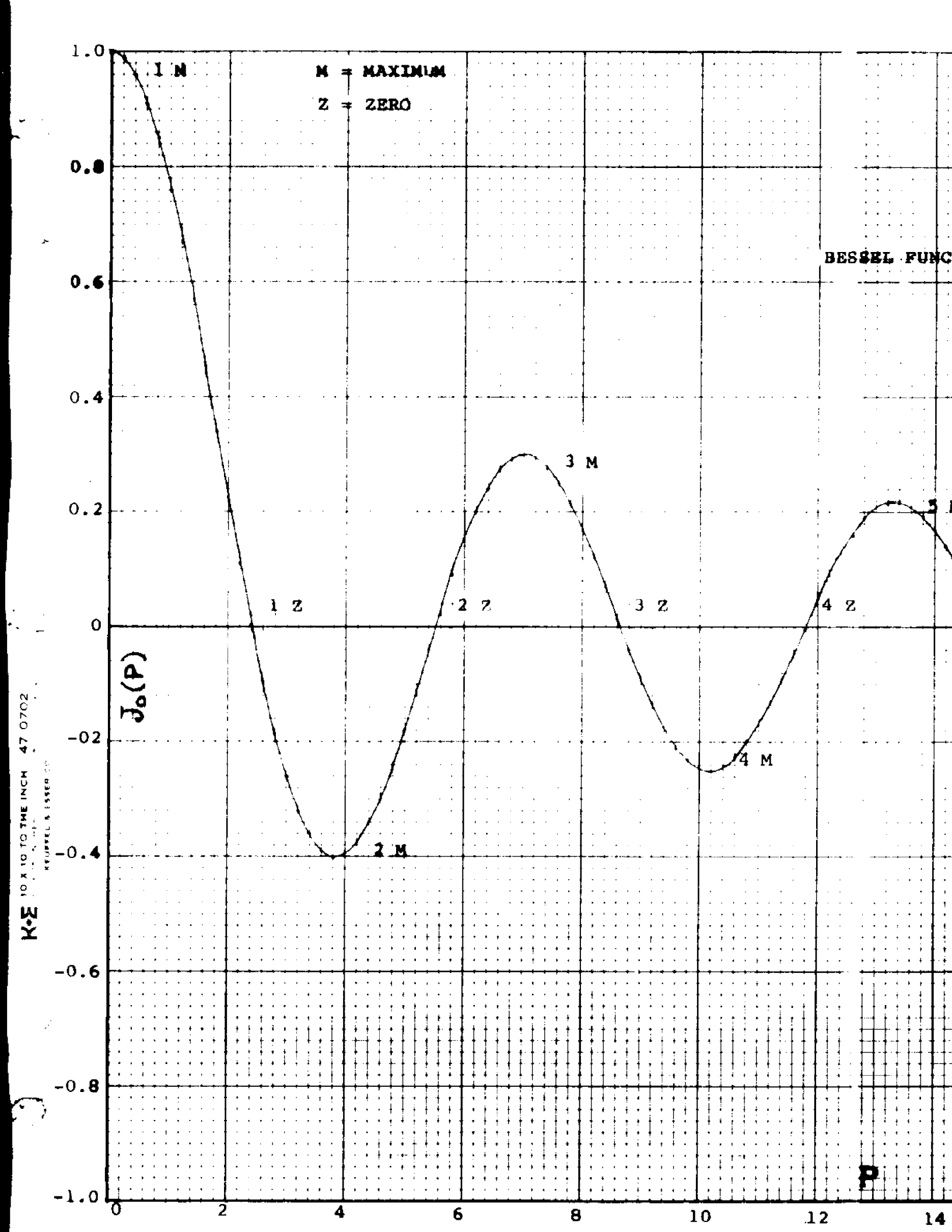
M = MAXIMUM
Z = ZERO
BESSEL FUNC
1 M
1 Z
2 Z
3 M
3 Z
4 Z
4 M
2 M
$J_0(P)$
P
1.0
0.8
0.6
0.4
0.2
0
-02
-0.4
-0.6
-0.8
-1.0
0
2
4
6
8
10
12
14
10 X 10 TO THE INCH 47 0702
KEUFFEL & ESSER

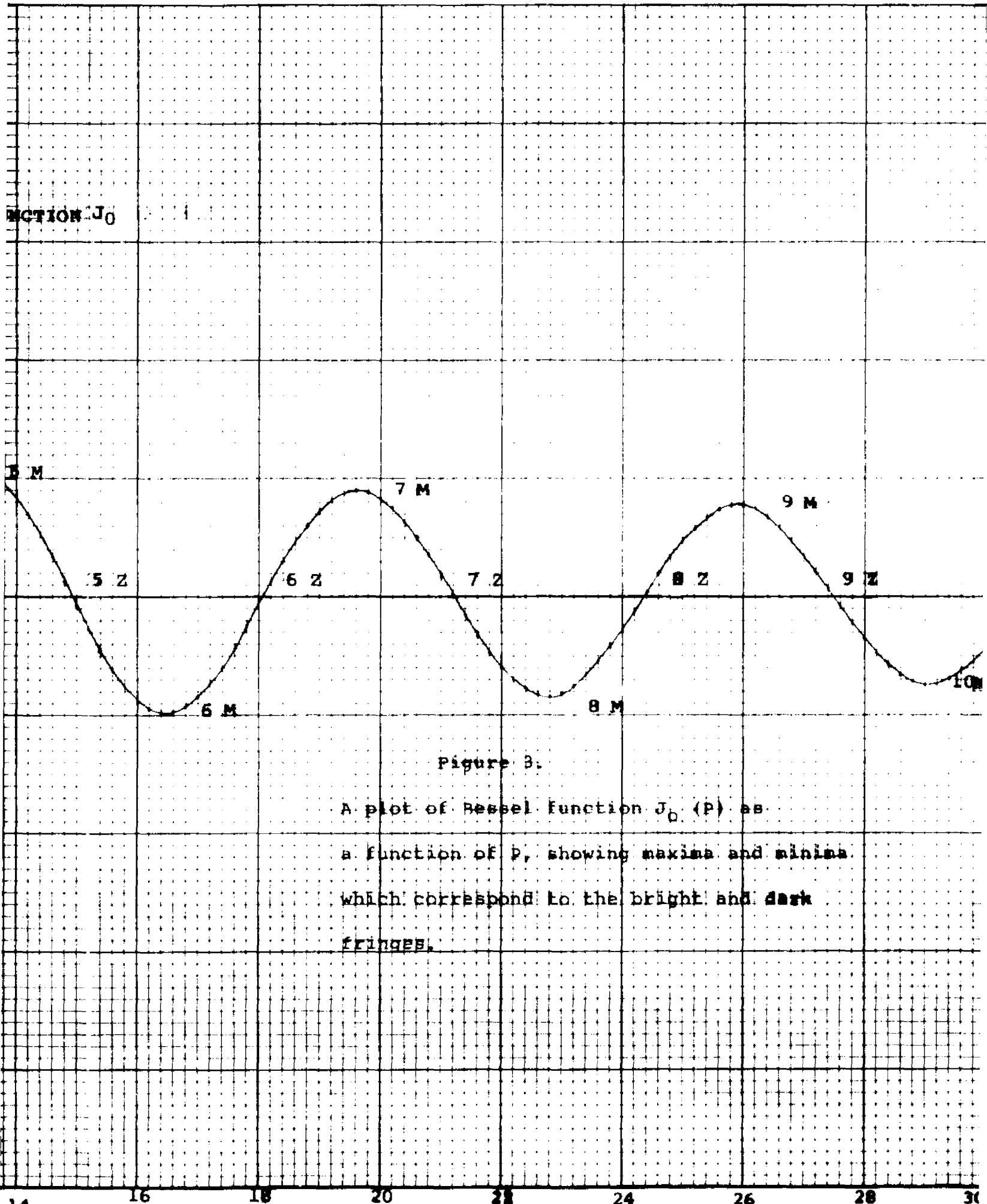

Figure 3.

A plot of Bessel function J_0 (P) as a function of P, showing maxima and minima which correspond to the bright and dark fringes.

Figure 3

Figure 4.

The value of vibration amplitudes represented by various zeros and maxima in the fringe pattern.

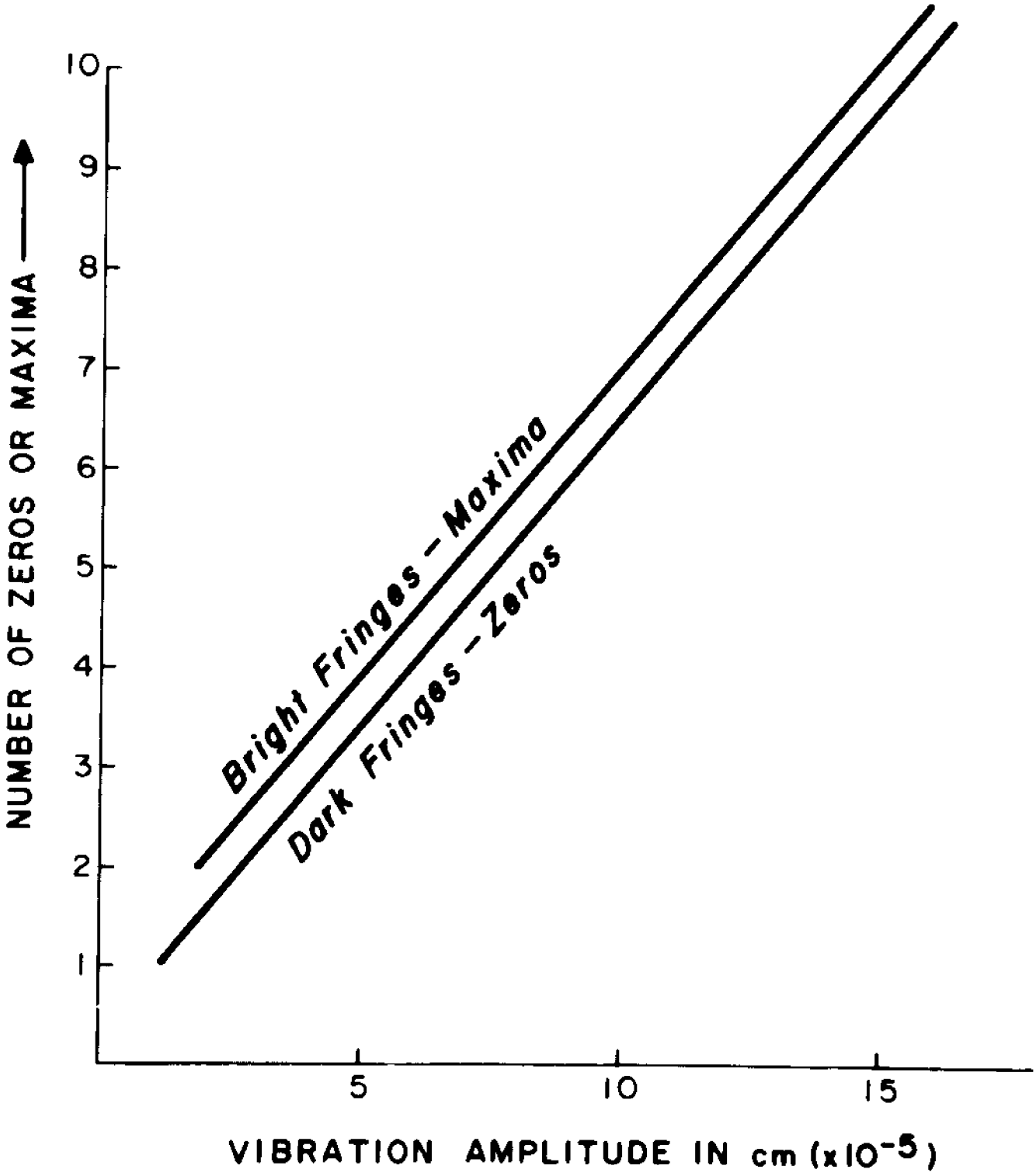
NUMBER OF ZEROS OR MAXIMA
10
9
8
7
6
5
4
3
2
1
Bright Fringes - Maxima
Dark Fringes - Zeros
5
10
15
VIBRATION AMPLITUDE IN cm (x10⁻⁵)

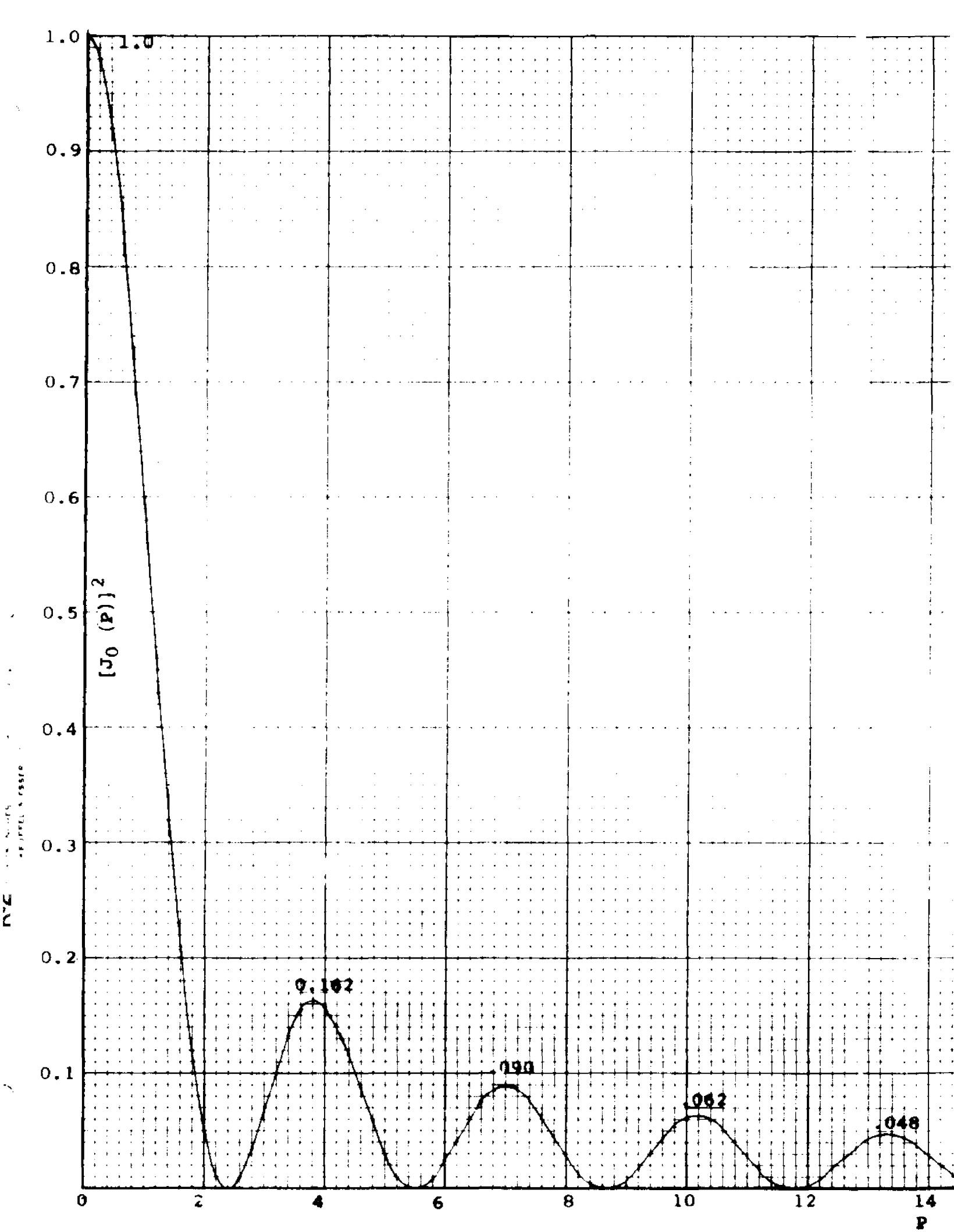
1.0
0.9
0.8
0.7
0.6
0.5
0.4
0.3
0.2
0.1
$[J_0(P)]^2$
1.0
.162
.090
.062
.048
0
2
4
6
8
10
12
14
P

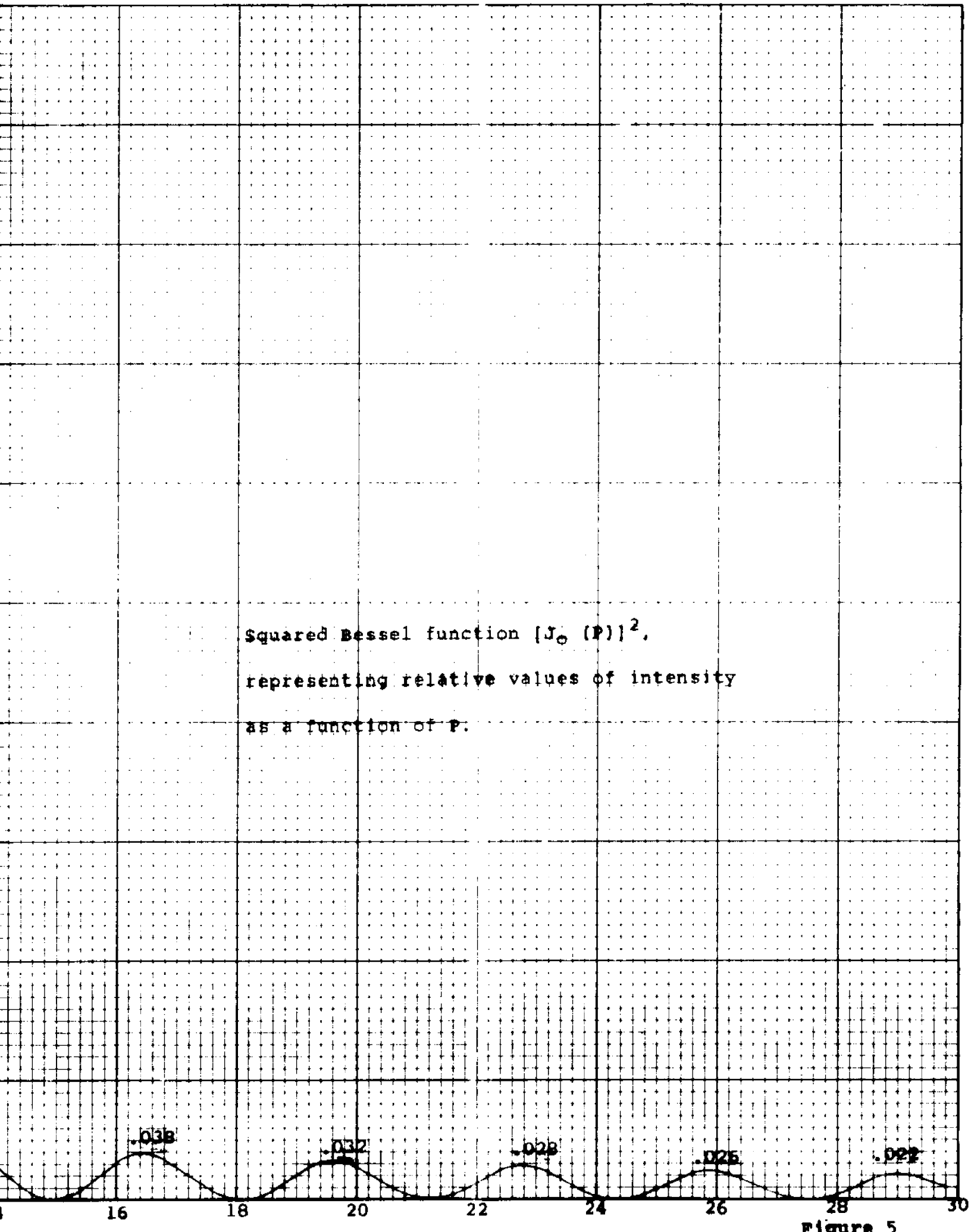

Squared Bessel function $[J_0(P)]^2$, representing relative values of intensity as a function of P.

Figure 5

Figure 6.

Changes in relative value of intensity as a function of vibration amplitude. The intensity of an object drops sharply as it begins to vibrate. The intensity at the second maximum is only 16% of the value at 1st maximum, when the object was stationary. Intensity of the succeeding maxima gradually decreases with higher vibration amplitudes.

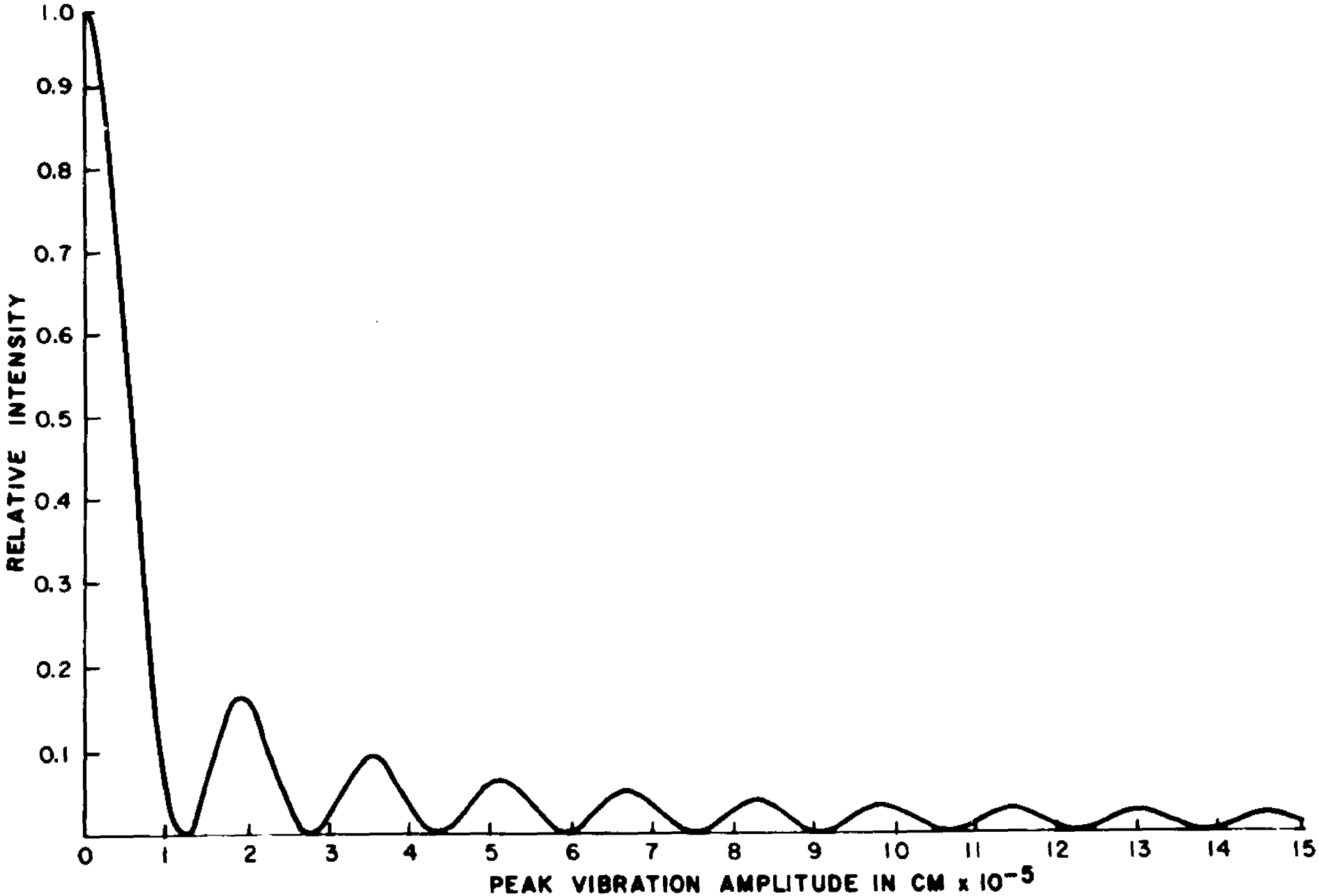
RELATIVE INTENSITY
1.0
0.9
0.8
0.7
0.6
0.5
0.4
0.3
0.2
0.1
0
1
2
3
4
5
6
7
8
9
10
11
12
13
14
15
PEAK VIBRATION AMPLITUDE IN CM x 10^{-5}

Figure 7.

Magnitude of error introduced, when angles Θ_2 and Θ_1 between direction of incident beam, direction of vibration, and axis of observation are not taken into account in calculating the vibration amplitude from the fringe number.

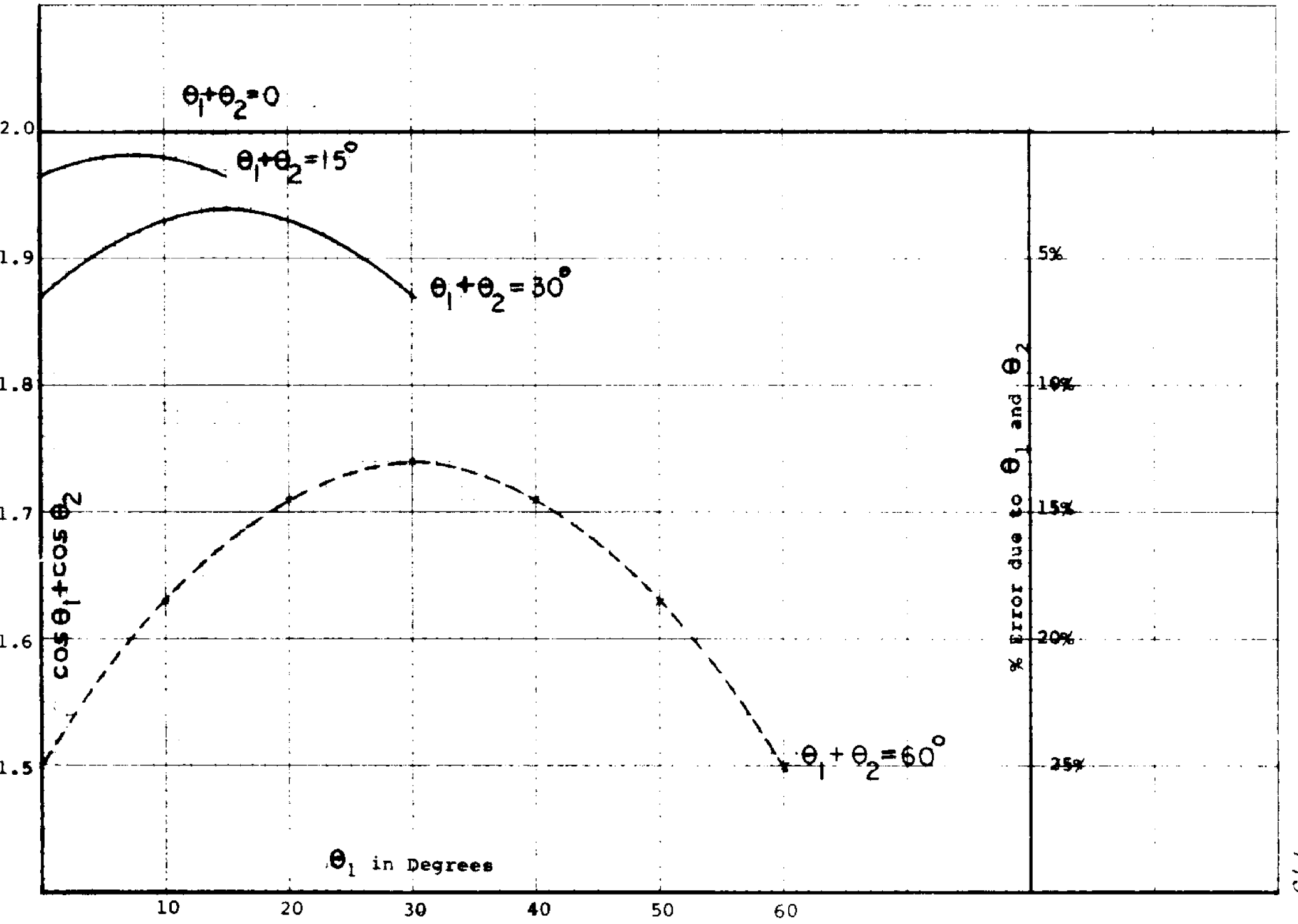
θ1+θ2=0
θ1+θ2=15°
θ1+θ2=30°
θ1+θ2=60°
2.0
1.9
1.8
1.7
1.6
1.5
cos θ1+cos θ2
5%
10%
15%
20%
25%
% Error due to θ1 and θ2
θ1 in Degrees
10
20
30
40
50
60

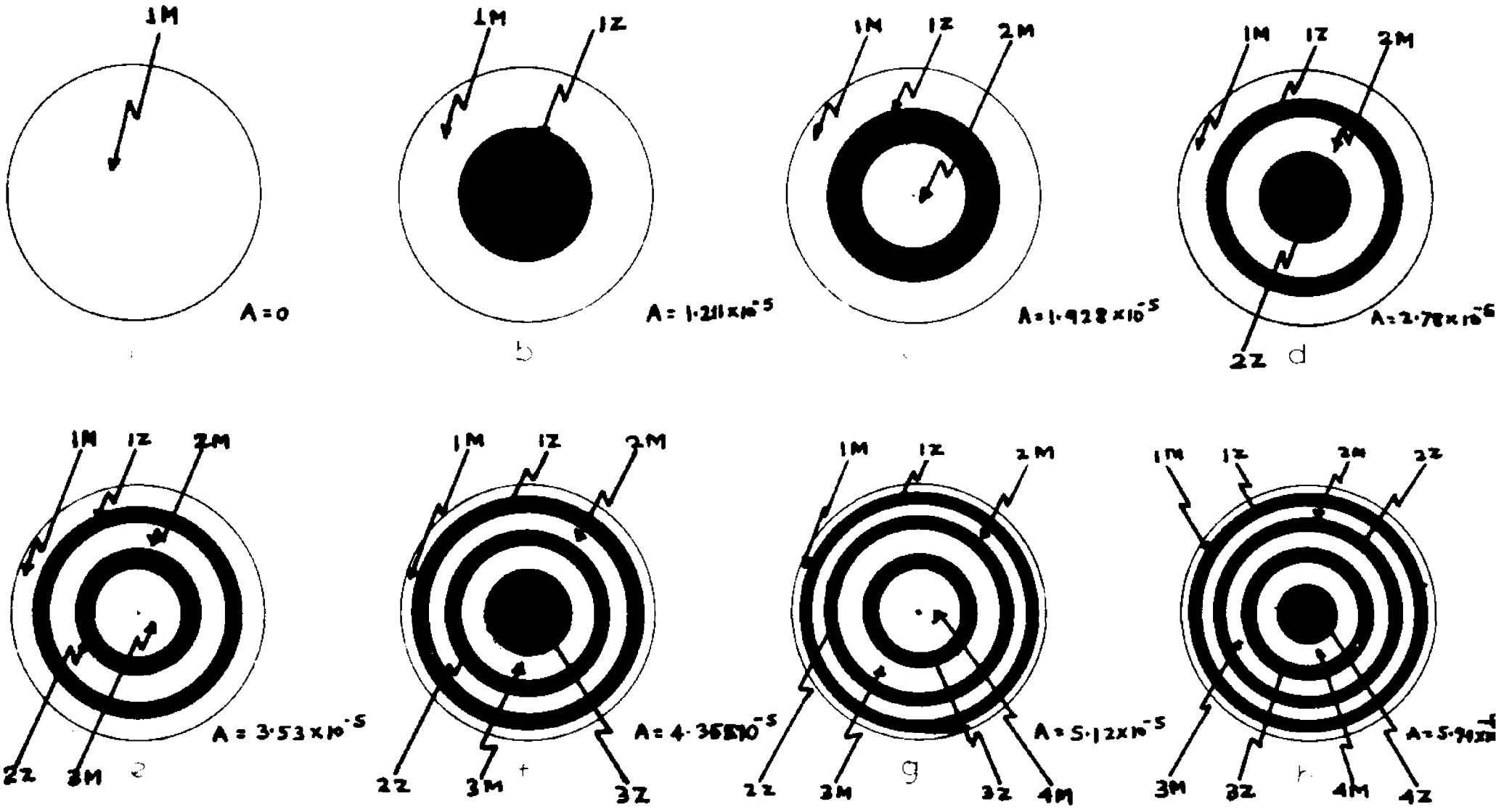

Formation of fringes on a circular membrane with increasing vibration amplitude and their identification by counting.

Figure 8

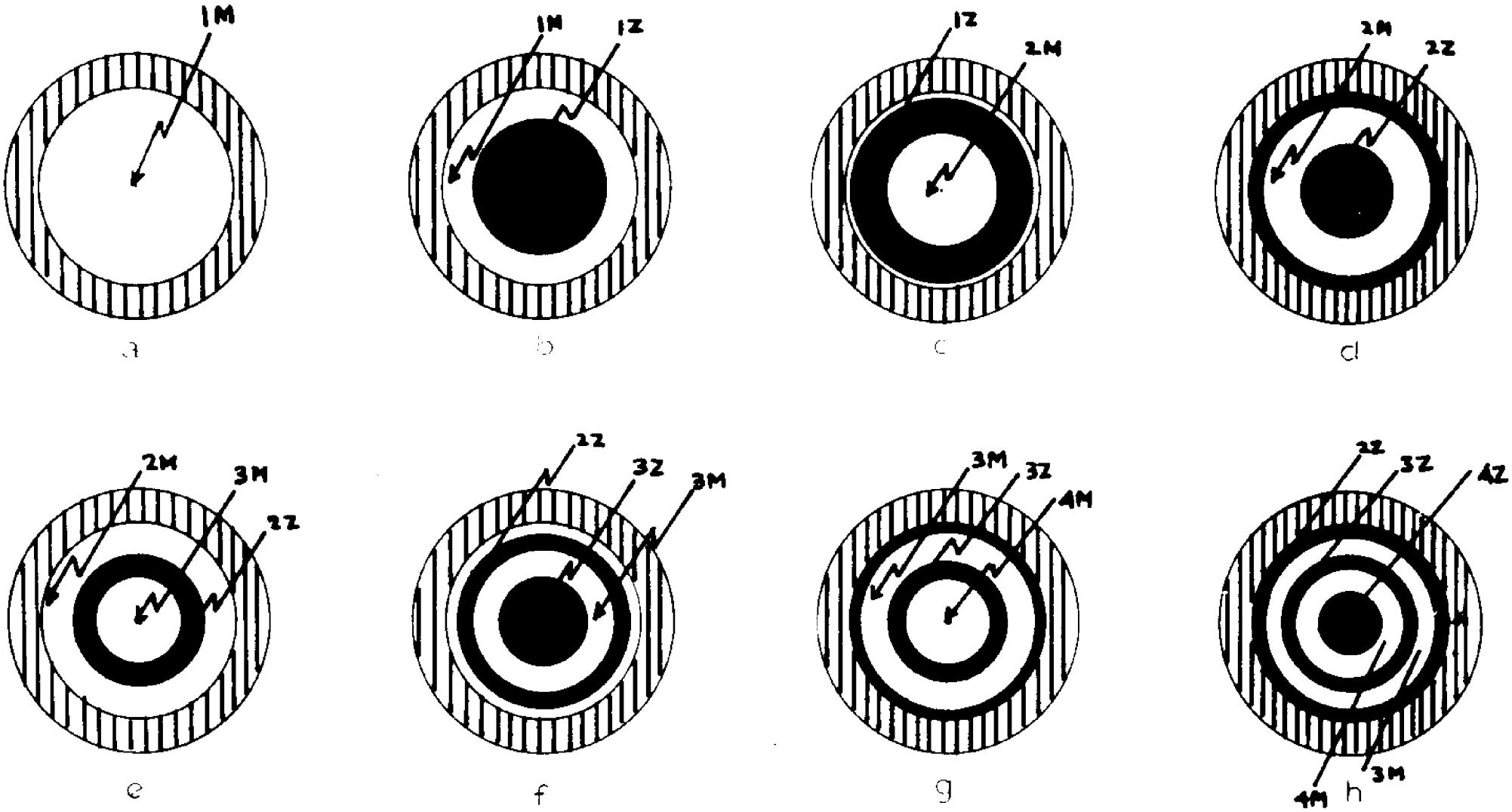

Problems in fringe identification when only part of the membrane is exposed to view.

Figure 9

a

-40 dB

b

-6 dB

c

-4 dB

d

-2 dB

e

0 dB

Figure 10
Gradual formation of the first dark fringe on a circular vibrating plate. Due to the finite range of amplitude over which a fringe develops, correct determination of a maximum or minimum can only be made with the aid of a series of holograms taken at small amplitude intervals.

Figure 11.

Experimental arrangement for time averaged holography.

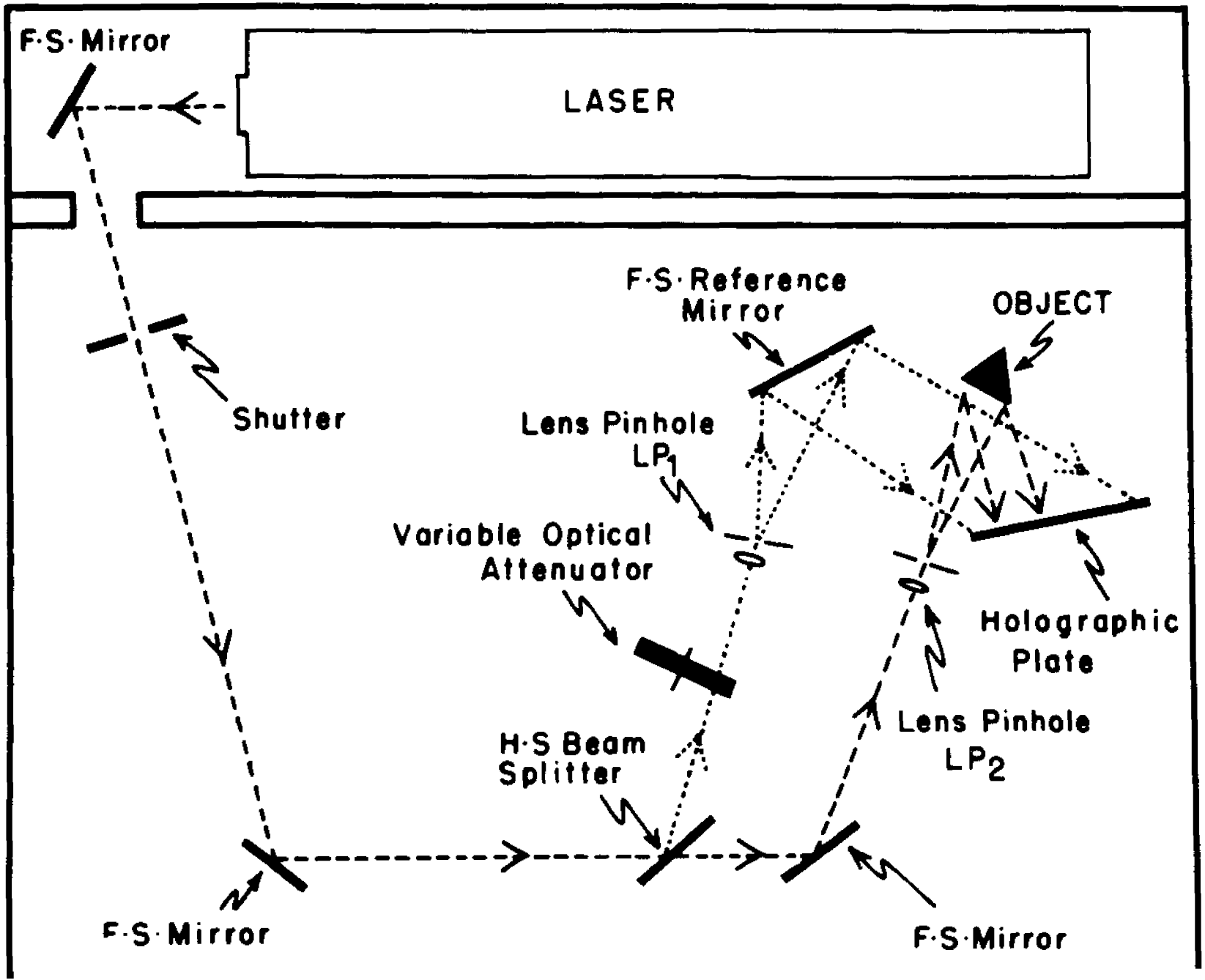
F·S·Mirror
LASER
F·S·Reference Mirror
OBJECT
Shutter
Lens Pinhole LP1
Variable Optical Attenuator
Holographic Plate
H·S Beam Splitter
Lens Pinhole LP2
F·S·Mirror
F·S·Mirror

Figure 12.

Vibration isolated table and enclosure for holographic set up. Mechanical vibrations and air currents must be minimized for successful holography.

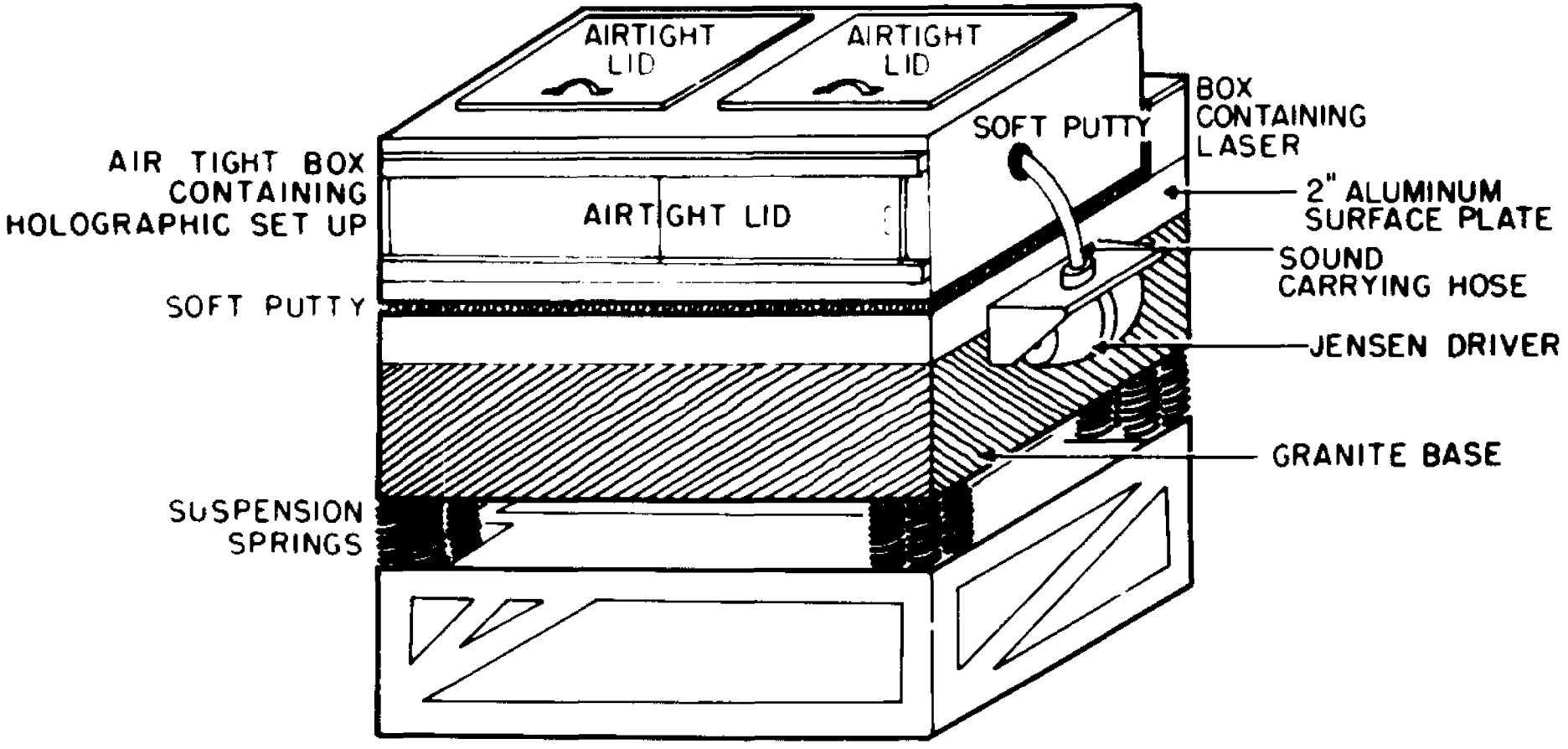
AIRTIGHT LID
AIRTIGHT LID
SOFT PUTTY
BOX CONTAINING LASER
AIR TIGHT BOX CONTAINING HOLOGRAPHIC SET UP
AIRTIGHT LID
2" ALUMINUM SURFACE PLATE
SOUND CARRYING HOSE
SOFT PUTTY
JENSEN DRIVER
GRANITE BASE
SUSPENSION SPRINGS

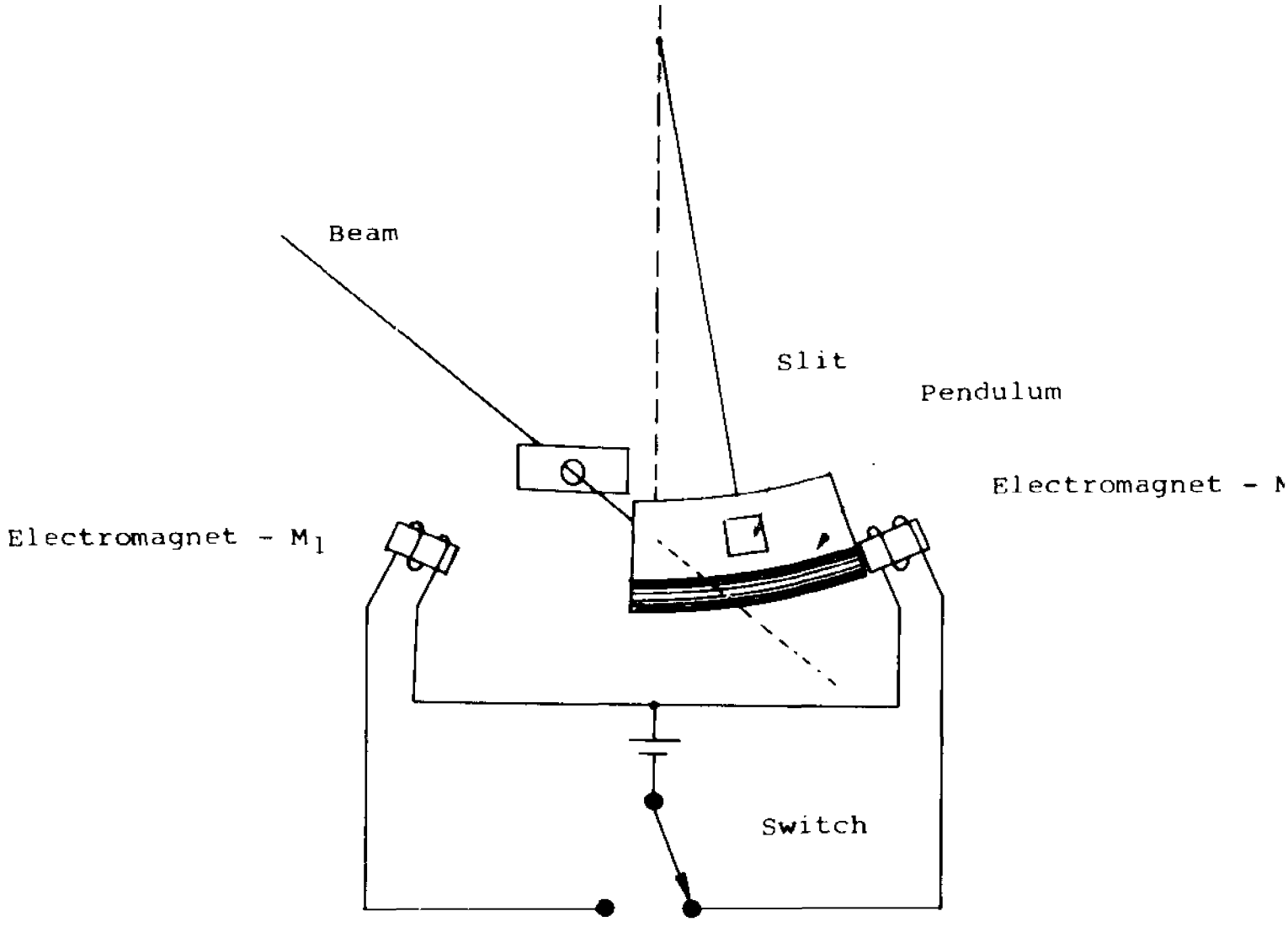

Figure 13.

Elements of a silent shutter. A pendulum carrying an adjustable slit is held by an electromagnet. When current is switched to the other electromagnet, the pendulum swings over and is held at the other end. The exposure time is varied by adjusting the width of the slit.

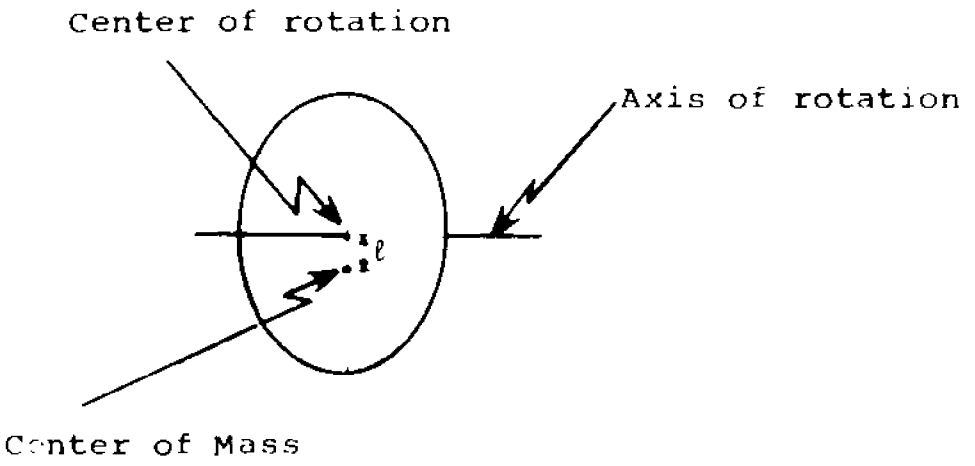

Figure 14. A compound pendulum

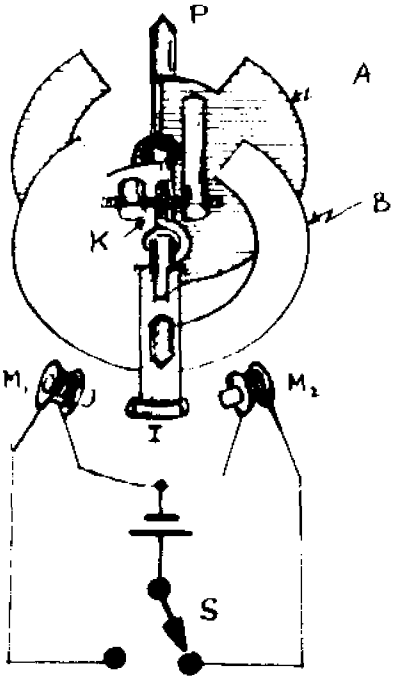

Figure 15. Components of the compound pendulum shutter P - pivot; A, B - plates forming the compound pendulum and the slit; K - screw for adjustment of slit width; I - soft iron pole piece; M_1, M_2 - electromagnets.

Figure 16.

Operating sequence of the silent shutter.

1. Shutter is held by the electromagnet M_2 in the off position.
2. Switching the current to electromagnet M_1 releases the shutter which swings over, making the exposure.
3. At the end of the swing the soft iron pole piece is held by electromagnet M_1 and the shutter stays in the off position.

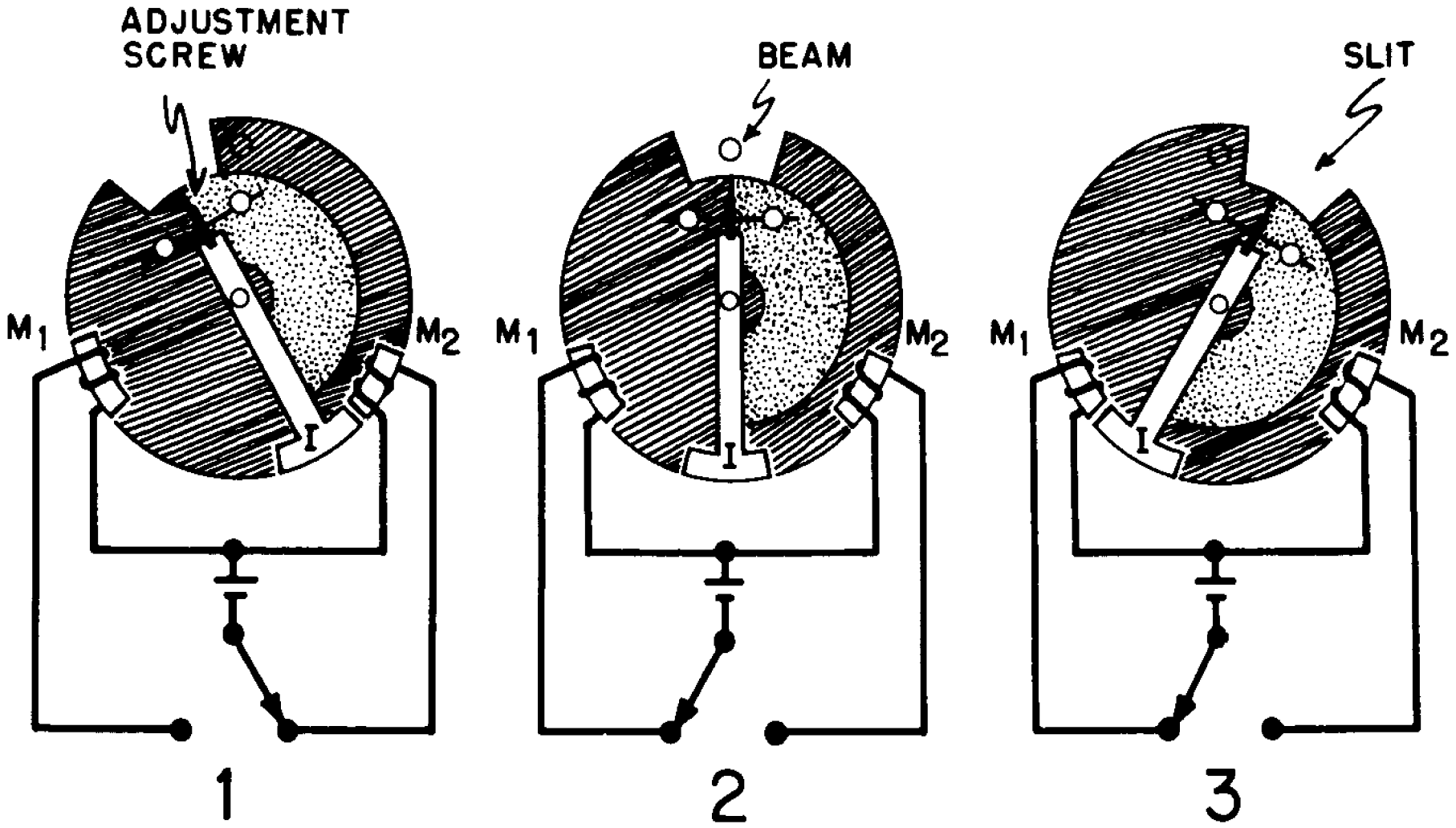
ADJUSTMENT SCREW
BEAM
SLIT
M1
M2
I
1
2
3

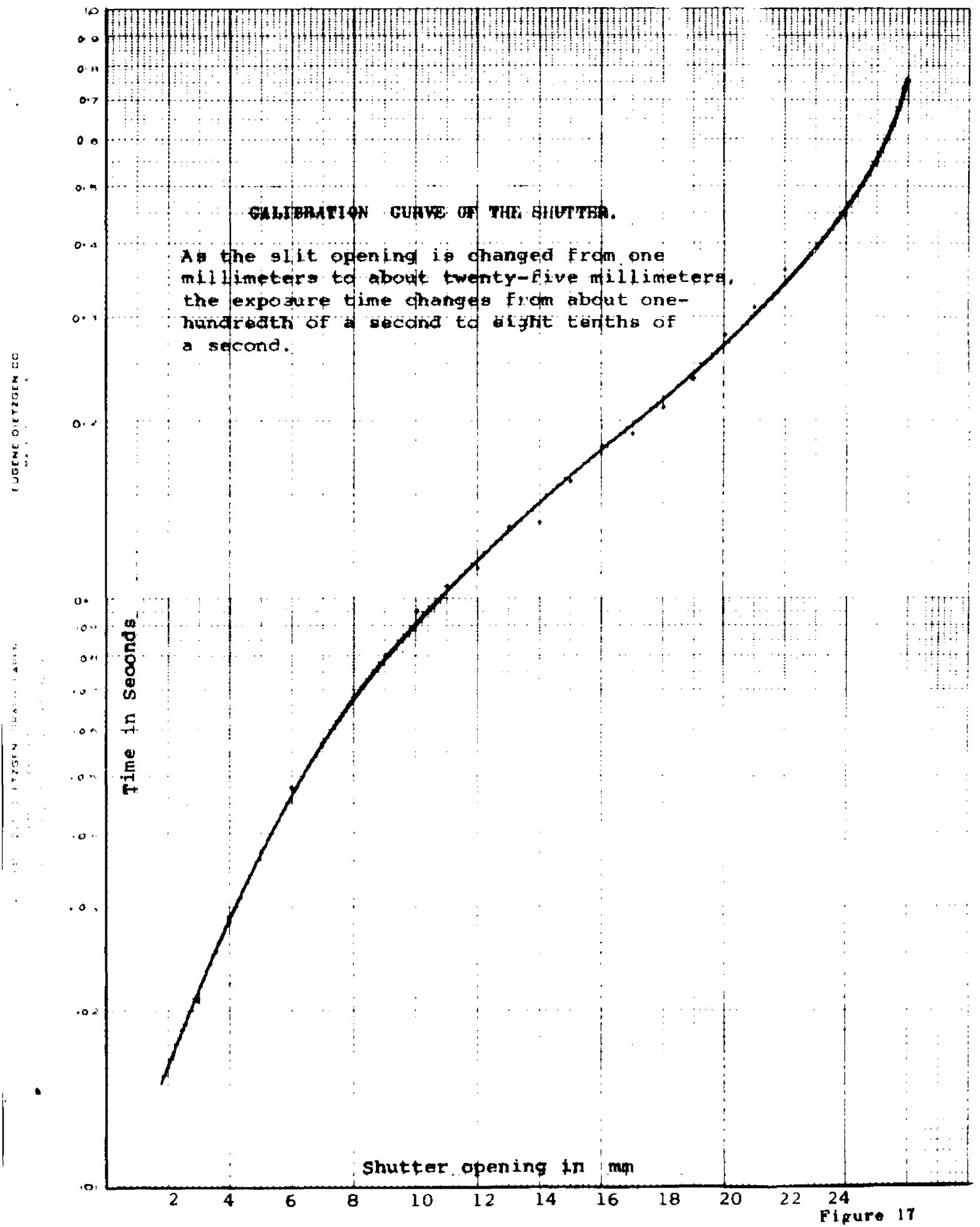
CALIBRATION CURVE OF THE SHUTTER.
As the slit opening is changed from one millimeters to about twenty-five millimeters, the exposure time changes from about one-hundredth of a second to eight tenths of a second.
Time in Seconds
Shutter opening in mm
2
4
6
8
10
12
14
16
18
20
22
24

Figure 17

Figure 18.

Air brush. Small quantities of bronze powder suspended in ether was sprayed on the tympanic membrane using this instrument. Very uniform thin coat was obtained.

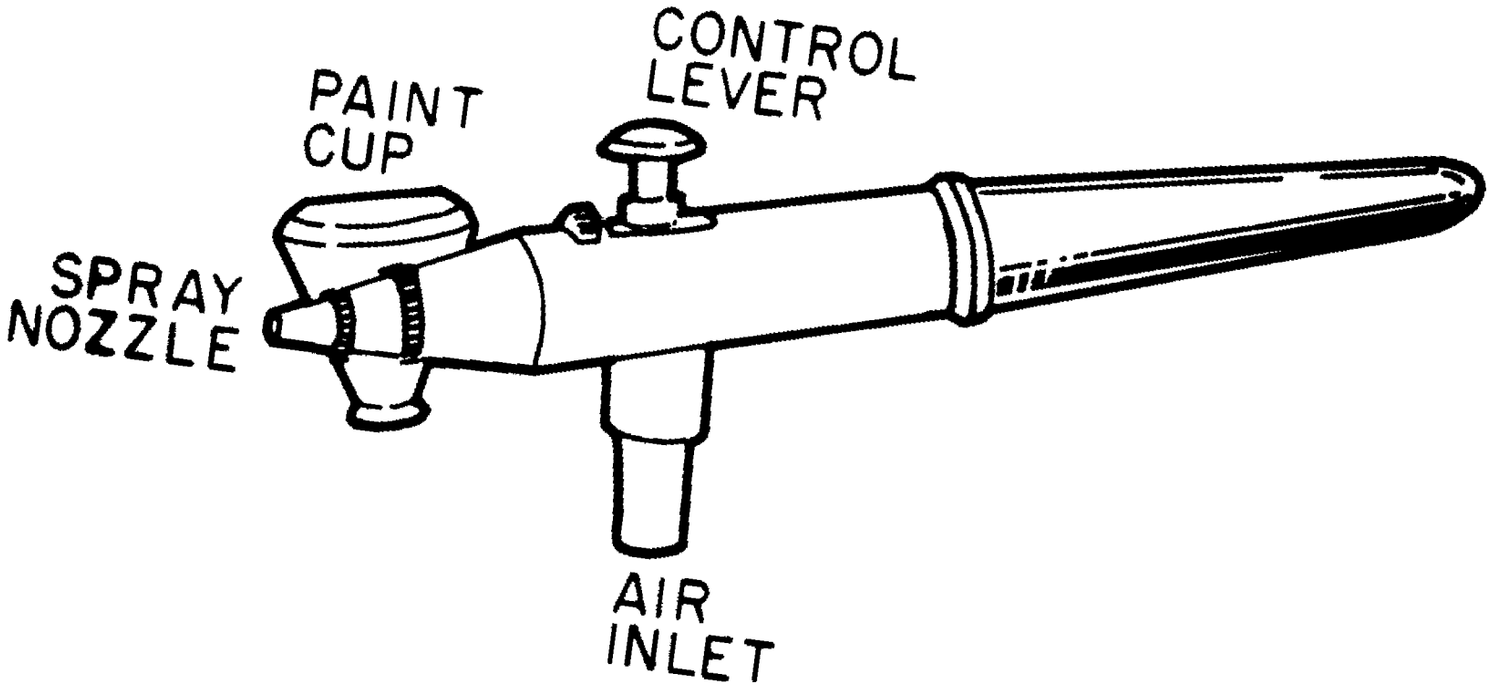
CONTROL
LEVER
PAINT
CUP
SPRAY
NOZZLE
AIR
INLET

Figure 19.

A series of holographic reconstructions of the cat tympanic membrane vibrating at 600 Hz. The reconstructions show the development of fringes on the tympanic membrane and on the malleus as the vibration amplitude is increased in two dB steps.

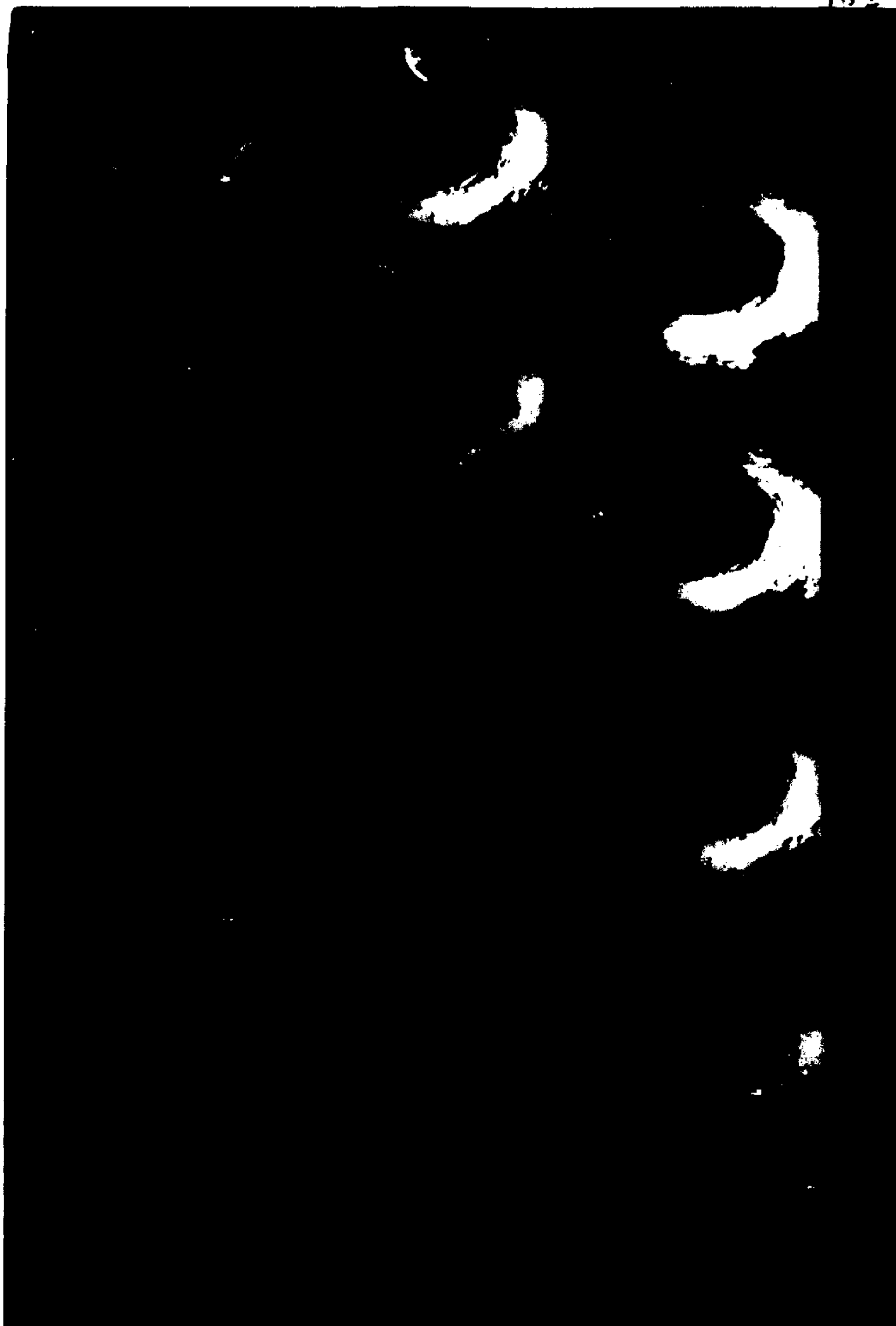

Figure 20.

A simplified line drawing of vibration pattern at 600 Hz, 111 dB SPL, with identification of the dark fringes.

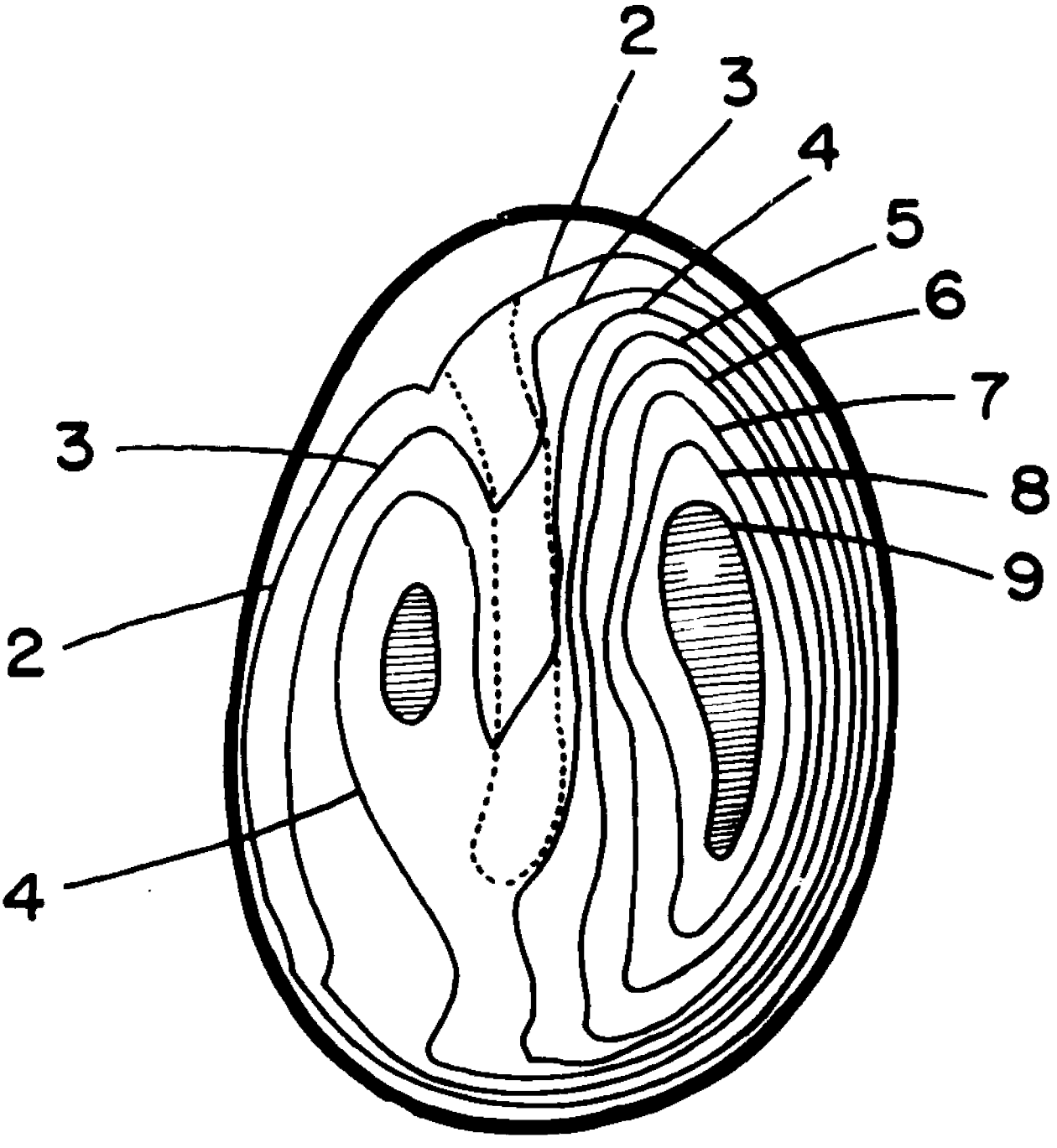
2
3
4
5
6
7
8
9
3
2
4

Figure 21.

Axis of rotation of the malleus, and the direction of fringes on the malleus are parallel to each other.

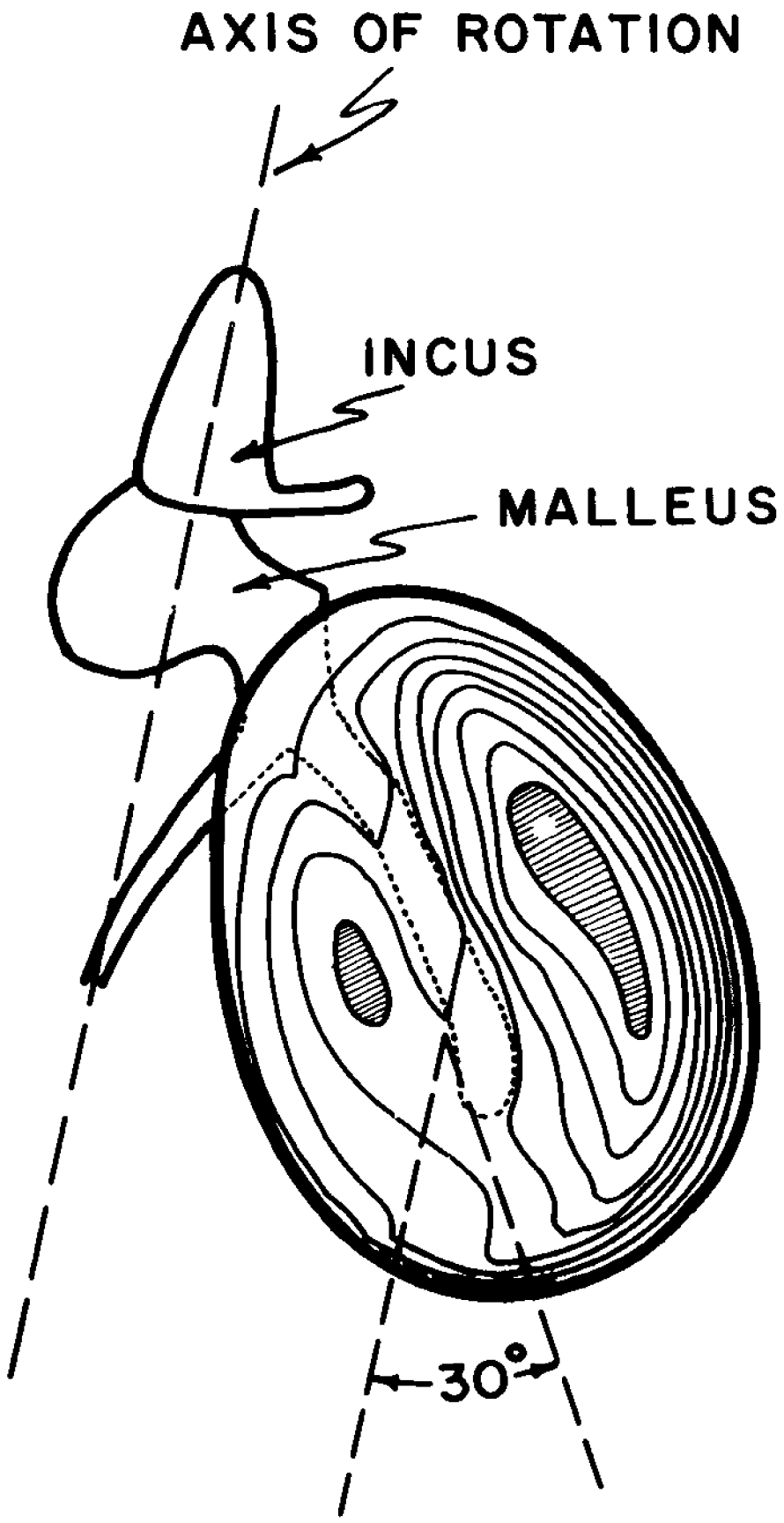
AXIS OF ROTATION
INCUS
MALLEUS
30°

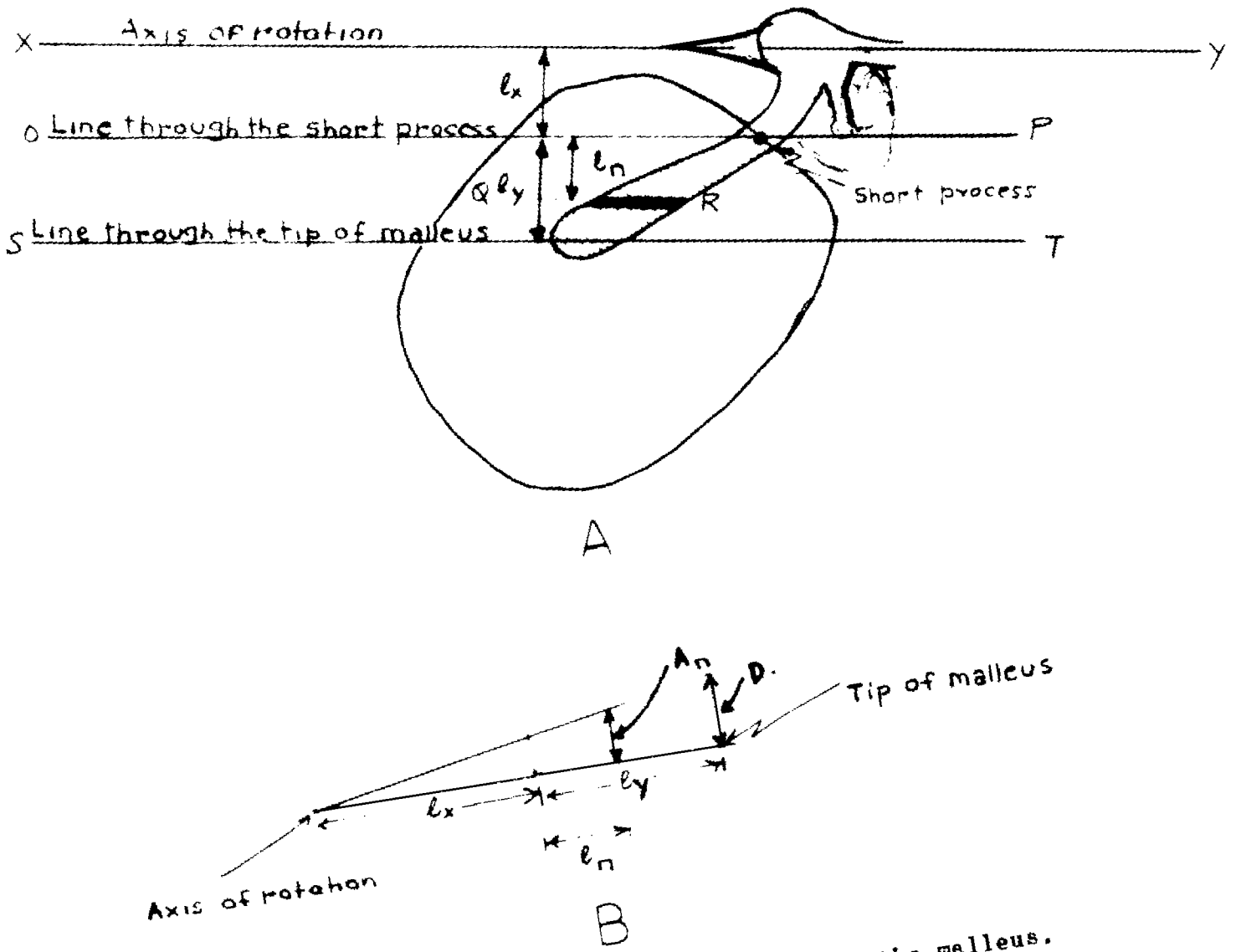

Figure 22. Geometry describing the rotation of the malleus.

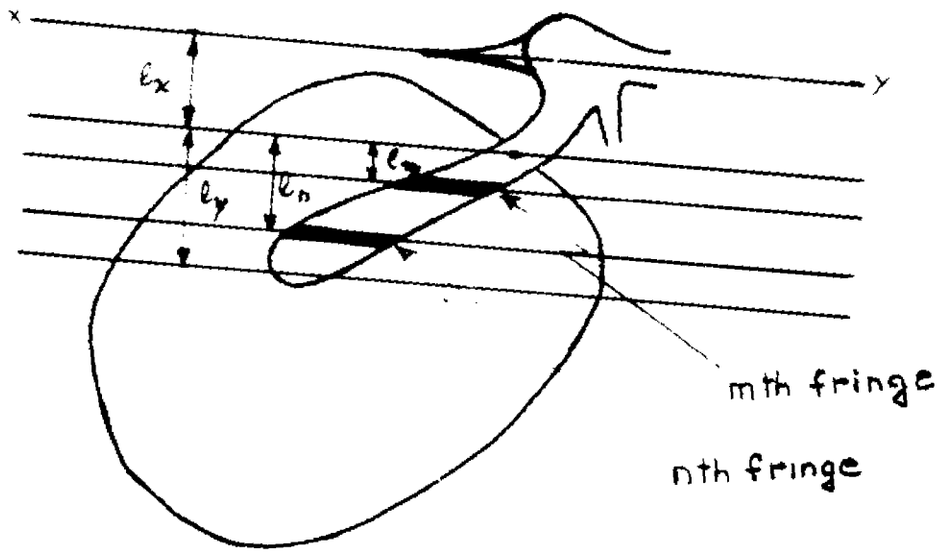

Figure 23. Perpendicular distance, of two fringes on the malleus from the short process, and of the short process from the axis of rotation.

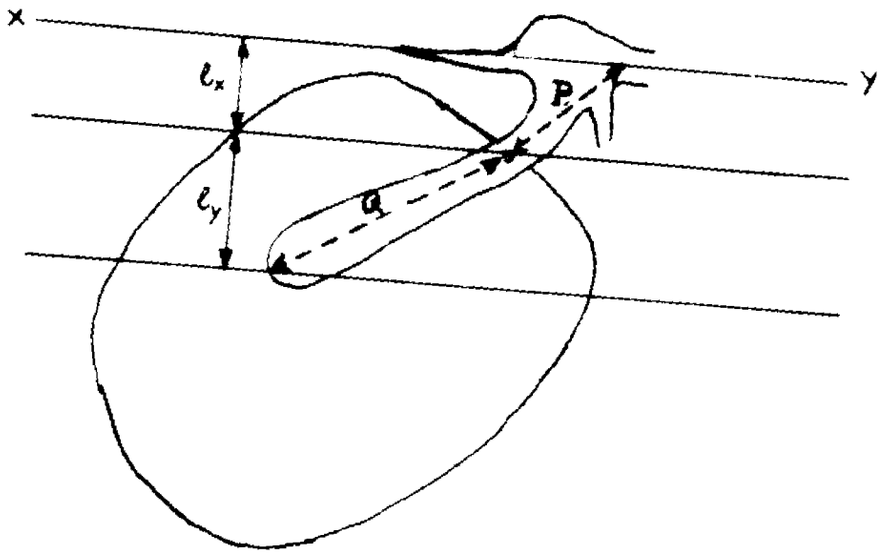

Figure 24. Distance between,(1) tip of the malleus and the short process, (2) short process and the axis of rotation.

Figure 25.

Effect of coating the tympanic membrane with bronze powder on the vibration amplitude of the malleus. 969 Hz, 108 dB SPL.
(A) Malleus coated alone.
(B) Tympanic Membrane coated.
There is no detectable change in the vibration amplitude of the malleus.

Figure 26.

SPL required to produce 10^{-7} cm umbo displacement, a comparison between holographic results and those obtained with interferometer. The agreement between the two sets of data is within five dB.

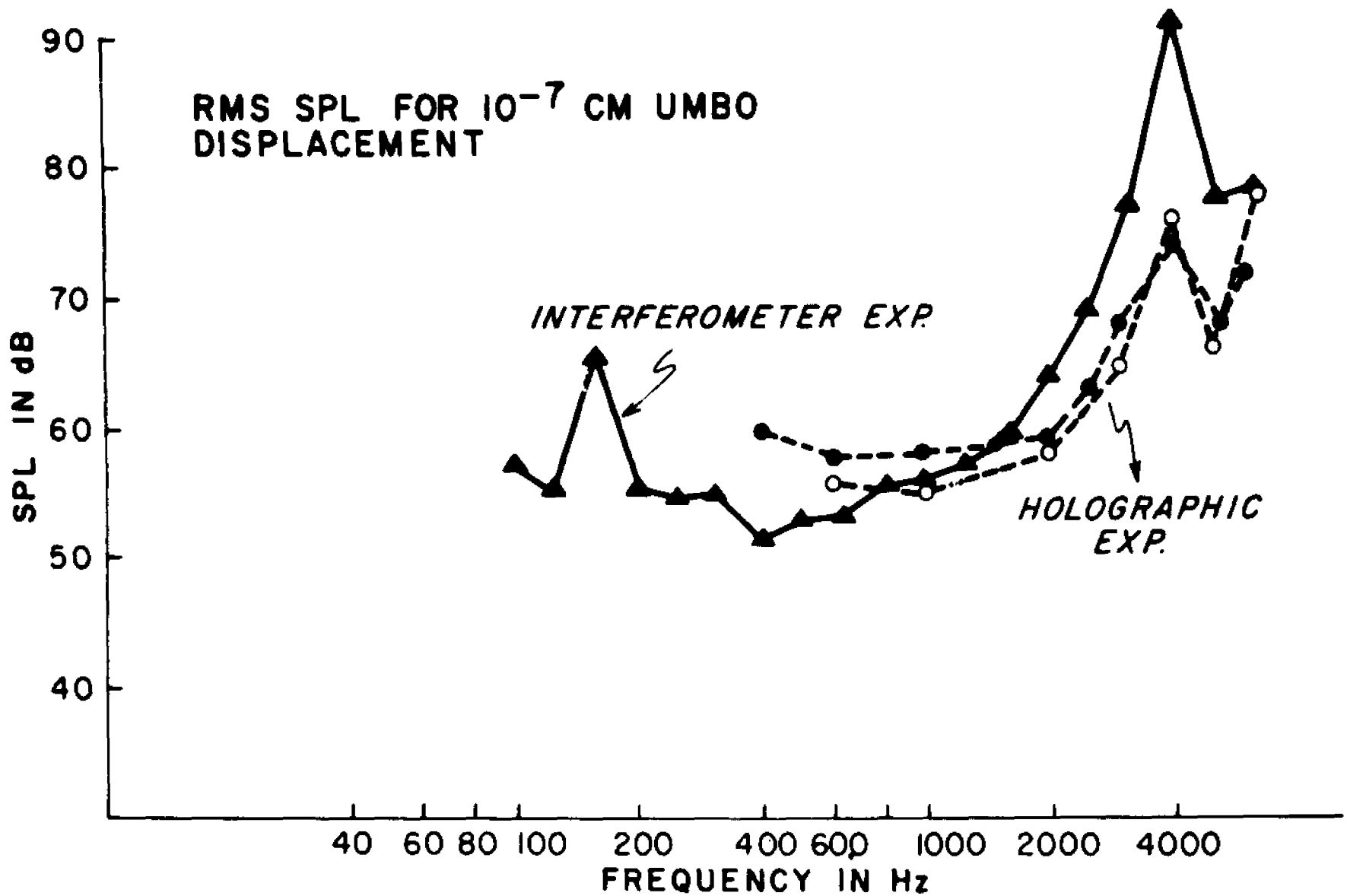
RMS SPL FOR 10^{-7} CM UMBO DISPLACEMENT
INTERFEROMETER EXP.
HOLOGRAPHIC EXP.
SPL IN dB
90
80
70
60
50
40
40 60 80 100 200 400 600 1000 2000 4000
FREQUENCY IN Hz

Figure 27.

Areas of approximately equal vibration amplitude cut out for determination of volume displacement.

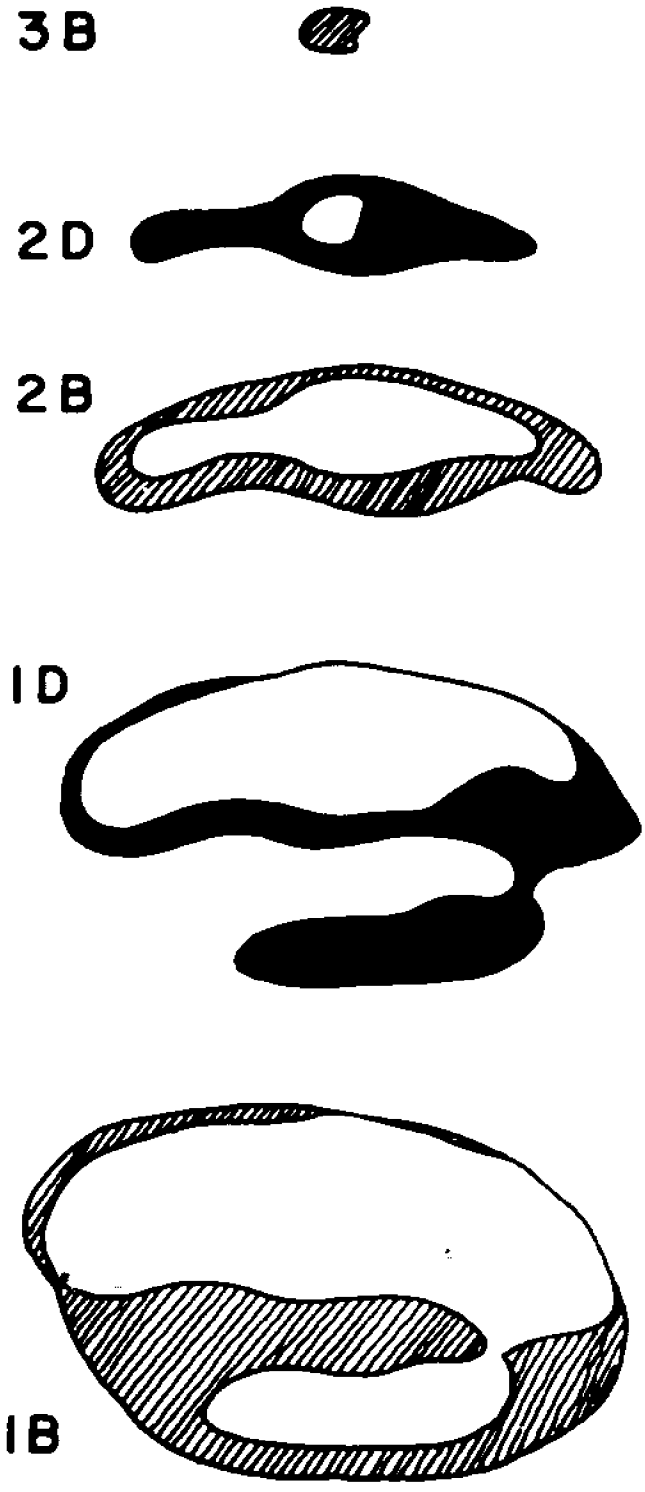
3B
2D
2B
1D
1B

Figure 28.

Volume displacement of the tympanic membrane as a function of frequency, calculated from the holographic data and from the middle ear impedance data. Close agreement between the two show that the use of fresh cadavers in holographic experiments was not detrimental to the vibrational properties of the tympanic membrane.

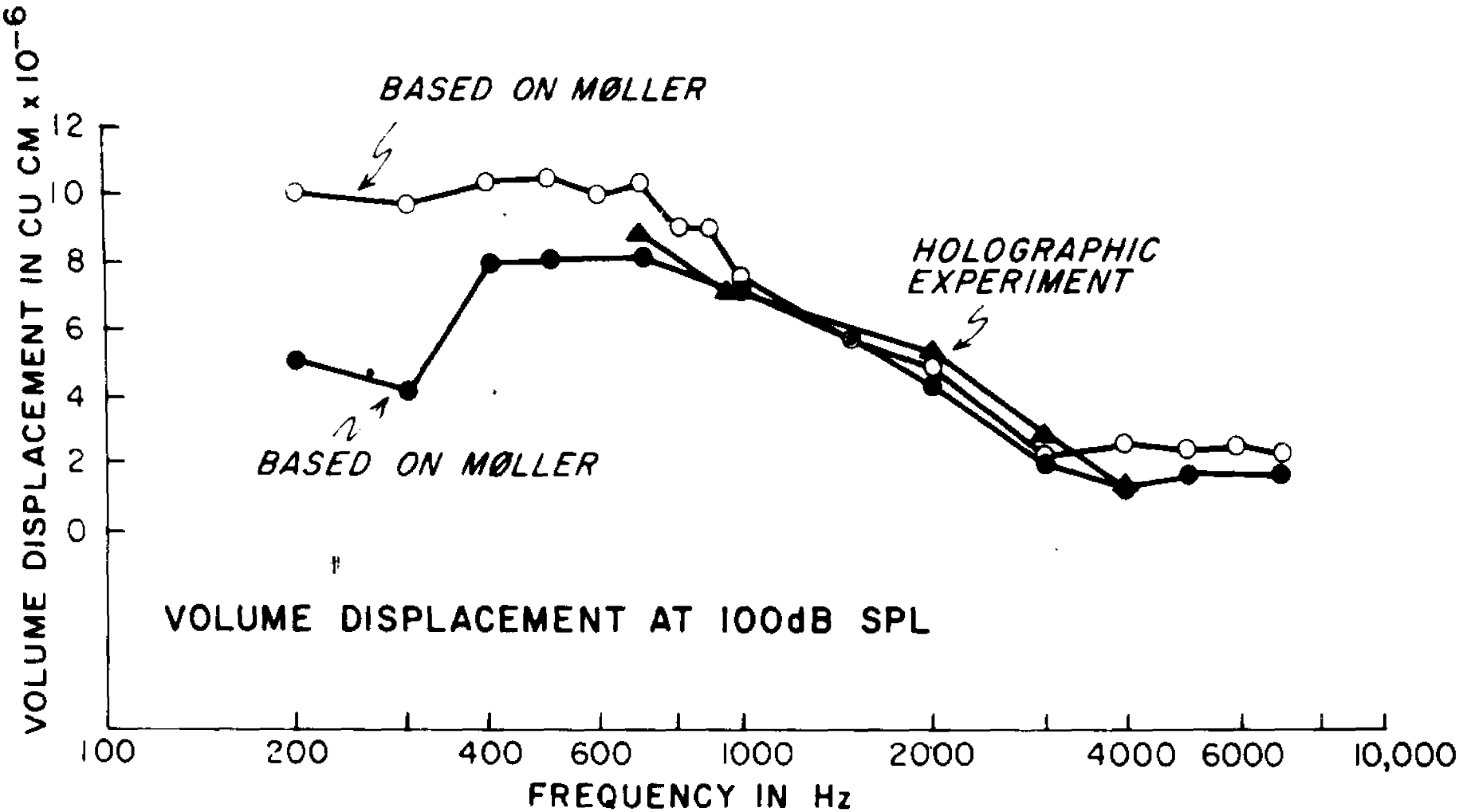
BASED ON MØLLER
HOLOGRAPHIC EXPERIMENT
BASED ON MØLLER
VOLUME DISPLACEMENT AT 100dB SPL
VOLUME DISPLACEMENT IN CU CM x 10⁻⁶
0
2
4
6
8
10
12
100
200
400
600
1000
2000
4000
6000
10,000
FREQUENCY IN Hz

Figure 29.

Vibration pattern of the cat tympanic membrane at four frequencies. Vibration pattern remains substantially unchanged up to a frequency around 3000 Hz.

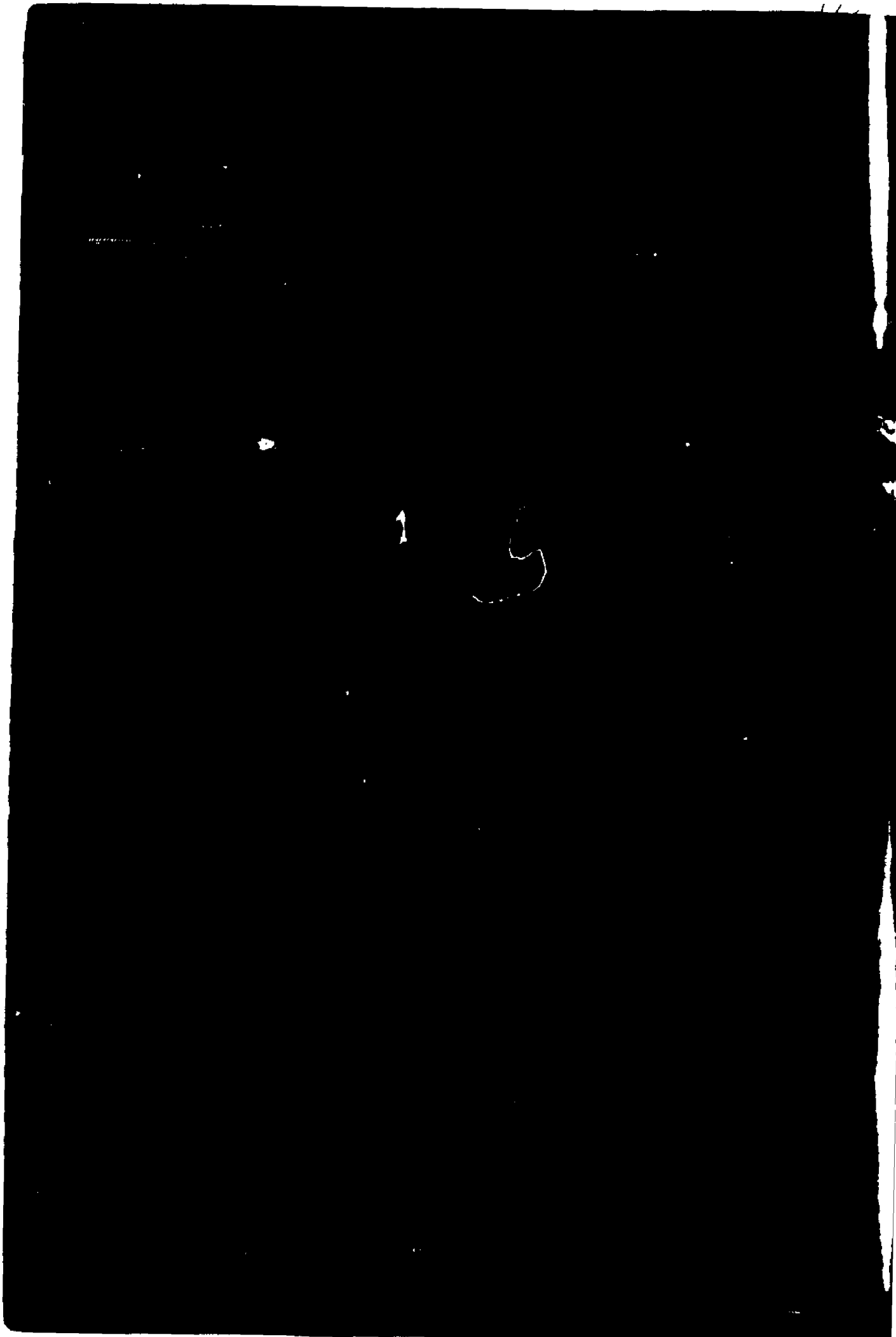

Figure 30.

Vibration pattern of the cat tympanic membrane at ten frequencies. Above 3000 Hz the vibration pattern changes sharply and above 4000 Hz the membrane vibrations break up in sections.

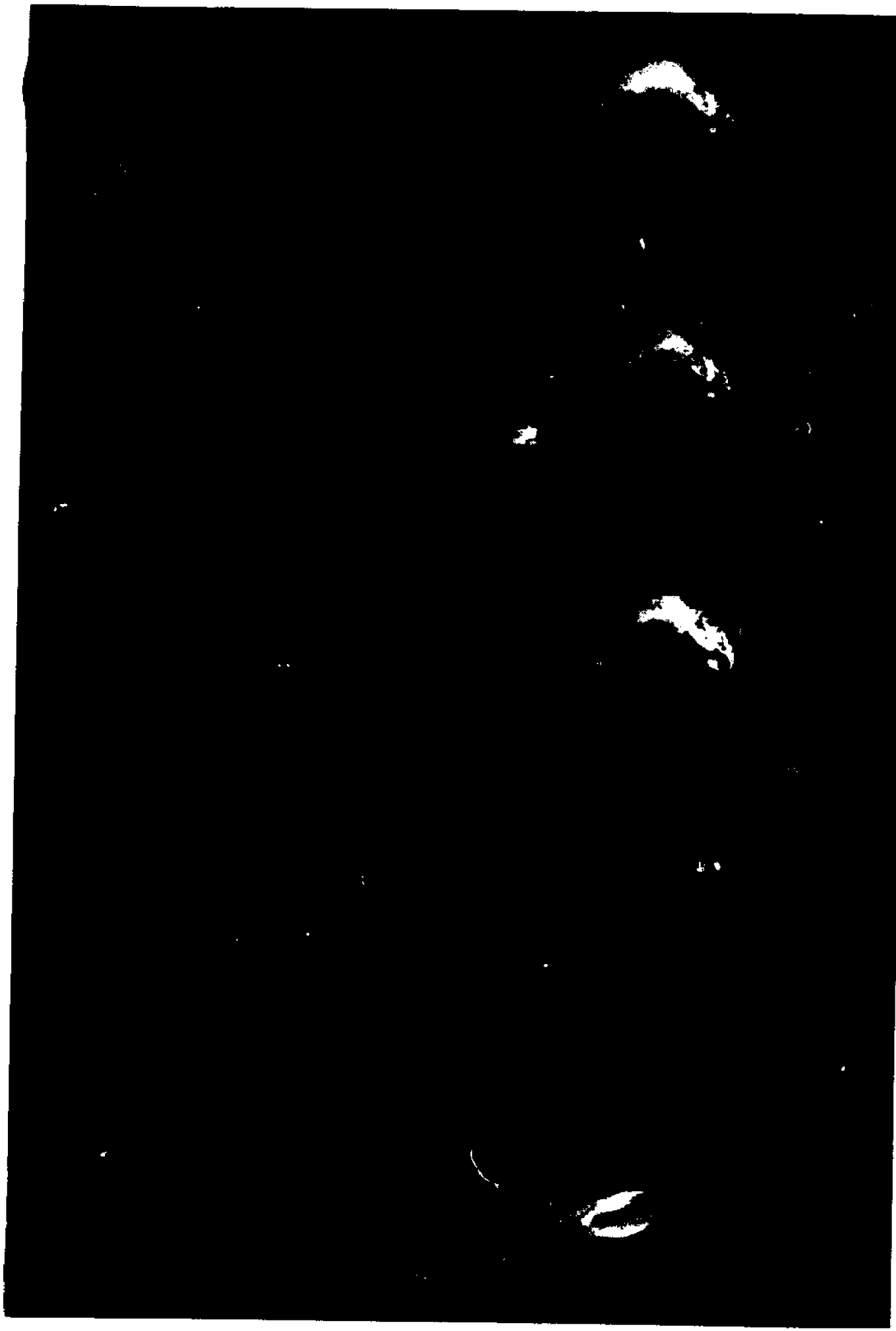

Figure 31.

Malleus, anterior and posterior amplitudes at 100 dB SPL (cat L). The maximum in the posterior region is highest in amplitude. The maximum in the anterior region is of about the same amplitude as that at the tip of the malleus.

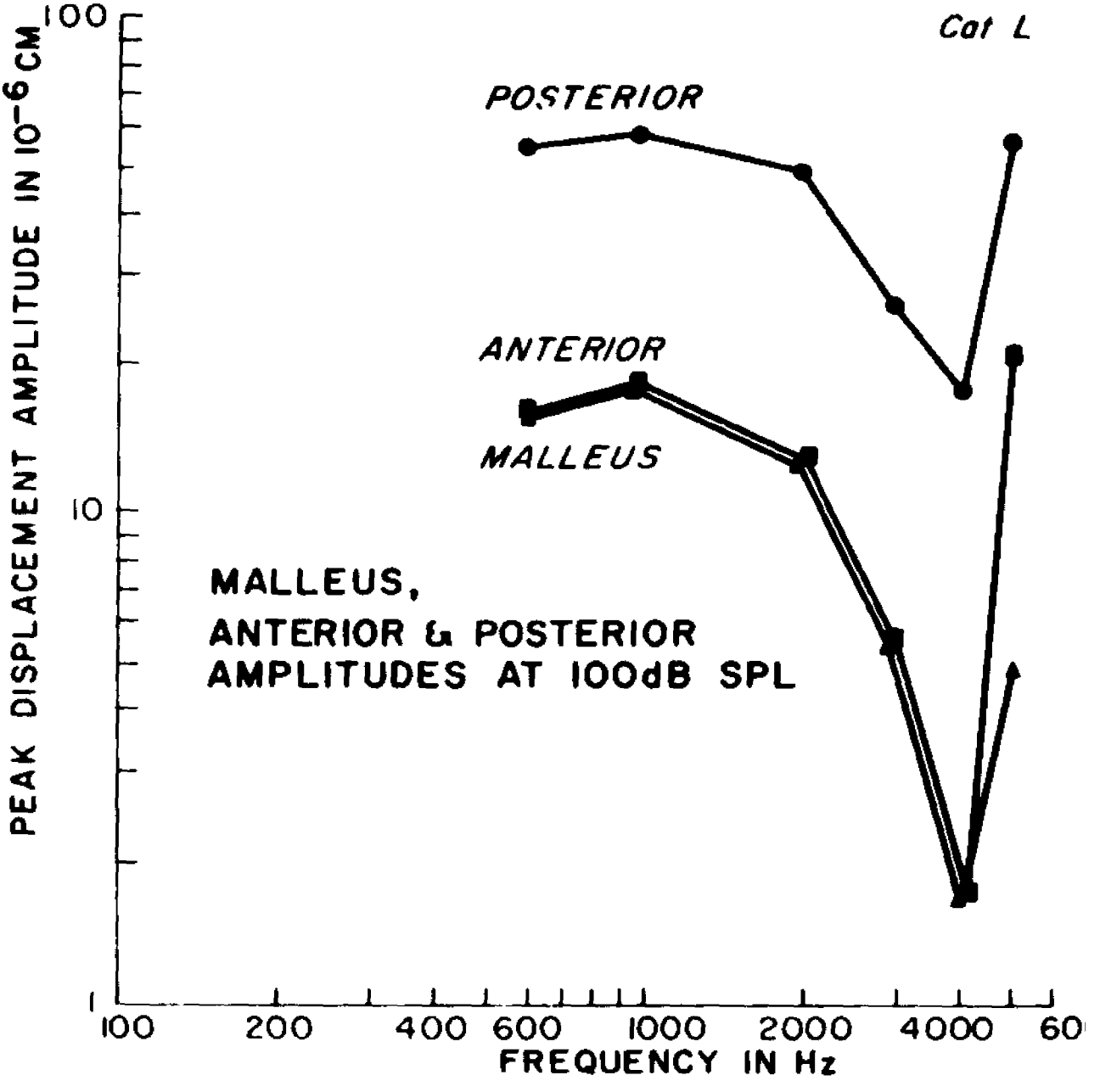
Cat L
POSTERIOR
ANTERIOR
MALLEUS
MALLEUS,
ANTERIOR & POSTERIOR
AMPLITUDES AT 100dB SPL
PEAK DISPLACEMENT AMPLITUDE IN 10^{-6} CM
100
10
1
100
200
400
600
1000
2000
4000
FREQUENCY IN Hz

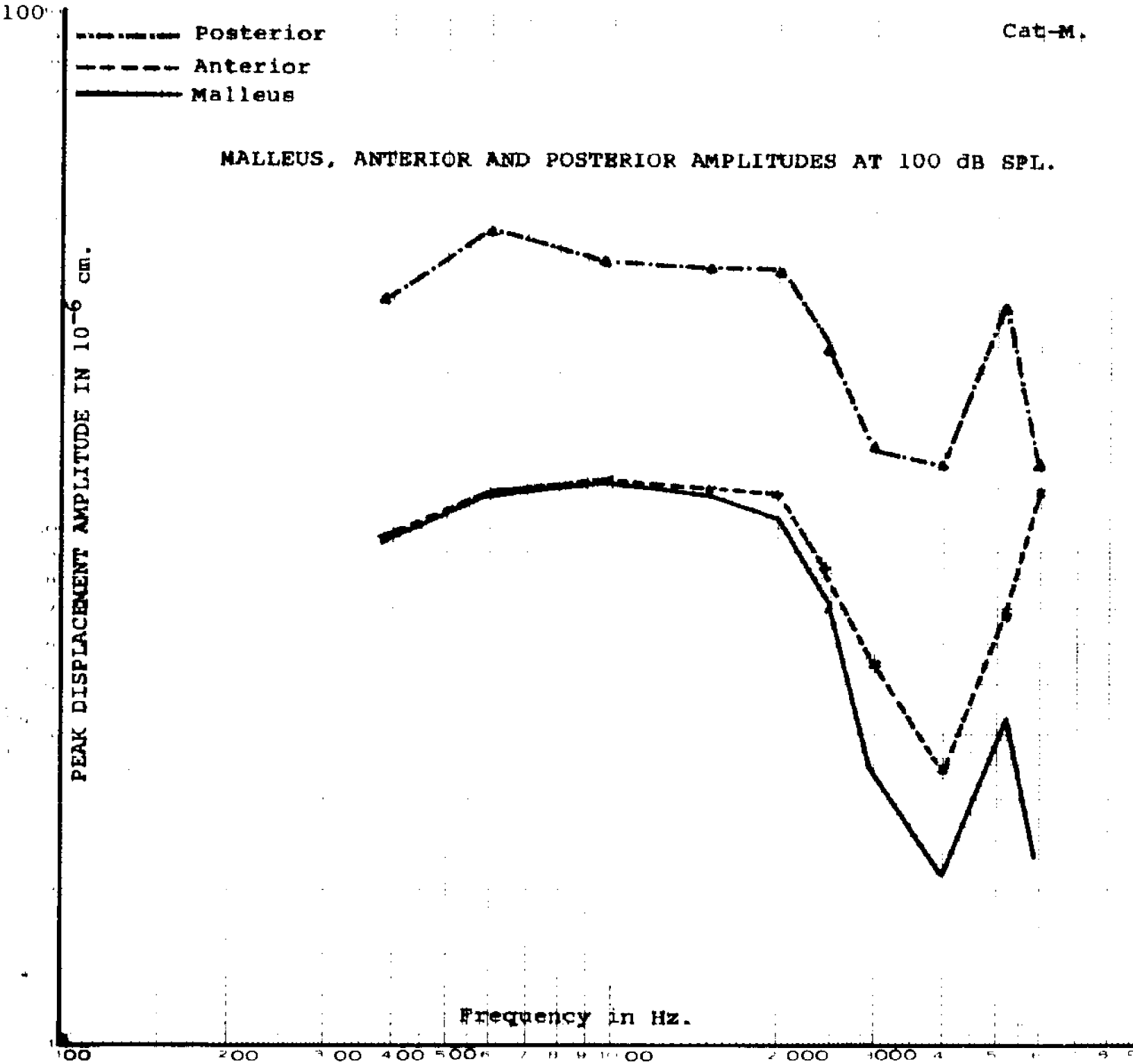
100
Posterior
Anterior
Malleus
Cat-M.
MALLEUS, ANTERIOR AND POSTERIOR AMPLITUDES AT 100 dB SPL.
PEAK DISPLACEMENT AMPLITUDE IN 10^{-6} cm.
Frequency in Hz.
100
200
300
400
500
1000
2000
3000

Figure 32.

Figure 33.

Ratio's between anterior, posterior, and mallar amplitudes. The point of maximum vibration in the anterior region has an amplitude between 1 and 1.3 times that of the mallar tip. For the point of maximum vibration in the posterior region below 2000 Hz, this ratio is about three. The averaged displacement over the entire tympanic membrane below 2000 Hz, is about 1.3 times that at the tip of the malleus.

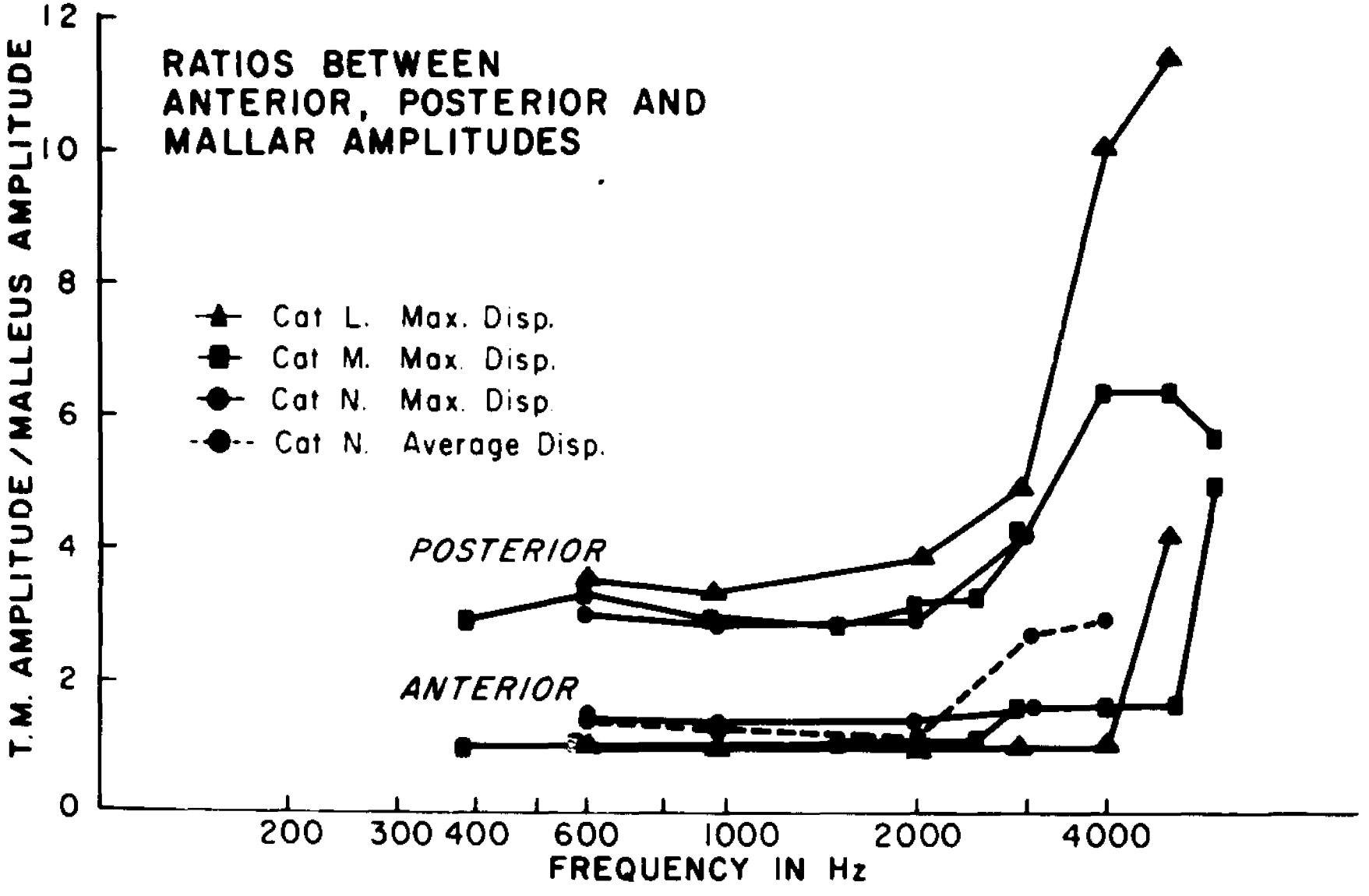
RATIOS BETWEEN
ANTERIOR, POSTERIOR AND
MALLAR AMPLITUDES
Cat L. Max. Disp.
Cat M. Max. Disp.
Cat N. Max. Disp.
Cat N. Average Disp.
POSTERIOR
ANTERIOR
T.M. AMPLITUDE / MALLEUS AMPLITUDE
0
2
4
6
8
10
12
200
300
400
600
1000
2000
4000
FREQUENCY IN Hz

Figure 34.

Malleus displacement amplitude at 100 dB SPL in three cats. Good agreement of data shows that the repeatability of these experiments is excellent.

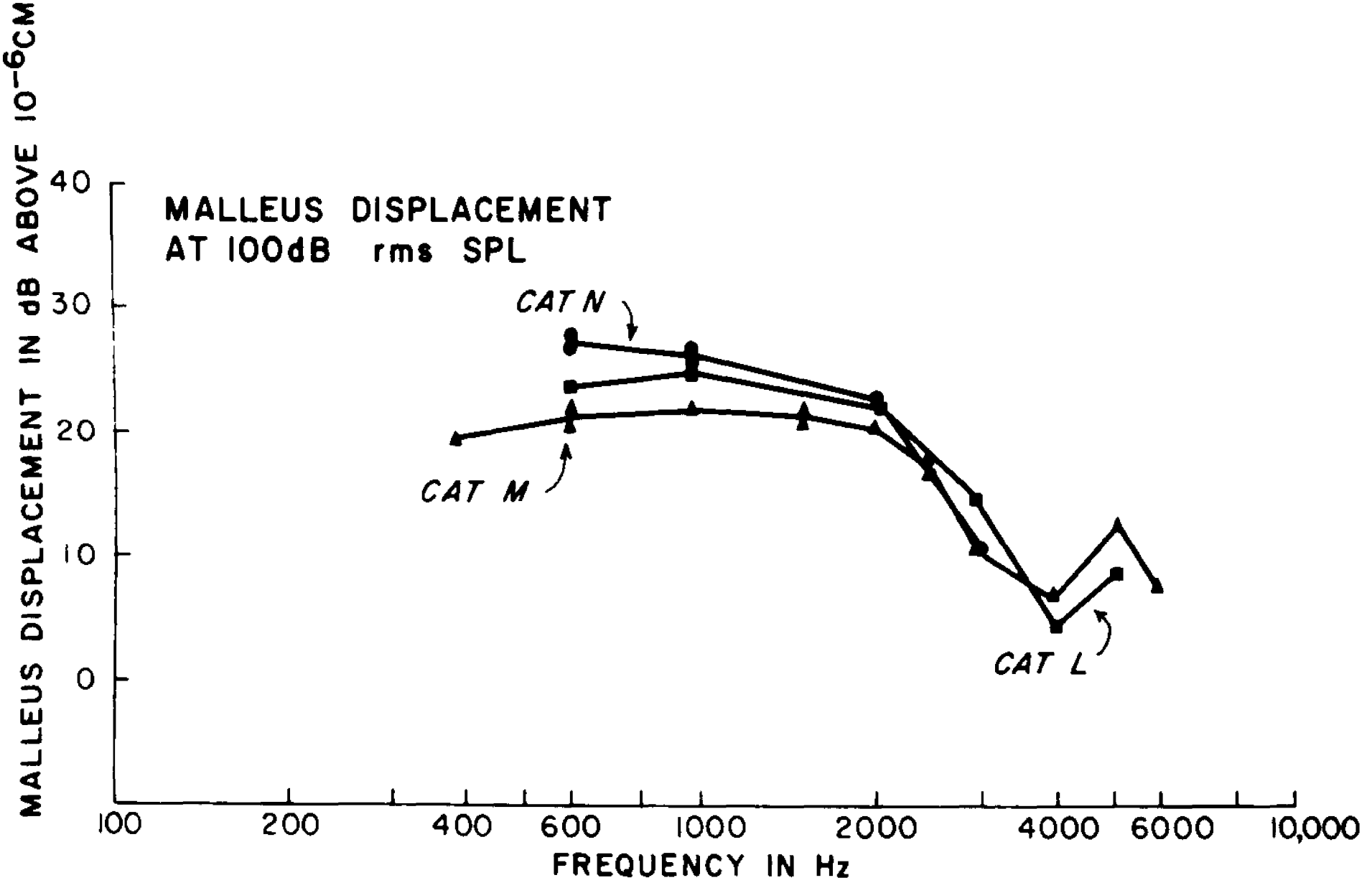
MALLEUS DISPLACEMENT
AT 100dB rms SPL
CAT N
CAT M
CAT L
MALLEUS DISPLACEMENT IN dB ABOVE 10^{-6}CM
40
30
20
10
0
100
200
400
600
1000
2000
4000
6000
10,000
FREQUENCY IN Hz

Figure 35.

Vibration patterns of tympanic membrane in man as measured by Bekesy, and in cat. Equal displacement lines on both show that the mode of vibration of the cat T. M. is quite different as compared to the human T. M.

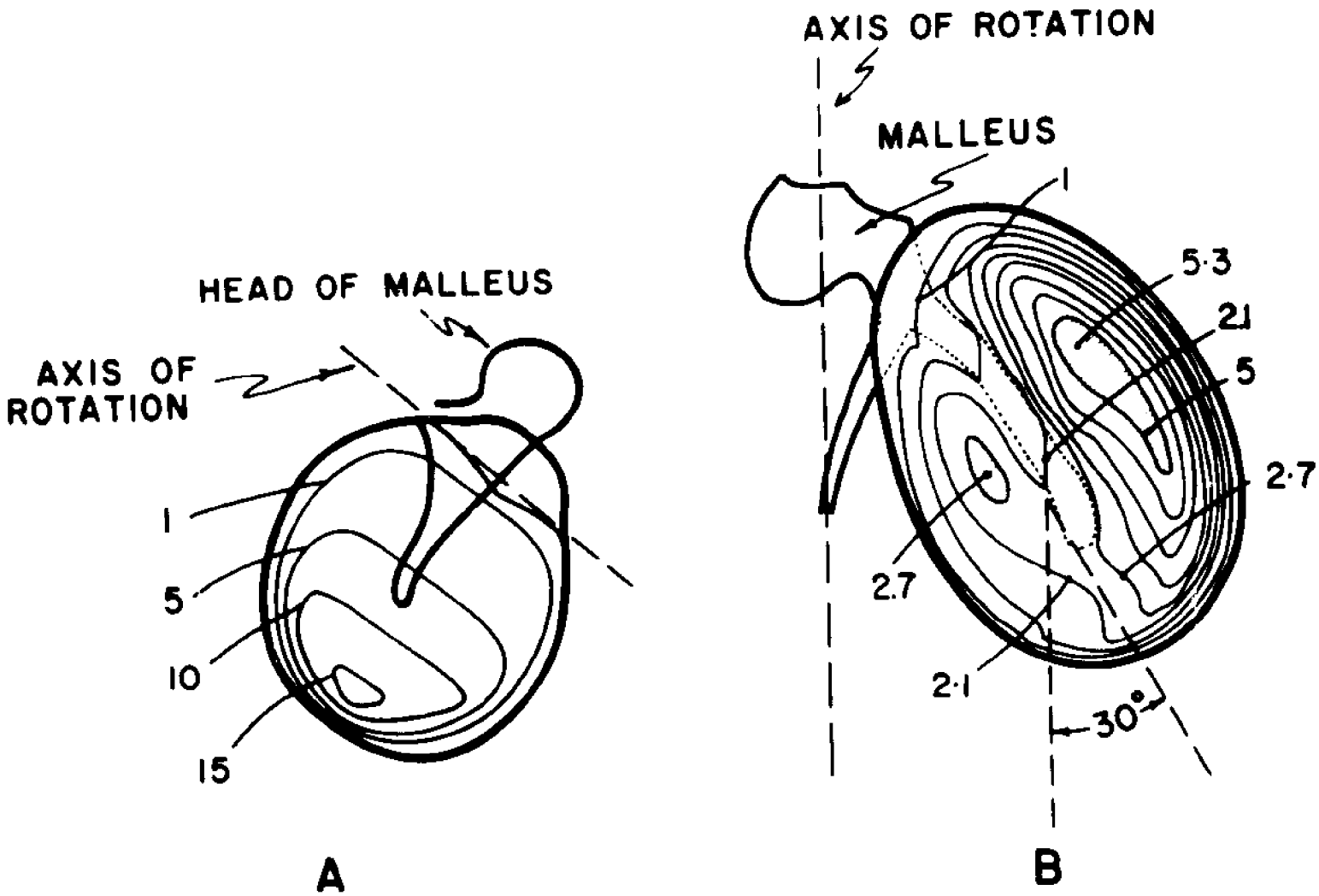
HEAD OF MALLEUS
AXIS OF ROTATION
1
5
10
15
A
AXIS OF ROTATION
MALLEUS
1
5·3
2·1
5
2·7
2·7
2·1
30°
B

Figure 36.

Vibration amplitude of the tympanic membrane along five crossections. The amplitude of the malleus at each point along its length is less than that of the T. M. adjacent to it on either side.

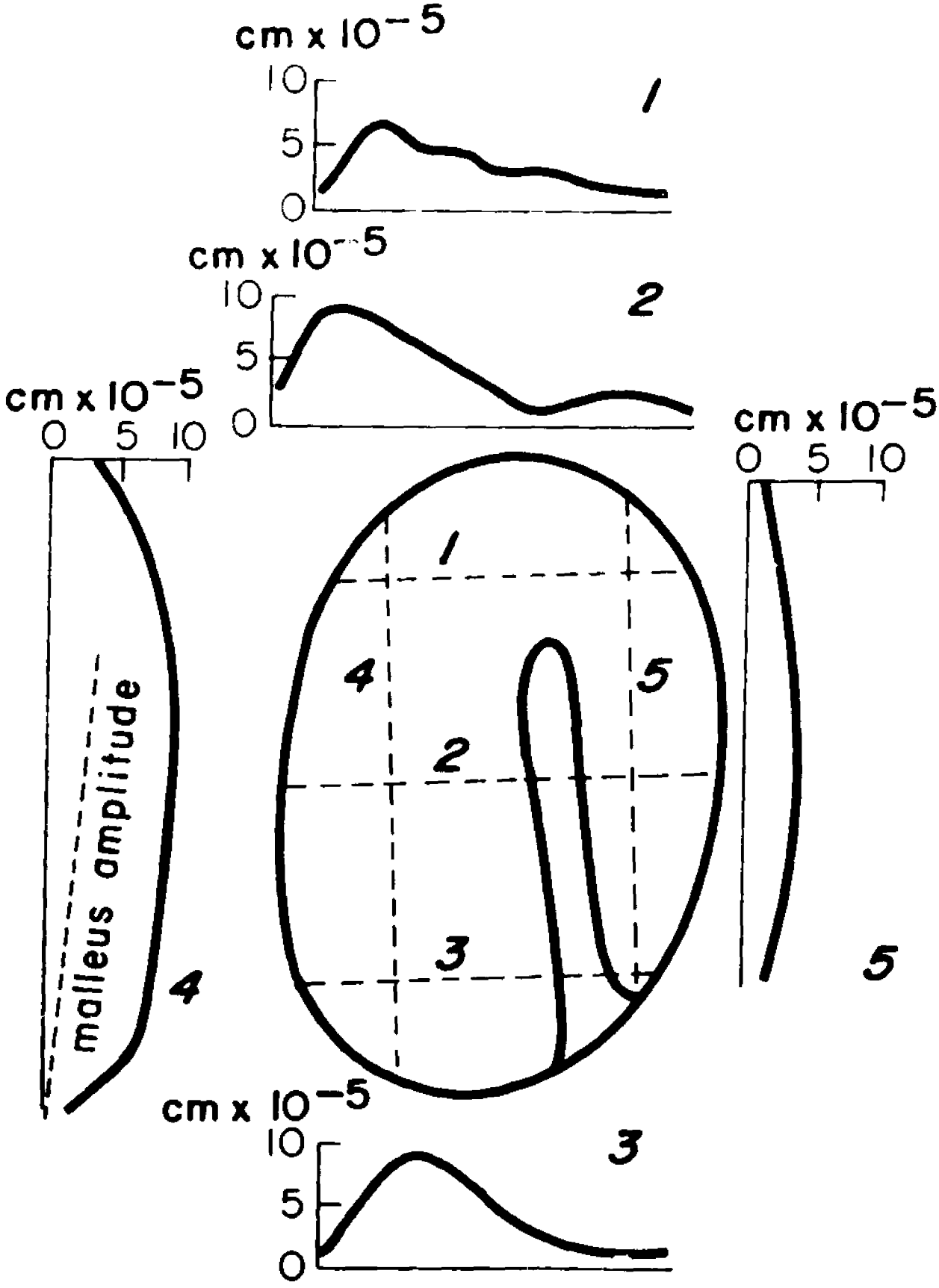
cm x 10⁻⁵
10
5
0
1
cm x 10⁻⁵
10
5
0
2
cm x 10⁻⁵
0 5 10
malleus amplitude
4
cm x 10⁻⁵
0 5 10
5
1
4
5
2
3
cm x 10⁻⁵
10
5
0
3

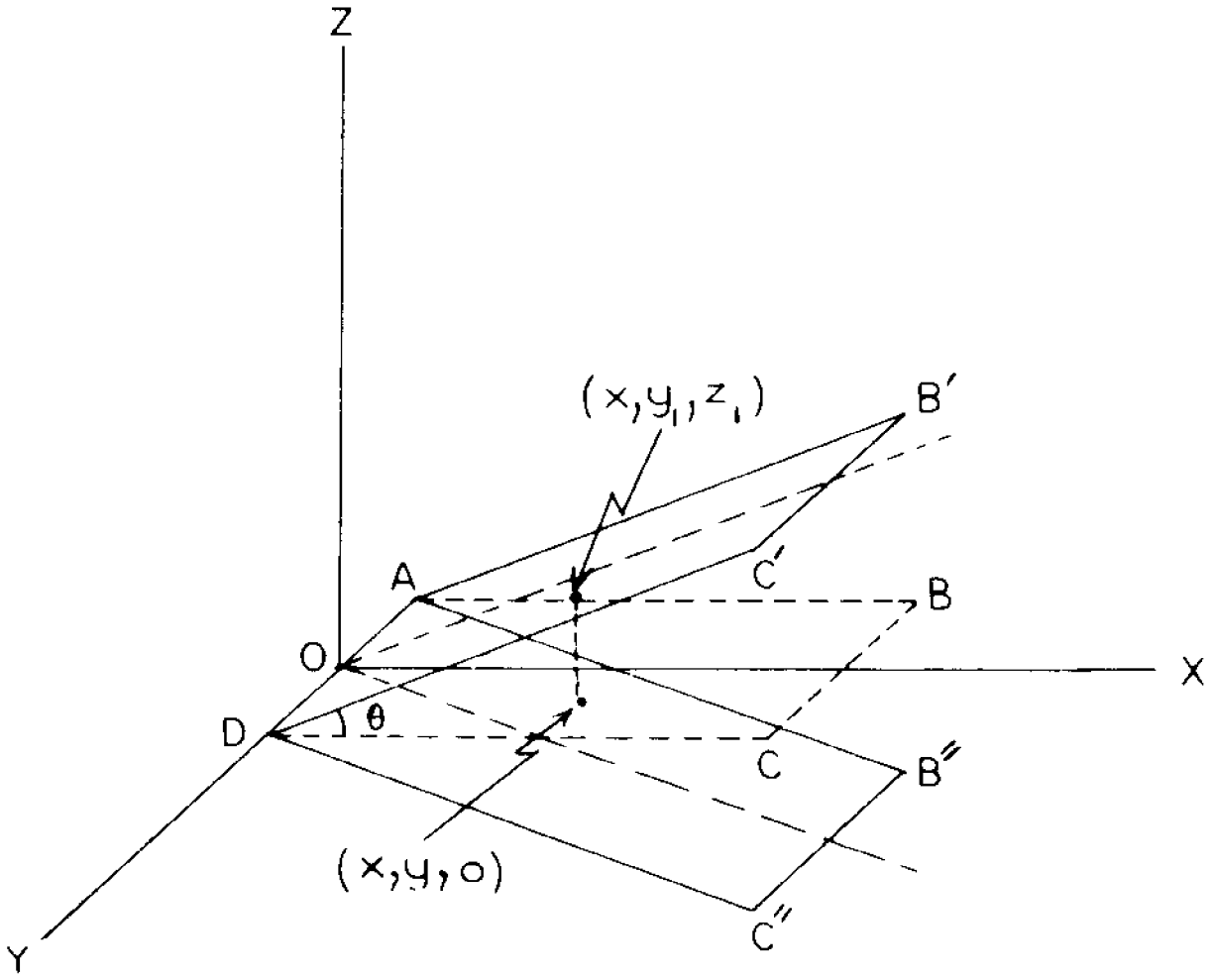

Figure 37.

Rotation of a plate around the y axis.

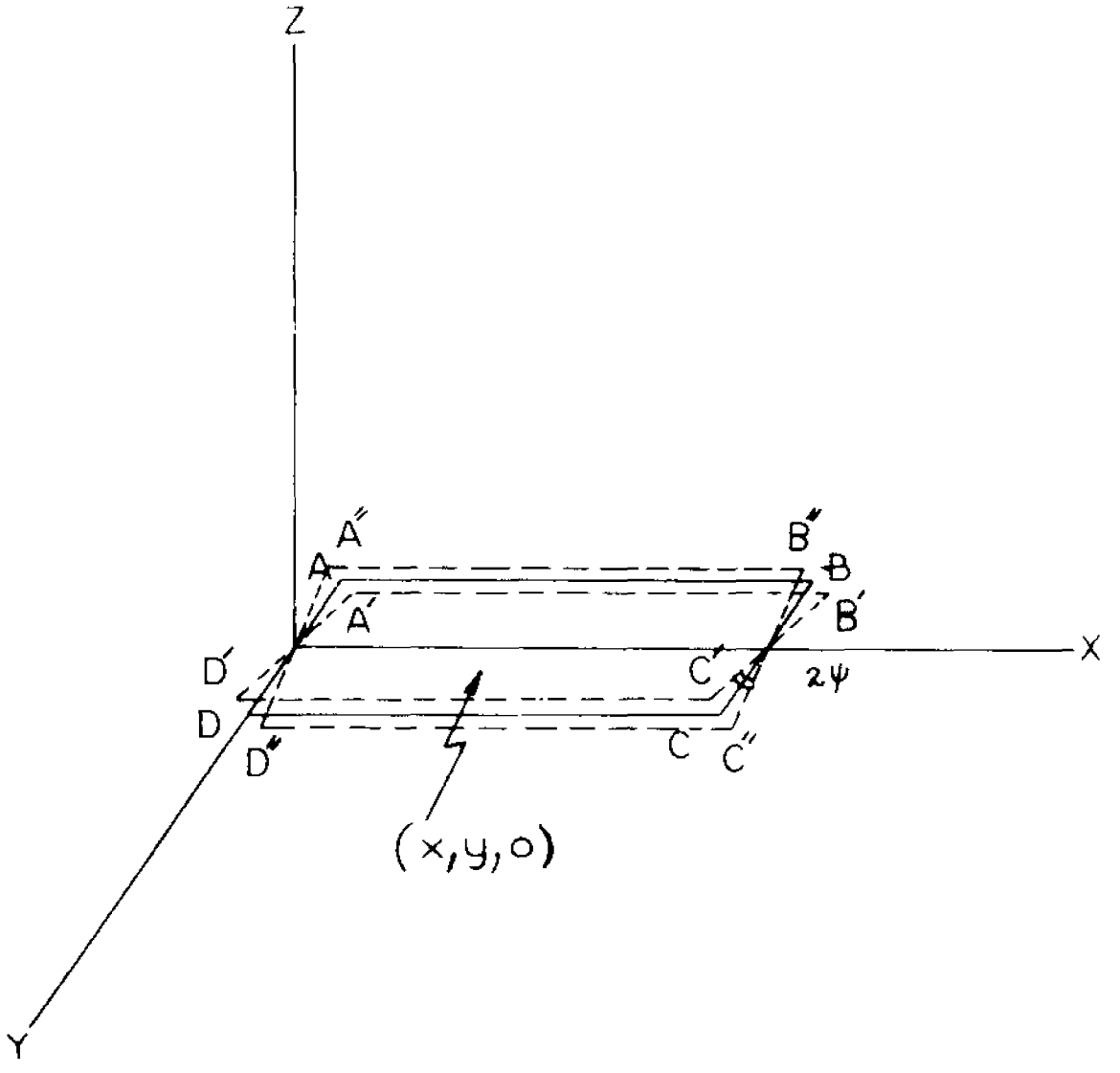

Figure 38.

Rotation of a plate around the x axis.

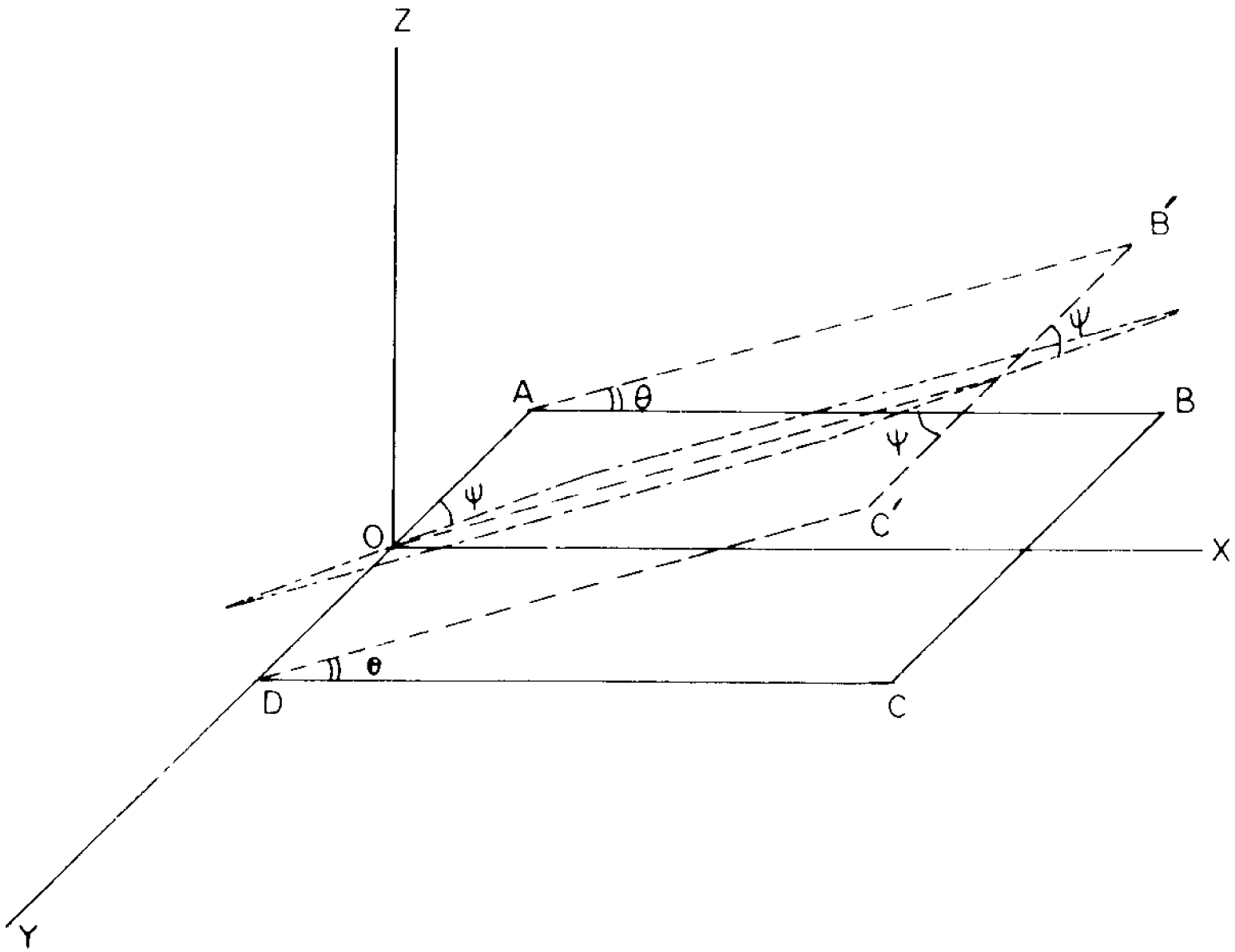

Figure 39.

Rotation of a plate around x and y axis.

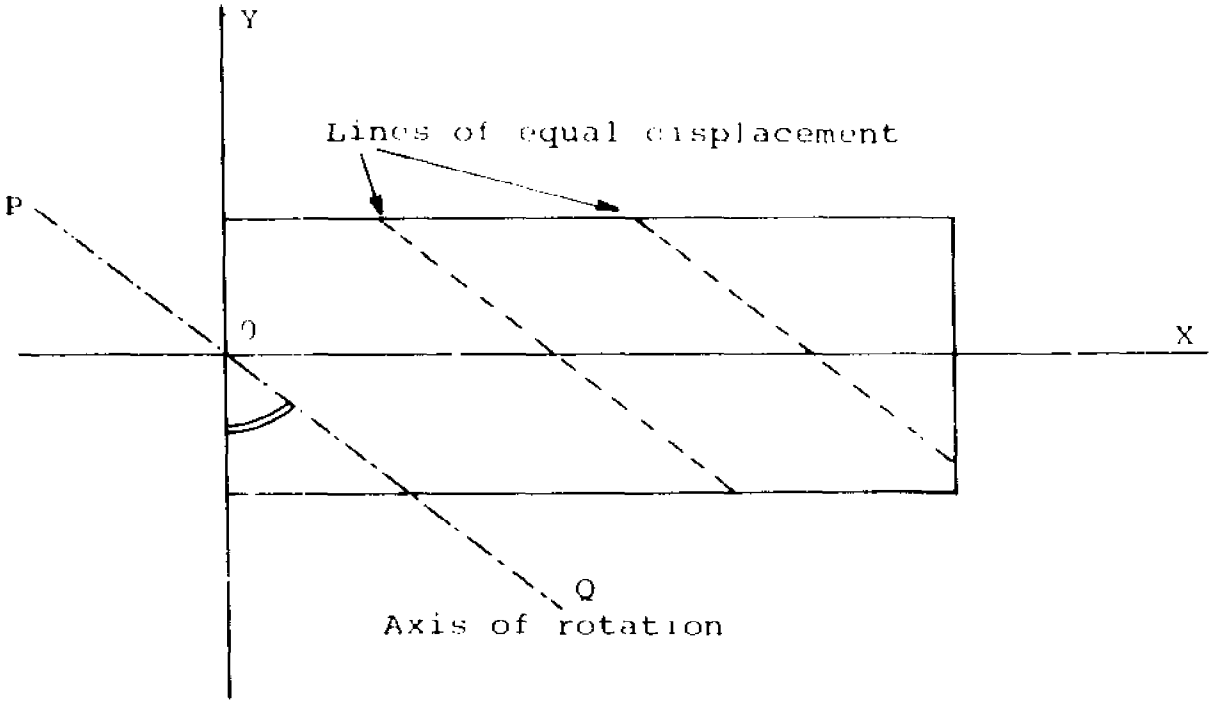

Figure 40.

Lines of equal displacement on a plate are parallel to its axis of rotation.

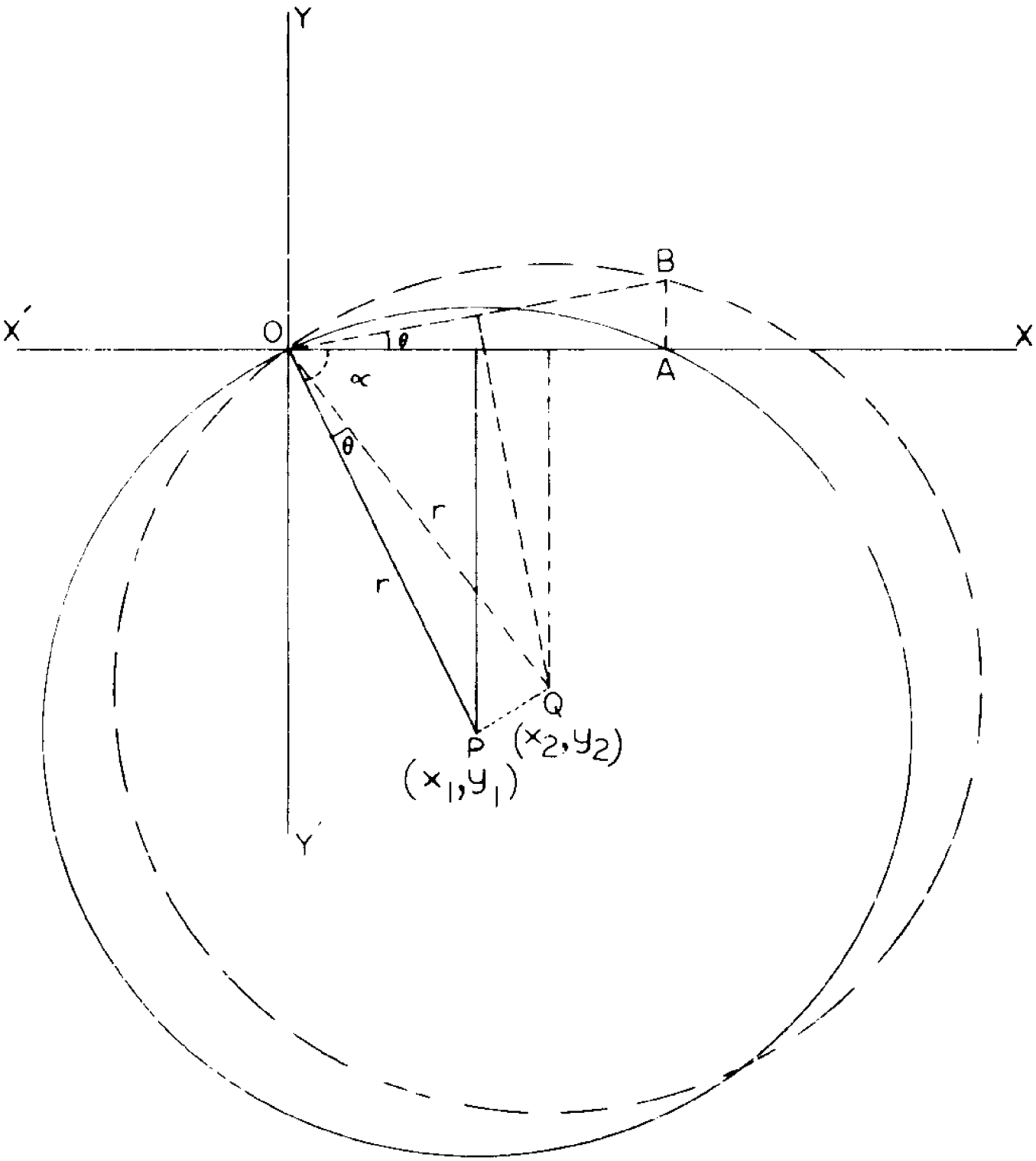

Figure 41.

Displacement of points on the segment of a circle when the chord is rotated through an angle θ .

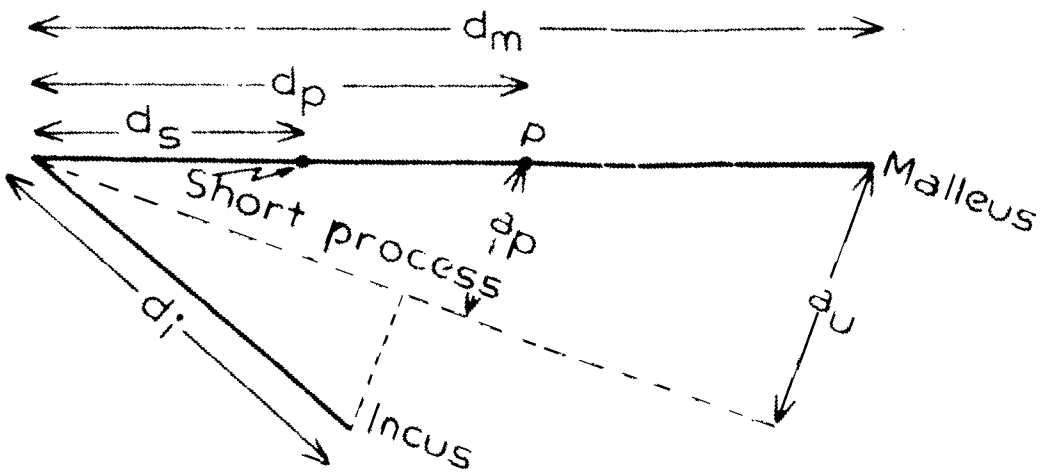

Figure 42.
Displacement of points along the malleus and incus.